Review

Catalytic wet peroxide oxidation: a route towards the application of hybrid magnetic carbon nanocomposites for the degradation of organic pollutants. A review

Rui S. Ribeiro [a], Adrián M.T. Silva [b], José L. Figueiredo [b], Joaquim L. Faria [b], Helder T. Gomes [a,*]

[a] Laboratory of Separation and Reaction Engineering — Laboratory of Catalysis and Materials (LSRE-LCM), Departamento de Tecnologia Química e Biológica, Escola Superior de Tecnologia e Gestão, Instituto Politécnico de Bragança, Campus de Santa Apolónia, 5300-857 Bragança, Portugal
[b] Laboratory of Separation and Reaction Engineering — Laboratory of Catalysis and Materials (LSRE-LCM), Departamento de Engenharia Química, Faculdade de Engenharia, Universidade do Porto, Rua Dr. Roberto Frias, 4200-465 Porto, Portugal

ARTICLE INFO

ABSTRACT

Several motivations have prompted the scientific community towards the application of hybrid magnetic carbon nanocomposites in catalytic wet peroxide oxidation (CWPO) processes. The most relevant literature on this topic is reviewed, with a special focus on the synergies that can arise from the combination of highly active and magnetically separable iron species with the easily tuned properties of carbon-based materials. These are mainly ascribed to increased adsorptive interactions, to good structural stability and low leaching levels of the metal species, and to increased regeneration and dispersion of the active sites, which are promoted by the presence of the carbon-based materials in the composites.

The most significant features of carbon materials that may be further explored in the design of improved hybrid magnetic catalysts are also addressed, taking into consideration the experimental knowledge gathered by the authors in their studies and development of carbon-based catalysts for CWPO. The presence of stable metal impurities, basic active sites and sulphur-containing functionalities, as well as high specific surface area, adequate porous texture, adsorptive interactions and structural defects, are shown to increase the activity of carbon materials when applied in CWPO, while the presence of acidic oxygen-containing functionalities has the opposite effect.

© 2016 Elsevier B.V. All rights reserved.

Contents

* Corresponding author.
  E-mail address: htgomes@ipb.pt (H.T. Gomes).

1. Introduction

With the increasing scarcity of clean water sources, wastewater treatment, and even reuse, became of utmost importance. Therefore, the development of efficient and economically viable technologies, able to meet increasingly demanding quality criteria for sustainable and safe urban water cycles and the use of treated wastewater as a reliable alternative water source, is presently of high priority in the policy agendas of European Union (EU) member states and many other countries around the world [1]. Therefore, the development of efficient technologies capable of degrading toxic, persistent and bio-recalcitrant organic pollutants commonly associated with negative impacts on conventional biological wastewater treatment processes, such as endocrine disrupting compounds, many types of pharmaceutical drugs including antibiotics, disinfection by-products, personal care products, metabolites, transformation products, pesticides, surfactants and biocides, has received a great deal of attention from the scientific community, in particular the so called Advanced Oxidation Processes (AOP) [1].

Among the AOP, catalytic wet peroxide oxidation (CWPO) is recognized as a low cost technology [2], since it operates with simple equipment and under mild conditions (e.g., at atmospheric pressure and low temperatures) [3]. CWPO employs hydrogen peroxide (H_2O_2) as oxidation source and a suitable catalyst to promote its partial decomposition to hydroxyl radicals ($HO^\bullet$), highly oxidizing species able to efficiently degrade most of the organic pollutants present in wastewaters [4,5]. Moreover, H_2O_2 is well-established as an environmentally-friendly agent, since its total decomposition products are oxygen and water, rendering CWPO-based water treatment technologies further attractive from an environmental point of view [3].

However, further optimization of catalyst design is still required in order to bring CWPO to the forefront of the most efficient AOP technologies. Bearing this in mind, the bibliometric analysis in Fig. 1 and the expertise gathered by the authors in their studies on carbon-based catalysts for CWPO prompted the preparation of this review on the synthesis of nanostructured hybrid magnetic carbon materials for CWPO applications. The background, main developments, and mechanistic aspects of the CWPO process, specially related with the application of carbon-based catalysts, are presented initially. Thereafter, the most significant results and conclusions reported in publications dealing with hybrid magnetic carbon catalysts for the degradation of organic pollutants by CWPO are thoroughly analysed and discussed. Since carbon materials present very specific features that may open prospects for the optimization of hybrid magnetic carbon materials for CWPO applications, the most significant results reported on the influence of carbon material properties on the efficiency of CWPO processes are also discussed in detail. In addition, all the pollutants used in the works reported in the literature on the application of carbon-based catalysts in CWPO processes are listed in Table 1.
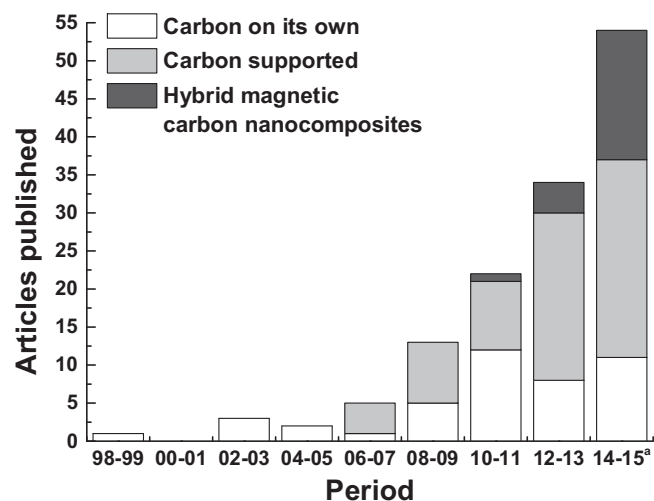

Fig. 1. Evolution of Scopus indexed original research articles dealing with the application of carbon-based materials in CWPO processes.
[a]Data collected from Scopus in November, 2015.

2. Catalytic wet peroxide oxidation: background, motivations and mechanistic aspects

2.1. The Fenton process

The catalytic oxidation of organic compounds using H_2O_2 as oxidant was first reported in the late XIX century, when the British researcher Henry John H. Fenton published his work on the oxidation of tartaric acid in the presence of iron salts [133]. In that work, it was demonstrated that tartaric acid can be oxidized by the interaction of small amounts of ferrous ion (Fe^{2+}) with distinct oxidizing agents, H_2O_2 leading to the best results. Fenton concluded that Fe^{2+} takes part in the reaction as catalyst, with a very small amount being enough to promote the complete degradation of an almost unlimited quantity of tartaric acid without being consumed.

In the 1930s, Fritz Haber and Joseph J. Weiss brought further insights on the phenomenon reported by Fenton, concluding that hydroxyl radicals ($HO^\bullet$) – generated from the reaction of H_2O_2 with the superoxide radical anion ($O_2^{\bullet-}$), the Haber-Weiss reaction [134] – were actually the active species responsible for the oxidation of tartaric acid, and not H_2O_2 itself. According to these authors, the interaction between H_2O_2 and Fe^{2+} in acidic media results in the decomposition of H_2O_2 through the oxidation of Fe^{2+} to ferric ion (Fe^{3+}), with the formation of hydroxide ions (OH^-) and $HO^\bullet$ radicals, as described by Eq. (1) [135].

$$H_2O_2 + Fe^{2+} \rightleftarrows OH^- + HO^\bullet + Fe^{3+} \tag{1}$$
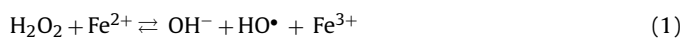
The participation of Fe^{2+} as catalyst in the oxidation process was finally demonstrated in the 1950s, in two works reported by Barb et al. [136,137]. These authors proposed a two-step mechanism in

Table 1
List of organic pollutants employed in the application of carbon-based catalysts in CWPO processes.

Class	Pollutant	Chemical formula	Articles published[a]	Reference(s)
Dyes	Methylene blue	$C_{16}H_{18}ClN_3S$	19	[6–24]
	Orange II	$C_{16}H_{11}N_2NaO_4S$	18	[19,25–41]
	Methyl orange	$C_{14}H_{14}N_3NaO_3S$	5	[17,42–45]
	Chromotrope 2R	$C_{16}H_{10}N_2Na_2O_8S_2$	3	[38,46,47]
	Crystal violet	$C_{25}H_{30}ClN_3$	2	[48,49]
	Reactive black 5	$C_{26}H_{21}N_5Na_4O_{19}S_6$	2	[48,50,51]
	Other	Not applicable	13	[6,7,49,51–60]
	Total		62	
Phenolic compounds	Phenol	C_6H_6O	31	[7,61–90]
	4-Chlorophenol	C_6H_5ClO	6	[91–96]
	Bisphenol A	$C_{15}H_{16}O_2$	6	[97–102]
	2-Nitrophenol	$C_6H_5NO_3$	2	[103,104]
	m-Cresol	C_7H_8O	2	[105,106]
	Other	Not applicable	5	[7,107–110]
	Total		52	
Real wastewater	Textile	Not applicable	8	[111–118]
	Cosmetic	Not applicable	1	[119]
	Pharmaceutical	Not applicable	1	[120]
	Salicylaldehyde production	Not applicable	1	[121]
	Winery	Not applicable	1	[122]
	Total		12	
Pharmaceuticals	17α-Methyltestosterone	$C_{20}H_{30}O_2$	2	[123,124]
	Ciprofloxacin	$C_{17}H_{18}FN_3O_3$	2	[125,126]
	Tetracycline	$C_{22}H_{24}N_2O_8$	1	[127]
	Total		5	
Herbicides	Amitrole	$C_2H_4N_4$	1	[128]
	Paraquat	$C_{12}H_{14}Cl_2N_2$	1	[129]
	Total		2	
Other			7	[76,81,85,108,130–132]

[a] Data collected from Scopus in November, 2015.

which Fe^{2+} is regenerated from the Fe^{3+} formed in the reaction described by Eq. (1):

- in the first step, H_2O_2 reacts with $HO^\bullet$ in solution, resulting in the formation of hydroperoxyl radicals ($HOO^\bullet$) and water, as described by Eq. (2);
- in the second step, $HOO^\bullet$ reduces Fe^{3+}, regenerating Fe^{2+} and closing the catalytic cycle, as described by Eq. (3).

$$H_2O_2 + HO^\bullet \rightarrow HOO^\bullet + H_2O \tag{2}$$

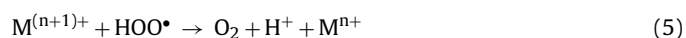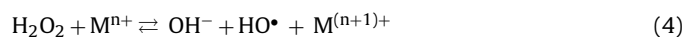$$Fe^{3+} + HOO^\bullet \rightarrow O_2 + H^+ + Fe^{2+} \tag{3}$$
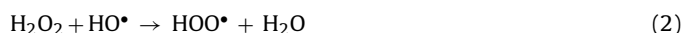
In recognition for the major contribution made by Fenton, the reported oxidation process in which homogeneous Fe^{2+} is used as catalyst is known as the Fenton process. Nowadays, it is widely known that $HO^\bullet$ radicals are powerful oxidants (standard reduction potential between +2.8 V and +2.0 V at pH 0 and 14, respectively) and serve as effective species in the destruction of a large range of organic pollutants [4,5]. As recently reviewed, the rate constant of the reaction described in Eq. (1) is 55 $M^{-1}\,s^{-1}$, much lower when compared with the rate constants of the reactions described in Eqs. (2) and (3), namely $3.30 \times 10^7\,M^{-1}\,s^{-1}$ and $7.82 \times 10^5\,M^{-1}\,s^{-1}$, respectively [138]. Therefore, although other reactions (such as non-efficient parasitic reactions) are involved in the Fenton process, the reaction described in Eq. (1) is expected to be the limiting step in the catalytic cycle. Nevertheless, some drawbacks leading to the increase of operation costs are commonly associated with the Fenton process, such as the need for a complicated final chemical and physically-driven separation step for the recovery or elimination of the Fe^{2+}/Fe^{3+} ions, often found in amounts exceeding the limits allowed by EU directives for treated waters (2 mg L^{-1}). In

addition, the Fenton process operates under pH values in the range 2.5–4.0 [139], originating acidic solutions which need neutralisation before being discharged into natural water courses. A tentative solution to overcome these constraints is the use of supported heterogeneous catalysts, whose advantages and disadvantages are discussed in the following Section.

2.2. Carbon-supported metal catalysts

Very distinct materials such as alumina, silica, mesoporous molecular sieves, zeolites, pillared clays, ion-exchange resins and nanometric diamonds have been used to support transition metals, mainly iron [5,90,138,140–146]. Nevertheless, the advantages of using carbon materials as supports for the preparation of highly dispersed metal catalysts are widely recognized. Since the first review on the subject by Ehrburger in 1984 [147], the application of carbon materials as catalyst supports has been the subject of several other comprehensive reviews [148–154], reflecting the increasing interest of the scientific community on carbonaceous supports. This interest may be attributed to some specific properties of carbon materials, such as: (i) stability in acidic/basic media; (ii) high specific surface area, leading to high dispersion and stability of the metal phases; (iii) possibility to control, to some extent, the porosity and the surface chemistry, improving diffusion of reactants and products to and from the surface and increasing metal dispersion by controlling polarity and hydrophobicity, respectively; (iv) easy recovery of expensive metal phases by burning away the carbon support; and (v) structural stability at high temperatures [154–156]. In addition, carbon materials are usually cheaper than other conventional catalyst supports [154].

Carbon-supported metal catalysts are typically prepared by techniques similar to those used with other supports, the most widely used being impregnation [154,155]. Nevertheless, several other methods have also been used for the preparation of carbon supported metal catalysts, such as precipitation or co-precipitation, liquid-phase reduction, chemical vapour deposition and physical vapour deposition [154]. Given the wide range of methods available for the preparation of supported metal catalysts and the interesting features of carbon materials, their application as supports for Fe species is the most straightforward tentative solution to overcome the drawbacks reported previously on the use of homogeneous Fe^{2+} catalysts in the Fenton process. In this way, it may be expected that the separation of the heterogeneous catalyst from the final treated waters becomes easier, since the active phase is immobilised on the surface of a support. Fe catalysts supported on carbon materials have been used in several works devoted to the catalytic oxidation of different compounds using H_2O_2 as oxidant [25,40,68,83,90,119,157], i.e., CWPO – catalytic wet peroxide oxidation. It should be noted that the term CWPO is here introduced to distinguish between the typical Fenton process and the processes involving heterogeneous supported catalysts or even other homogeneous catalysts, since other metals have also been found as active species for CWPO applications, provided that the metal presents two possible oxidation states (e.g., M^{n+} and $M^{(n+1)+}$, where M represents the metal symbol) [145]. Thus, the catalytic reactions described by Eqs. (1) and (3) can be replaced by more general reactions, as described by Eqs. (4) and (5).

$$H_2O_2 + M^{n+} \rightleftarrows OH^- + HO^\bullet + M^{(n+1)+} \qquad (4)$$

$$M^{(n+1)+} + HOO^\bullet \rightarrow O_2 + H^+ + M^{n+} \qquad (5)$$

Although the use of supported catalysts facilitates the final separation step, this alternative poses other difficulties, namely the loss of catalyst activity due to metal leaching. In this Section we will present some illustrative examples of this catalyst deactivation phenomenon that typically occurs during CWPO of organic pollutants in aqueous phase. For that purpose, supported catalysts based on carbon materials with very distinct properties are considered. The description of the catalyst, the process operating conditions and the catalytic performance of each catalyst (pollutant removal and Fe leached to the treated waters) found in the following examples are summarized in Table 2.

A carbon-supported Fe catalyst was prepared by Zazo et al. [90] and subsequently tested in the CWPO of phenol. The catalyst was prepared by incipient-wetness impregnation of a commercial activated carbon, as described in Table 2. As observed, complete removal of the initial phenol content was obtained in CWPO experiments performed during 4 h at 30 °C and $pH_{solution} = 3$. Nevertheless, a Fe leaching of 2.40 mg L^{-1} was determined at the end of the process. In addition, due to the Fe leaching, the authors concluded that this supported catalyst would undergo a significant loss of activity when subjected to continuous experiments [90].

Two distinct carbon materials were used as supports in the work reported by Ramirez et al. [25], namely an activated carbon obtained by carbonization of olive stones and a carbon aerogel prepared from resorcinol and formaldehyde. The supported catalysts were prepared by incipient-wetness impregnation with a ferrous acetate solution. The Fe leaching in the CWPO of orange II at 30 °C and $pH_{solution} = 3$ was 0.87 mg L^{-1} and 0.97 mg L^{-1}, with the activated carbon and the carbon aerogel support, respectively. The authors concluded that Fe leached from the support leads to a progressive deactivation in consecutive reaction cycles, which is an important limitation for their industrial application.

Carbon nanotubes and carbon nanofibers have also been used as supports for Fe species in CWPO applications. Rodríguez et al. [40] reported the use of supported Fe catalysts prepared by incipient-wetness impregnation of carbon nanotubes, carbon nanofibers and activated carbon. As observed in Table 2, the three catalysts lead to high removals of orange II in CWPO experiments, performed at 30 °C and $pH_{solution} = 3$. However, very high levels of Fe leaching were determined in the treated waters, limiting the stability and durability of the catalysts.

So far, it has been shown that most of the carbon-supported metal catalysts do not exhibit suitable stability for CWPO applications, mainly as a result of metal leaching. At the same time, since the report of Lücking et al. in 1998 [91], different carbon materials have been recognized as active metal-free catalysts for CWPO. In this way, active metals are not required to promote the generation of HO$^\bullet$, thus avoiding the need for a metal separation step at the end of the CWPO treatment. The application of carbon materials directly as catalysts in CWPO processes will be discussed in detail in the next Sections.

2.3. Carbon materials as catalysts on their own

The application of carbon materials directly as catalysts was recognized a long time ago [158]. Back in 1969, Robert W. Coughlin noticed the increasing importance of carbons in several catalytic processes, which was ascribed to some of their properties, such as the crystalline structure, microscopic physical structure, electronic properties and surface chemistry, as well as to the presence of impurities [158]. Since then, the use of carbon materials as catalysts on their own has been the subject of several works, in parallel with the development of new types of nanostructured carbon materials [155]. Comprehensive reviews on the subject with extensive detail may be found in the book published in 2009 by Serp and Figueiredo [154] and in the book published in 2015 by Serp and Machado [159].

In the particular case of CWPO, carbon materials (without any supported metal phase) were first reported as active and stable catalysts by Lücking et al. in 1998 [91]. To the best of our knowledge, this work also reported for the first time the application of carbon supported catalysts in CWPO. At that time, the authors highlighted the difficulty to retain homogeneous catalysts in the process as the main disadvantage on the use of iron salts directly in solution (in the Fenton process), and the leaching of the metal phase from the support material as the main disadvantage of the application of supported metal catalysts in CWPO. Bearing this in mind, Lücking et al. [91] compared the performances of distinct materials in the CWPO of 4-chlorophenol, at $pH_{solution} = 3$, namely iron powder, iron supported on activated carbon, graphite and three activated carbons of distinct origins (without any supported metal phase). As summarized in Table 3, the results have shown that both iron powder and iron supported on activated carbon catalysts owe their activity to the Fe ions leached to the solution (300 and 56.0 mg L^{-1}, respectively, in batch experiments), which subsequently act as homogeneous catalysts; on the contrary, both activated carbon and graphite were found to act as heterogeneous catalysts in the decomposition of H_2O_2 and in the oxidation of 4-chlorophenol [91]. In support of this observation, graphite revealed much higher activity in the CWPO of 4-chlorophenol in comparison with homogeneous Fe^{2+} (1 mg L^{-1}, twice the amount leached to the treated water when graphite was used as catalyst) [91].

The results reported by Lücking et al. [91] prompted the scientific community to further explore the use of carbon materials without any supported metal phase in CWPO. Since the ability of carbon materials to selectively decompose H_2O_2 into HO$^\bullet$ is of major importance to the global process performance, this reaction was also the subject of specific research. In a previous publication, our group proposed a mechanism for the decomposition of H_2O_2 when carbon materials are used as catalysts [160], based on experimental results and on other findings reported in the literature

Table 2

Representative examples on the use of carbon-supported metal catalysts in CWPO processes: description of the catalyst, operating conditions and catalytic performance of each catalyst (pollutant removal and Fe leached to the treated waters).

Authors	Catalyst	Operating conditions	Pollutant	H_2O_2 stoichiometric ratio[a]	Pollutant removal	$[Fe]_{leaching}$ $(mg\,L^{-1})$
Zazo et al. [90]	Fe (4 wt.%) supported on a commercial activated carbon by incipient-wetness impregnation with an iron nitrate solution, followed by calcination at 200 °C for 4 h	Batch experiments [Catalyst] = 0.5 g L^{-1} [H_2O_2]$_0$ = 0.50 g L^{-1} T = 50 °C pH$_{solution}$ = 3 t = 4 h	Phenol (100 mg L^{-1})	1.0	100.0% (50.0 mg g^{-1} h^{-1})	2.40
	Same activated carbon, but without impregnation of Fe				58.0% (29.0 mg g^{-1} h^{-1})	Not addressed
Ramirez et al. [25]	Fe (7 wt.%) supported on activated carbon (prepared by carbonization of olive stones) by incipient-wetness impregnation with a ferrous acetate solution, followed by calcination under N$_2$ atmosphere at 200 °C for 2 h	Batch experiments [Catalyst] = 0.2 g L^{-1} [H_2O_2]$_0$ = 0.20 g L^{-1} T = 30 °C pH$_{solution}$ = 3 t = 4 h	Orange II (35 mg L^{-1})	1.3	98.0% (42.9 mg g^{-1} h^{-1})	0.87
	Same activated carbon, but without impregnation of Fe	Same conditions as above, except that t = 35 h			98.0% (4.90 mg g^{-1} h^{-1})	Not addressed
	Fe (7 wt.%) supported on carbon aerogel (prepared by polymerization of an organic resorcinol-formaldehyde solution) by incipient-wetness impregnation with a ferrous acetate solution, followed by calcination under N$_2$ atmosphere at 200 °C for 2 h	Same conditions as above, except that t = 4 h			98.0% (42.9 mg g^{-1} h^{-1})	0.97
	Same carbon aerogel, but without impregnation of Fe	Same conditions as above, except that t = 15 h			98.0% (9.33 mg g^{-1} h^{-1})	Not addressed
Rodríguez et al. [40]	Fe (5 wt.%) supported on carbon nanotubes (prepared by chemical vapour deposition) by incipient-wetness impregnation with an unknown Fe precursor, followed by heating under N$_2$ atmosphere at 350 °C for 4 h	Batch experiments [Catalyst] = 2.0 g L^{-1} [H_2O_2]$_0$ = 0.35 g L^{-1} T = 30 °C pH$_{solution}$ = 3 t = 2 h	Orange II (66 mg L^{-1})	1.2	94.0% (15.5 mg g^{-1} h^{-1})	25.2
	Fe (5 wt.%) supported on commercial carbon nanofibers (origin not specified) by using the same incipient-wetness impregnation procedure as described above				100.0% (16.5 mg g^{-1} h^{-1})	22.7
	Fe (5 wt.%) supported on a commercial activated carbon by using the same incipient-wetness impregnation procedure as described above				94.0% (16.2 mg g^{-1} h^{-1})	50.1

[a] Obtained by dividing the amount of H_2O_2 employed by the stoichiometric amount needed for the complete mineralization of the pollutant considered.

[2,161–172]. The proposed mechanism, given in Table 4, consists of the following steps:

- [H_2O_2] decomposes via HO$^\bullet$ formation, with the participation of reduced active sites [AS], i.e., electron donor sites existing at the carbon surface (e.g. basic oxygen containing groups, such as chromene and pyrone, basic nitrogen containing functionalities or delocalized π-electrons at the carbon basal planes), as described by Eq. (6);
- [H_2O_2] adsorbed over the oxidized active sites [AS$^+$], i.e., electron acceptor sites, decomposes to HOO$^\bullet$ and H$^+$, regenerating [AS], as described by Eq. (7);
- Adsorbed HOO$^\bullet$ and H$^+$ produce atomic oxygen (which may remain trapped in the surface and accounts for the formation of carbon surface oxides) and water when in contact with reducing

active sites [S] existing at the carbon surface, as described by Eq. (8);
- Due to self-annihilation, H_2O_2 in the bulk can be decomposed to HOO$^\bullet$, HO$^\bullet$, O$_2$ and water, by reaction with HOO$^\bullet$, HO$^\bullet$ and O$_2^{\bullet-}$, as described by Eqs. (10)–(12). Due to the low bimolecular reaction rate, Eqs. (11) and (12) will have a negligible contribution to this self-annihilation process. H_2O_2 in the bulk may also be decomposed by dissociation as a weak acid, as described by Eq. (9);
- Finally, the radicals HO$^\bullet$, HOO$^\bullet$ and O$_2^{\bullet-}$ can react with themselves resulting mainly in O$_2$, water and some minor amounts of regenerated H_2O_2 (Eqs. (14)–(20)); HOO$^\bullet$ can also be decomposed by a first order process, as described by Eq. (13).

Most of the reactions given in Table 4 are widely accepted in AOP [173,174], in addition to the catalytic surface reactions described by

Table 3
Summary of the comparative study reported by Lücking et al. in 1998 [91], in which carbon materials without any supported metal phase were first shown as active and stable catalysts for CWPO. Data include description of the catalyst, operating conditions and catalytic performance of each catalyst [pollutant removal in terms of dissolved organic carbon (DOC) and Fe leached to the treated waters].

Authors	Catalyst	Operating conditions	Pollutant	H_2O_2 stoichiometric ratio[a]	Pollutant removal[b]	$[Fe]_{leaching}$ (mg L^{-1})
Lücking et al. [91]	Iron powder (95 wt.% Fe, Isocommerz VE Außen- und Binnenhandelsbetrieb BT Herzberg/E)	Batch experiments [Catalyst] = 1.0 g L^{-1} [H_2O_2]$_0$ = 5.30 g L^{-1} T = 30 °C pH$_{solution}$ = 3 t = 6 h			64.0%	300
	Graphite (99.8 wt.% C, Laborchemie Apolda GmbH)	Same conditions as above, except that t = 96 h	4-Chlorophenol (1000 mg L^{-1})	1.2	30.0%	0.50
	Homogeneous Fe^{2+} (for comparison purposes)	Same conditions as above, except that [catalyst] = 1 mg L^{-1} and t = 144 h			8.0%	Not applicable
	Activated carbon (RFZ1, from Norit), followed by impregnation with iron hydroxide (ash content ca. 15–20 wt.%)	Batch and continuous experiments [Catalyst] = 1.0 g L^{-1} [H_2O_2]$_0$ = 5.30 g L^{-1} T = 30 °C (batch)			80.9% (batch) 41.0% (continuous, 32 d) 17.0% (continuous, 160 d)	56.0 (batch) 14.8 (continuous, 32 d) 0.32 (continuous, 160 d)
	Activated carbon (F-300, from Chemviron Carbon)	T = 20 °C (continuous) pH$_{solution}$ = 3 t = 800 h (batch) t = 160 d (continuous)	4-Chlorophenol (1000 mg L^{-1})	1.2	70.1% (batch) 18.0% (continuous, 32 d) 8.0% (continuous, 160 d)	<2.00[c] (batch) 0.46 (continuous, 32 d) 0.18 (continuous, 160 d)
	Activated carbon (Darco GCW, from Norit)				65.7% (batch) 15.0% (continuous, 32 d) 10.0% (continuous, 160 d)	<2.00[c] (batch) 0.48 (continuous, 32 d) 0.20 (continuous, 160 d)
	Activated carbon (ROW 0.8, from Norit)				72.2% (batch) 13.0% (continuous, 32 d) 6.0% (continuous, 160 d)	<2.00[c] (batch) 0.12 (continuous, 32 d) 0.11 (continuous, 160 d)

[a] Obtained by dividing the amount of H_2O_2 employed by the stoichiometric amount needed for the complete mineralization of the pollutant considered.
[b] Dissolved organic carbon (DOC) removal.
[c] Not specified.

Table 4
Reaction mechanisms for H_2O_2 decomposition.

Reaction	Comment/Rate	
$[H_2O_2 + S] \rightarrow HO^\bullet + OH^- + [S^+]$	Catalytic surface reaction [160]	(6)
$[H_2O_2 + S^+] \rightarrow [HOO^\bullet + H^+ + S]$	Catalytic surface reaction [160]	(7)
$[HOO^\bullet + H^+ + S] \rightarrow H_2O + [O^\bullet + S^+]$	Catalytic surface reaction [160]	(8)
$H_2O_2 \rightleftarrows H^+ + HO_2^-$	pK_a = 11.75 [165]	(9)
$H_2O_2 + HO^\bullet \rightarrow H_2O + HOO^\bullet$	2.7×10^7 M^{-1} s^{-1} [162]	(10)
$H_2O_2 + HOO^\bullet \rightarrow HO^\bullet + H_2O + O_2$	3 M^{-1} s^{-1} [167]	(11)
$H_2O_2 + O_2^{\bullet-} \rightarrow HO^\bullet + OH^- + O_2$	0.13 M^{-1} s^{-1} [172]	(12)
$HOO^\bullet \rightarrow O_2^{\bullet-} + H^+$	1.58×10^5 s^{-1} [161]	(13)
$O_2^{\bullet-} + H^+ \rightarrow HOO^\bullet$	1×10^{10} M^{-1} s^{-1} [161]	(14)
$HO_2^- + HO^\bullet \rightarrow HOO^\bullet + OH^-$	7.5×10^9 M^{-1} s^{-1} [163]	(15)
$HO^\bullet + HOO^\bullet \rightarrow H_2O + O_2$	6.6×10^9 M^{-1} s^{-1} [164]	(16)
$HO^\bullet + HO^\bullet \rightarrow H_2O_2$	5.5×10^9 M^{-1} s^{-1} [162]	(17)
$HOO^\bullet + HOO^\bullet \rightarrow H_2O_2 + O_2$	8.3×10^5 M^{-1} s^{-1} [161]	(18)
$HO^\bullet + O_2^{\bullet-} \rightarrow OH^- + O_2$	8×10^9 M^{-1} s^{-1} [169]	(19)
$HOO^\bullet + O_2^{\bullet-} \rightarrow HO_2^- + O_2$	9.7×10^7 M^{-1} s^{-1} [161]	(20)

Adapted from [160].

Eqs. (6)–(8). In particular, the mechanism of H_2O_2 decomposition for CWPO applications is especially relevant when leading to the formation of HO$^\bullet$, since these species present higher redox potential (2.80 V) than that of HOO$^\bullet$ (1.70 V) and of H_2O_2 itself (1.77 V) [175].

Since the report of Lücking et al. [91], very distinct materials such as activated carbons [6,7,39,46,47,72,88,129,171,176–178], graphite [61,66,81,91,122,177], carbon nanotubes [59,65,83,103], carbon blacks [66,177], carbon aerogels [41], activated carbon xerogels [38], glycerol-based carbon materials [104], graphene-based materials [34,62,107] and others [81,111], have been reported as active and efficient catalysts for CWPO. The most significant findings will be discussed in detail in the following Sections.

3. The influence of carbon material properties on the efficiency of catalytic wet peroxide oxidation processes

Although carbon materials are known to be active in reactions typically catalysed by metals, the number of industrial applications in which carbon materials are used as catalysts on their own is still rather limited [155]. This fact may be partially explained by the relatively poor knowledge on the properties of these materials that influence their efficiency as catalysts [154]. In the particular case of CWPO, the development of suitable carbonaceous materials (without any supported metal) has been intensively explored in recent years [145]. Several efforts have been made in order to understand the effect of the carbon material properties on their catalytic performance. In this Chapter we will present some examples of how

Table 5
Summary of the comparative study performed by Domínguez et al. [177]: description of the catalyst, operating conditions and values of the apparent H_2O_2 global decomposition rate constants (k_d). Fe leaching was not addressed in this study.

Authors	Catalyst	Operating conditions	k_d (h^{-1})
Domínguez et al. [177]	Activated carbon (AC-M) 4.0 wt.% ashes (0.04 wt.% Fe) $S_{BET} = 1019 \, m^2 \, g^{-1}$		1.01
	Graphite (G-S) 0.5 wt.% ashes (0.44 wt.% Fe) $S_{BET} = 12 \, m^2 \, g^{-1}$		0.87
	Activated carbon (AC-P) 1.0 wt.% ashes (0.01 wt.% Fe) $S_{BET} = 931 \, m^2 \, g^{-1}$	Batch experiments [Catalyst] = 2.5 g L^{-1} $[H_2O_2]_0 = 25.0$ g L^{-1}	0.57
	Carbon black (CB-V) 1.0 wt.% ashes (0.00 wt.% Fe) $S_{BET} = 233 \, m^2 \, g^{-1}$	T = 80 °C $pH_{solution} = 3.5$ t = 2 h	0.42
	Graphite (G-F) 0.20 wt.% ashes (0.00 wt.% Fe) $S_{BET} = 7 \, m^2 \, g^{-1}$		0.05
	Carbon black (CB-C) 0.0 wt.% ashes (0.00 wt.% Fe) $S_{BET} = 75 \, m^2 \, g^{-1}$		0.03

the efficiency of CWPO is influenced by distinct properties of the carbon materials, such as metal impurities, surface chemistry, textural and structural features and adsorptive interactions. During the development of a highly efficient and optimized carbon material for CWPO, all these features should be taken into account.

3.1. Metal impurities

The presence of metal impurities in the carbonaceous materials, mainly iron, typically resulting from their origin and synthesis procedures, is expected to increase their catalytic activity. It is thus natural that the ash content has been considered as one of the most important features of carbon materials affecting their activity in CWPO applications [81,88,176,179].

In a work performed with carbon materials with very distinct structural, textural and surface chemical properties, Domínguez et al. [177] have concluded that the presence of metals in the ashes, in particular iron, is the most important factor regarding the catalytic activity observed for each catalyst. Specifically, two activated carbons (AC-M and AC-P), two carbon blacks (CB-C and CB-V) and two graphites (G-S and G-F) were tested in the catalytic decomposition of H_2O_2 at 80 °C and $pH_{solution} = 3.5$. As observed in Table 5, the catalytic activity follows the order: AC-M > G-S > AC-P > CB-V > G-F > CB-C, which may be explained in terms of the specific surface area and Fe content of each carbon material. For instance, the lowest catalytic activity of CB-C is consistent with its lowest specific surface area and absence of Fe on its ashes (cf. Table 5). On the contrary, AC-M possesses the highest amount of ashes and the largest specific surface area. However, the second highest activity shown by G-S, with a very low specific surface area ($12 \, m^2 \, g^{-1}$) but a high Fe content (0.44 wt.%), led the authors to conclude about the prevalence of the Fe content effect over that of the specific surface area [177]. Nevertheless, it should be emphasized that higher H_2O_2 decomposition rates do not necessarily mean higher generation of highly reactive $HO^\bullet$ and higher efficiency of pollutant removal by CWPO. In some cases, H_2O_2 can be decomposed to oxygen via parasitic reactions (cf. Table 4), not resulting in the generation of effective $HO^\bullet$ for CWPO. Therefore, in order to ascertain the exact mechanisms involved, it is necessary to determine the yield of $HO^\bullet$ radicals formed during the catalytic decomposition of H_2O_2 or, better still, to evaluate the degradation of a model pollutant by CWPO in the presence of the catalysts considered.

Our group also demonstrated the synergistic effect that can arise from the presence of very stable metal species in the com-

position of carbon materials, resulting as impurities from their synthesis procedure [103]. In that work, the catalytic activity of commercial carbon nanotubes (CNT, supplied by Arkema Inc., with contents of alumina and iron oxide under 7 wt.% and 5 wt.%, respectively) was compared to the possible effect of homogeneous catalysis promoted by the amount of Fe leached during the CWPO of 2-nitrophenol (2-NP). For that purpose, the influence of the amount of Fe leached to the solution during the performed experiments ($0.02 \, mg \, L^{-1}$) was evaluated using Fe^{3+} as catalyst with the same concentration as in the 2-NP treated solution. This effect, together with pure adsorption and non-catalytic removals, is given in Fig. 2a. As observed, the contributions of homogeneous Fe, pure adsorption and non-catalytic removal are negligible, suggesting that CNT are active heterogeneous catalysts for CWPO. Furthermore, as observed in Fig. 2b, X-ray diffraction (XRD) analysis of the CNT before and after CWPO show that no significant distortion of CNT structure results from their use in the CWPO process. This suggests the presence of highly stable metal species in the composition of these CNT, mainly iron oxides, which may contribute to their high catalytic performance in the CWPO of 2-NP (cf. Fig. 2a).

3.2. Surface chemistry

The availability of active sites at the surface of carbon materials also plays a significant role on their performance as catalysts [180]. Indeed, the catalytic performance of carbon materials has long been linked to their surface chemistry [158,181,182]. Nevertheless, only recent advances on characterization techniques allowed to establish useful relationships between the catalytic performances and the presence of functional groups on the surface of carbon materials [180]. Important conclusions have been obtained by studying carbon materials with very similar structural and textural properties, but with different amounts of surface groups [180]. In general, carbon materials used in catalysis have a graphitic structure and a variety of surface functional groups is formed due to the presence of heteroatoms (such as O, N, H, Cl, S, among others) bonded to the edges of the graphene layers and defects in the carbon materials [180].

Several reviews on characterization techniques and functionalization methods have been published in recent years regarding carbon materials for catalytic applications [155,156,180,183–185]. Therefore, in this Section, we will limit our presentation to some illustrative examples of the influence of key surface chemical features of carbon materials on their performance in CWPO processes.
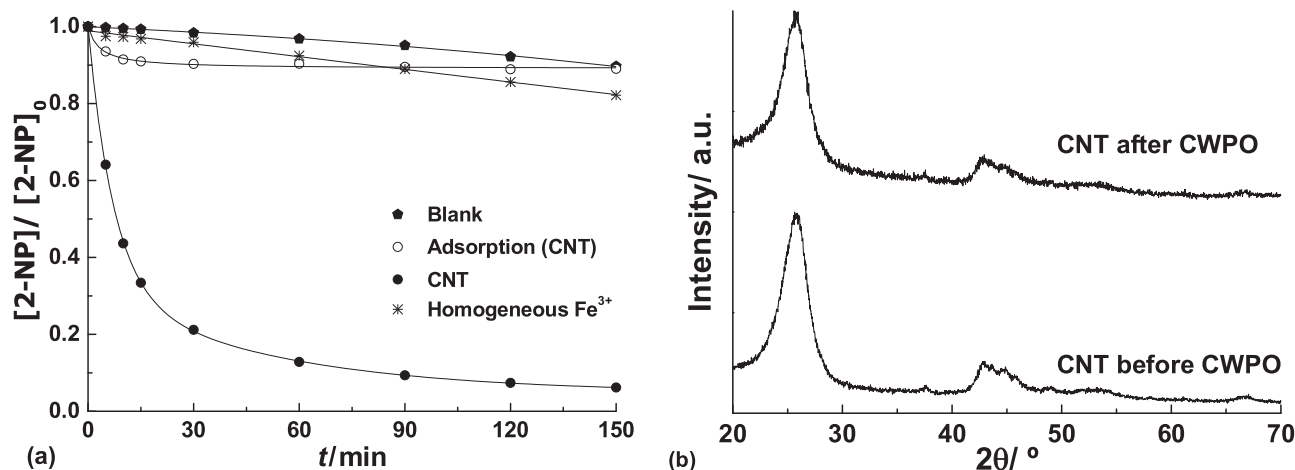
Fig. 2. Study performed with CNT: (a) removal of 2-nitrophenol (2-NP) obtained as a function of time when using CNT (0.1 g L^{-1}), homogeneous Fe^{3+} (0.02 mg L^{-1}) and non-catalytic removal (blank), with [2-NP]$_0$ = 100 mg L^{-1}, T = 50 °C, pH 3 and, in CWPO runs, [H$_2$O$_2$]$_0$ = 1.18 g L^{-1}; (b) XRD spectra of the CNT before and after the CWPO process. Reprinted from [103], Copyright© 2013, with permission from Elsevier [License number: 3761821508483].

3.2.1. Acidic oxygen-containing functionalities

When a carbon catalyst is used in CWPO, HO$^\bullet$ radicals are formed by decomposition of H$_2$O$_2$ with the participation of reducing active sites existing on its surface, as previously described by Eq. (6) (cf. Table 4). For this reaction to take place, an electron must be transferred from the active site to the H$_2$O$_2$ molecule. Acidic oxygen-containing functionalities present at the surface of a carbon material have an electron-withdrawing capacity [6,154], therefore their presence is expected to limit the catalytic performance of these materials in CWPO processes. In addition, the number of available electron rich donating active sites is expected to decrease with the increase of acidic functionalities, since these functional groups are generated in the same active sites by capture of the available unpaired π electrons [154].

The work reported by Soria-Sánchez et al. [59] is an illustrative example of the negative effect of oxygen-containing surface groups on the catalytic performance of carbon materials in CWPO. Five commercial carbon materials were initially considered: multi-walled carbon nanotubes (CNTs-N), carbon nanofibers (CNFs), high surface area graphite (HSAG) and two activated carbons (AC and NORIT). All these carbon materials were further oxidized with nitric acid (using distinct procedures) and their activity in the CWPO of the organic dye C. I. reactive red 241 was compared to that of the pristine materials. The main results obtained in this comparative study are given in Fig. 3, where the oxidized samples are denoted by the prefix "ox/". As observed, the oxidized samples are less active than the pristine samples. This effect is particularly significant in the case of the CNTs, in which it is shown that the catalytic activity largely disappears upon the introduction of acidic oxygen-containing functionalities, as evidenced by pH point of zero charge (PZC) measurements, thermogravimetric analysis performed under He and surface/semi-quantitative (XPS) analysis [59].

The influence of oxygen-containing functionalities has also been studied by our group, using activated carbon xerogels as catalysts for the removal of two azo dyes by CWPO [38]. Three activated carbon xerogels were produced from the same organic resorcinol-formaldehyde xerogel (RFX), upon alkali activation with dry KOH, using successively increasing mass ratios of KOH/RFX (1:1, 2:1 and 4:1, resulting in the materials denoted as ACX-K1, ACX-K2 and ACX-K4, respectively), followed by pyrolysis at 700 °C. The result was a set of activated carbon xerogels with very similar structure and porous texture, but with distinct surface chemical features, as determined by slurry pH measurements, elemental analysis and by Fourier transform infrared spectroscopy (FTIR). The sequence of the

catalytic activity of these activated carbon xerogels is the opposite of their oxygen content. This relationship is clearly visible when the pollutant removals (in the circumstance the dye Chromotrope 2R, C2R) obtained by CWPO are plotted against the oxygen content of the catalysts (Fig. 4), especially at T = 30 °C, where a linear correlation is suggested.

3.2.2. Basic active sites

As recognized in recent comprehensive reviews, the basicity of carbon materials is mainly governed by the presence of some oxygen-containing functionalities (e.g., chromene, pyrone, and quinones) [186–188] and by non-heteroatomic Lewis base sites, characterized by regions of π-electron density on the carbon basal planes [187,189,190]. It should be noted, however, that the extent of contribution of these functionalities and Lewis base sites to the overall basicity of carbon materials has not yet been fully defined [154,191].

Contrarily to the acidic oxygen-containing functionalities, basic groups are electron donating species (i.e., reducing species), which is a necessary condition to promote the decomposition of H$_2$O$_2$ to HO$^\bullet$, through the reaction described by Eq. (6) (cf. Table 4). Therefore, basic functionalities are widely recognized as active sites for the catalytic decomposition of H$_2$O$_2$ during CWPO processes [6,7,91,160,166,171]. Among these, the presence of basic nitrogen-containing groups has been related with increased rates of H$_2$O$_2$ decomposition [178,179].

The positive effect of basic groups on the catalytic performance of carbon materials in CWPO processes was well illustrated by Santos et al. [6]. In this work, three carbon materials were tested in the CWPO of dye solutions, namely a commercial activated carbon (AC$_0$) and two additional materials obtained from it by different functionalization treatments: liquid phase oxidation with nitric acid (AC$_a$) and thermal treatment at 700 °C in H$_2$ atmosphere (AC$_b$). In this way, samples with different surface chemistry were produced (as shown by PZC measurements, temperature-programmed desorption (TPD) analysis and determination of acidic/basic active sites by a titration method) while maintaining the original textural properties as much as possible [6]. The adsorption and CWPO removals of CI reactive red 241 obtained with these three catalysts are shown in Fig. 5. As observed, dye removal decreases when the oxidized sample (AC$_a$) is used in CWPO, in comparison to the pristine sample (AC$_0$). This observation is in agreement with the negative effect of acidic oxygen-containing functionalities addressed in the previous Section. In contrast, the efficiency of
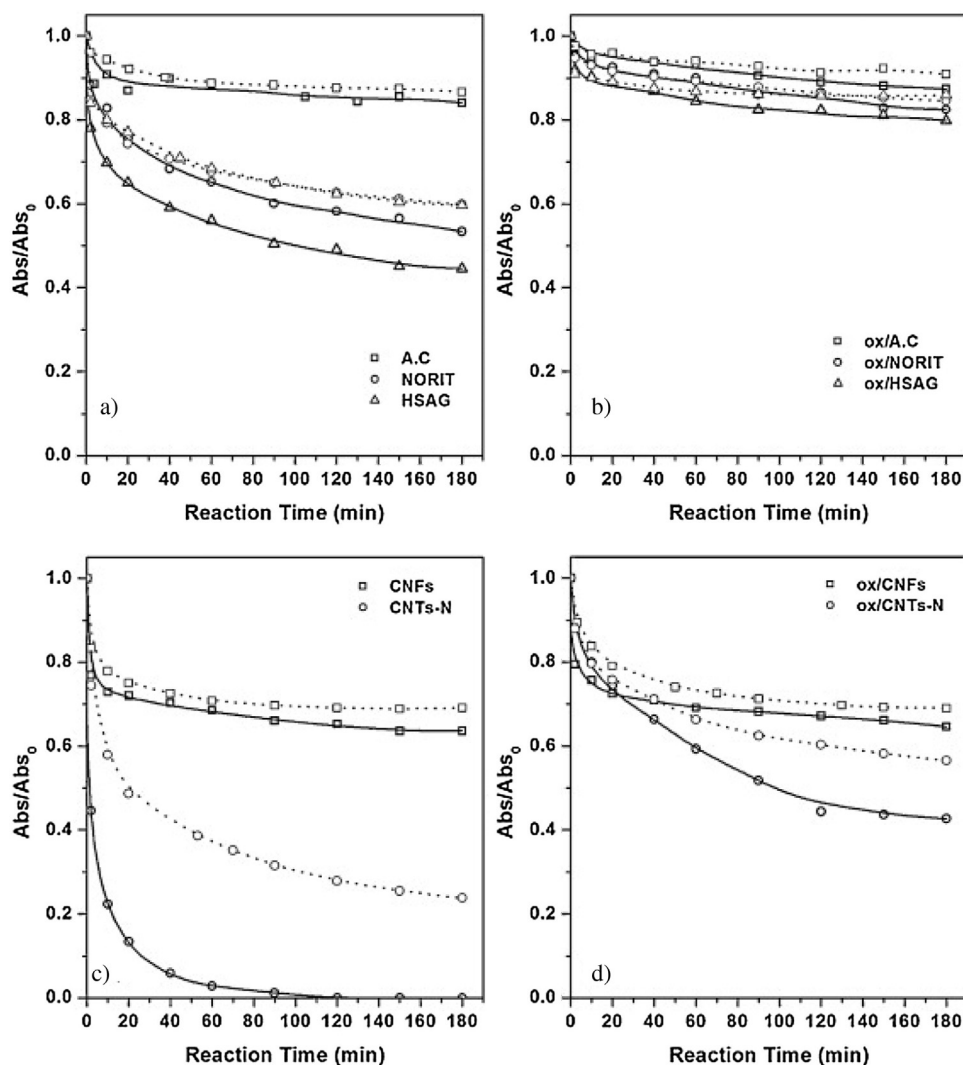
Fig. 3. CWPO (solid lines) and adsorption (dotted lines) removal of C. I. reactive red 241 obtained as a function of time when using different carbon materials: (a) AC, NORIT and HSAG, (b) ox/AC, ox/NORIT and ox/HSAG, (c) CNFs and CNTs and (d) ox/CNFs and ox/CNTs. Experiments performed with [C. I. reactive red 241]$_0$ = 200 mg L^{-1}, [catalyst/adsorbent] = 2.0 g L^{-1}, T = 25 °C, pH 3.5 and, in CWPO runs, [H$_2$O$_2$]$_0$ = 34.0 g L^{-1}. Reprinted from [59], Copyright© 2012, with permission from Elsevier [License number: 3761870125753].

the CWPO process increases when the sample subjected to thermal reduction (AC$_b$) is used as catalyst. This effect was ascribed to the increased amount of free electrons on the graphene basal planes of activated carbon (corresponding to Lewis basicity) [6].

Further insights on the influence of basic active sites at the surface of carbon materials have also been given by our group, in another work carried out with the objective of quantifying the HO$^\bullet$ radicals formed during the catalytic H$_2$O$_2$ decomposition process [160]. Three activated carbons with different chemical properties were tested, as characterized by PZC measurements, TPD analysis and determination of acidic/basic active sites determination by a titration method. In order to maintain, as much as possible, similar structural properties between the catalysts, two samples were prepared from the same commercial activated carbon (AC), one by liquid phase oxidation of AC with sulphuric acid (ACS), and the other (ACNUT) by a series of successive treatments: liquid phase oxidation of AC with nitric acid, followed by hydrothermal treatment with urea at 200 °C and thermal treatment at 800 °C under N$_2$ atmosphere. When the yield of HO$^\bullet$ formed during the H$_2$O$_2$ decomposition process (Y$_{HO^\bullet}$) is plotted against the amount of basic active sites at the surface of the carbon materials used in this work

(cf. Fig. 6), a linear relationship is suggested [160]. This further highlights the positive effect of basic groups on the CWPO processes.
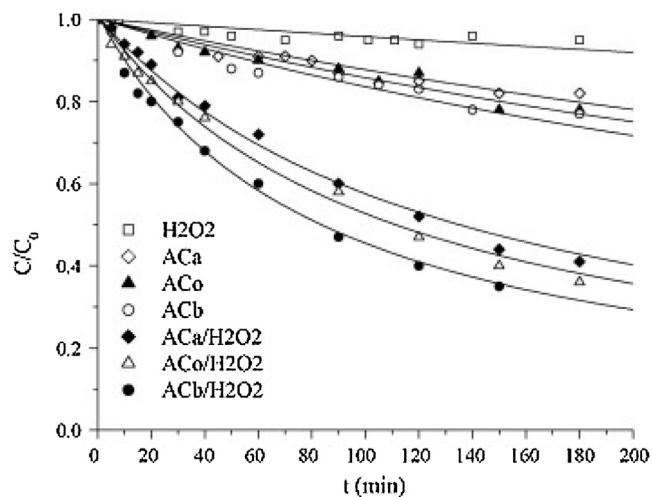
3.2.3. Sulphur-containing functionalities

The presence of sulphur-containing functionalities at the surface of carbon materials has also been related with enhanced performances of the CWPO process in the work of Gomes et al. [46], in which four different activated carbon samples with varying surface chemistry and increased acidic character were used in the CWPO of C2R. The materials were prepared by liquid phase treatments of a commercial sample (AC), namely with H$_2$O$_2$ (ACHP), sulphuric acid (ACSA) and nitric acid (ACNA). The results obtained in pure adsorption and in CWPO runs are shown in Fig. 7a and b. As expected, in general, the catalytic performance of the catalysts was found to be inversely proportional to their acidic character (cf. Fig. 7b). Nevertheless, the removal of C2R obtained with the ACSA sample falls out of this correlation [46]. This was explained in terms of the introduction of sulphur-containing groups on the carbon surface: on one hand, the hydrophilic character of sulphur-containing functionalities enables a more intimate contact between the aqueous solution and the surface of ACSA, increasing the adsorption of C2R and H$_2$O$_2$ molecules – essential steps for further reaction of
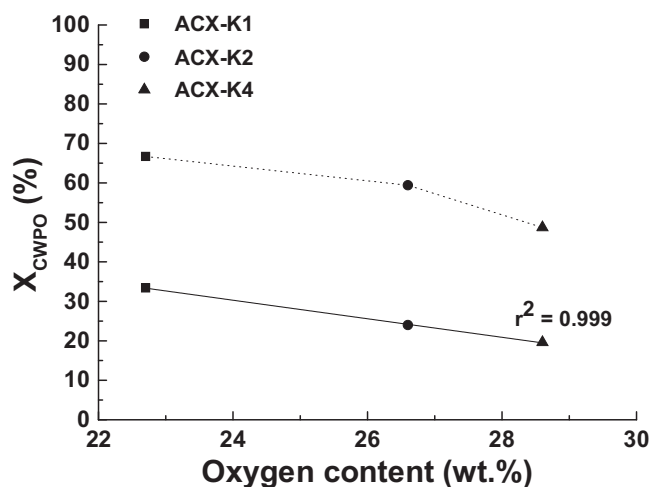
Fig. 4. Removal of Chromotrope 2R by CWPO obtained after 150 min (X_{CWPO}, after subtracting the adsorption removals) vs. oxygen content of the activated carbon xerogel catalysts. Experiments performed with $[Chromotrope\ 2R]_0 = 100\,mg\,L^{-1}$, $[catalyst/adsorbent] = 0.1\,g\,L^{-1}$, T = 50 °C (dotted line) and T = 30 °C (solid line), pH 3 and $[H_2O_2]_0 = 1.18\,g\,L^{-1}$.
Data from [38].

Fig. 6. Yield of HO• obtained in the H_2O_2 decomposition ($Y_{HO•}$) after 150 min of reaction with the pristine activated carbon (AC) and with the modified activated carbons ACS and ACNUT vs. the amount of basic active sites. Experiments performed with $[catalyst] = 0.1\,g\,L^{-1}$, T = 50 °C, pH 3 and $[H_2O_2]_0 = 1.18\,g\,L^{-1}$. Points represent experimental data, while line represents the linear fitting ($r^2 = 0.97$). Reprinted from [160], Copyright© 2013, with permission from Elsevier [License number: 3761870884392].

Fig. 5. Removal of C. I. reactive red 241 (initial concentration = $50\,mg\,L^{-1}$) by adsorption (ACx) and CWPO (ACx/H_2O_2) obtained as a function of time when using different activated carbon materials ($2.2\,g\,L^{-1}$). Experiments performed at room temperature, pH 3 and, in CWPO runs, $[H_2O_2]_0 = 51.0\,g\,L^{-1}$. Non-catalytic removal (blank) is also given for comparison. Reprinted from [6], Copyright© 2008, with permission from Elsevier [License number: 3761870653269].

the pollutant molecules with HO• formed at the catalyst surface from the decomposition of H_2O_2; on the other hand, increased rates of HO• formation in the vicinity of the pollutant were ascribed to the presence of thiol groups on the surface of ACSA – which, as described in Eq. (21), may react with H_2O_2 with formation of HO• [46]. Although based on the different pollutant removals obtained, the enhanced production of HO• claimed by the authors was not sustained by any direct or indirect measurement – a question that should be addressed in future works proposing new mechanisms for the catalytic decomposition of H_2O_2.

$$H_2O_2 + SH \rightleftarrows OH^- + HO• + SH^+ \qquad (21)$$
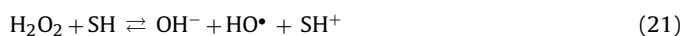
Gomes et al. [47] have further explored the influence of sulphur-containing functionalities, leading to additional insights on the reaction mechanisms involved in CWPO using activated carbons treated with sulphuric acid. The influence of sulphur-containing

functionalities on the catalytic decomposition of H_2O_2 was also recently addressed by our group [160]. Five samples were prepared from the same commercial activated carbon (AC) and then used as catalysts for the decomposition of H_2O_2: the first sample resulted from the liquid phase oxidation of AC with sulphuric acid (ACS), while the others were prepared by a series of successive treatments, namely liquid phase oxidation of AC with nitric acid (ACN), followed by hydrothermal treatment of ACN with urea at 200 °C (ACNU) and a final thermal treatment of ACNU at 800 °C under N_2 atmosphere (ACNUT). When the apparent H_2O_2 global decomposition rate constant (k_d) is plotted against the amount of acidic active sites of the catalysts (cf. Fig. 8), the deviant behaviour of ACS becomes evident. This was ascribed to the role of sulphur-containing groups in the catalytic decomposition of H_2O_2, as previously discussed. In addition, it was remarked that the acidic functionalities present at carbon surfaces cannot be analysed only in terms of quantity, but also by their quality [160]; while acidic oxygen-containing functional groups are known to influence negatively the CWPO process, the presence of acidic sulphur-containing functionalities were found to have a positive effect.

### 3.3. Textural and structural features

Any carbon material suitable for catalysis must present adequate textural properties, in order to guarantee that diffusion limitations and deactivation phenomena are minimized [155,192]. Nowadays, it is recognized that the activity of a catalyst is mainly determined by the nature, concentration and accessibility of its active sites, and only under particular conditions this is proportional to the specific surface area [180]. Nevertheless, linear correlations are obtained in several cases, especially when catalysts with different specific surface area are prepared from the same precursor material (thus ensuring that the intrinsic site activity is the same for each catalyst) [180]. Indeed, it has been shown in several works that textural and structural properties of carbon materials should also be taken into account when developing catalysts for application in CWPO processes, in addition to their metal impurities and surface chemical features [91,104,107,166,171,177]. Some illustrative examples of these correlations will be given in this Section.
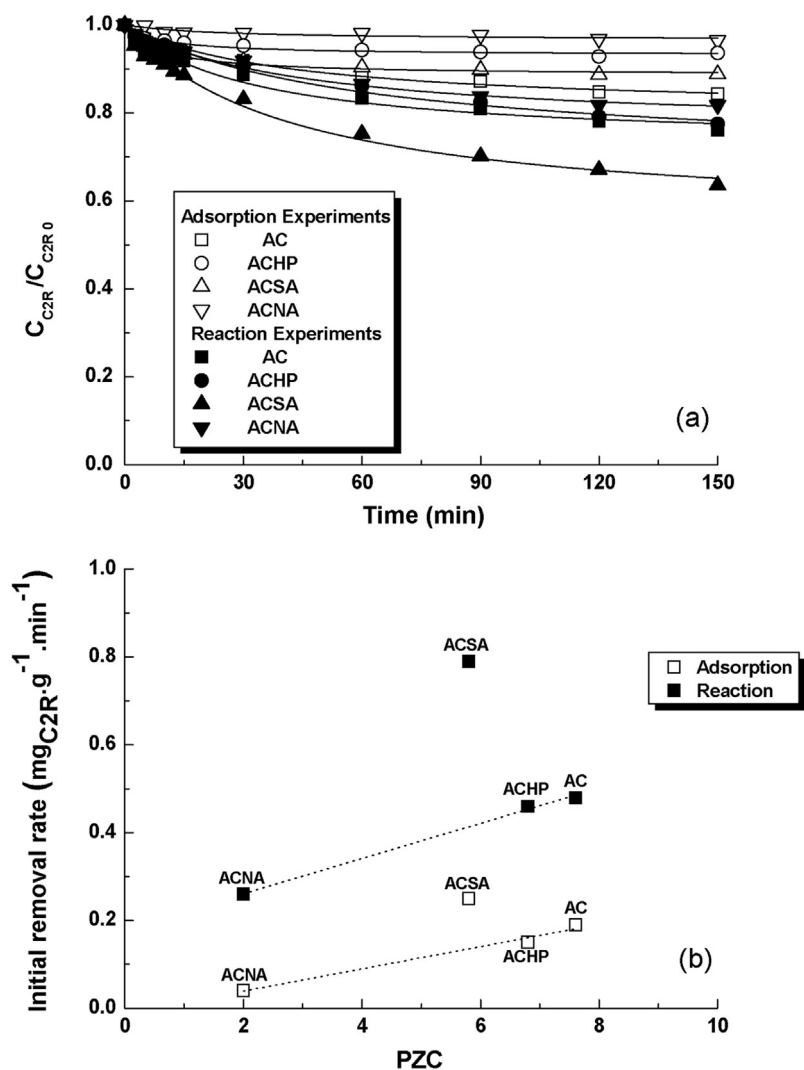
Fig. 7. Chromotrope 2R removal in adsorption and CWPO experiments: (a) concentration decay curves and (b) initial removal rates, as function of the PZC (pH at the point of zero charge) of the different activated carbon materials. Experiments performed with [Chromotrope 2R]$_0$ = 100 mg L^{-1}, [catalyst/adsorbent] = 0.5 g L^{-1}, T = 50 °C, pH 3 and [H$_2$O$_2$]$_0$ = 1.18 g L^{-1}. Reprinted from [46], Copyright© 2010, with permission from Elsevier [License number: 3761871081226].

### 3.3.1. Surface area and porosity

Most heterogeneous catalysts are porous solids [192], their texture being mainly determined by the preparation method [192–195]. Since the catalytic reaction occurs (or is initiated) on the surface of the catalyst, its area is expected to strongly affect the catalytic activity [192]. In addition, the reactants must diffuse through the porous system in order to reach the active sites and then, after reaction, the products have to leave the catalyst [192]. Therefore, the textural and morphological parameters of carbon materials should also be taken into account to fully understand their performance in CWPO. Indeed, the surface available and the extent of porosity are expected to play an important role in the case of catalytic H$_2$O$_2$ decomposition [166]. For instance, the catalytic active sites will be widely distributed on carbons with a relatively high specific surface area, in such a way that H$_2$O$_2$ decomposition is enhanced, whereas inhibiting phenomena may prevail on densely distributed active sites [166]. In this context, 2D graphene-based materials can be a promising alternative to porous carbon materials, since their highly accessible specific surface area is expected to provide a perfect environment for higher turnover rates [196]. Nevertheless, in order to discriminate the effect of textural and morphological parameters of carbon materials on their catalytic performance, it must be ensured that the intrinsic activity of the
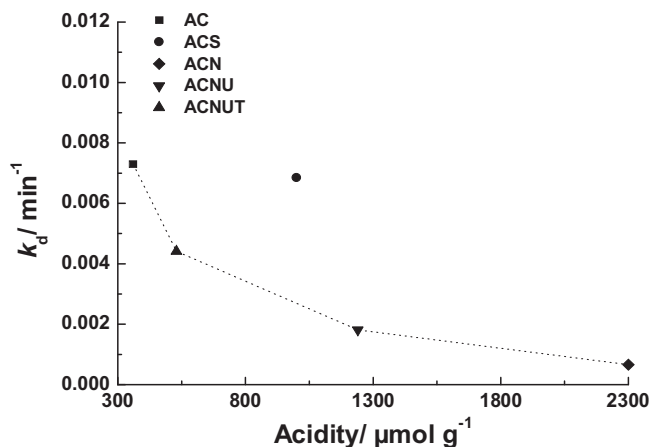
Fig. 8. Apparent H$_2$O$_2$ global decomposition rate constants (k$_d$) obtained after 150 min of reaction with the pristine AC and with the modified activated carbons ACS, ACN, ACNU and ACNUT vs. the amount of acidic active sites. Experiments performed with [catalyst] = 0.1 g L^{-1}, T = 50 °C, pH 3 and [H$_2$O$_2$]$_0$ = 1.18 g L^{-1}. Reprinted from [160], Copyright© 2013, with permission from Elsevier [License number: 3761880098821].
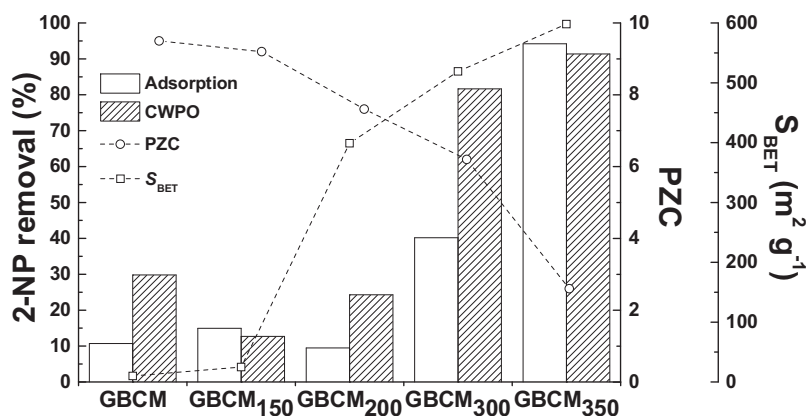
Fig. 9. 2-Nitrophenol removal obtained after 4 h in adsorption and CWPO runs (bars/left axis), as a function of the PZC (pH at the point of zero charge, circles/right axis) and specific surface area (S_{BET}, squares/right axis) of the different carbon materials produced from glycerol. Experiments performed with $[2-NP]_0 = 100\,mg\,L^{-1}$, [catalyst/adsorbent] $= 1.0\,g\,L^{-1}$, T $= 50\,°C$, pH 3 and, in CWPO runs, $[H_2O_2]_0 = 1.78\,g\,L^{-1}$.
Adapted from [104].
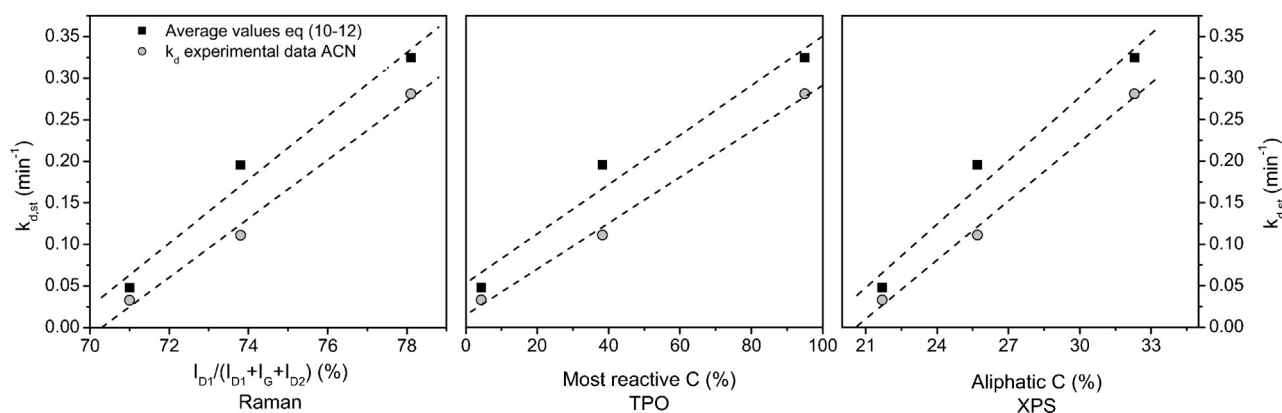
Fig. 10. Apparent global H_2O_2 decomposition rate constants (k_d) vs. Raman (left), TPO (middle) and XPS (right) parameters related with the structural ordering of the activated carbons considered. Squares represent kinetic values obtained based on empirical equations, considering activated carbons without oxygen-containing surface groups; circles represent experimental values. Experiments performed with [catalyst] $= 0.5\,g\,L^{-1}$, T $= 50\,°C$, pH 3 and $[H_2O_2]_0 = 0.50\,g\,L^{-1}$. Reprinted from [171], Copyright© 2011, with permission from Elsevier [License number: 3761880337816].

surface of each catalyst is the same, which is a complex process that only occurs under very particular conditions [180].

Lücking et al. [91] (refer to Section 2.3 for details) highlighted the granular structure and high specific surface area of activated carbons as advantages of these materials when used as CWPO catalysts in fixed bed reactors, their long-term stability being confirmed by continuous experiments.

Domínguez et al. [177] (refer to Section 3.1 for details) have concluded that the most important factor determining the catalytic activity of a wide range of carbon materials is their content in metals, followed by their specific surface area.

The interplay between chemical and textural properties has also been addressed by our group in a work dealing with the application of carbon materials produced from glycerol (GBCM—glycerol-based carbon materials) in the CWPO of 2-NP [104]. GBCM was prepared by partial carbonization of glycerol, followed by calcination under N_2 atmosphere at 800 °C for 4 h. GBCM was further activated under oxidative atmosphere (air) during 60 min at different temperatures, in the range 150–350 °C, in order to produce several other materials, labelled as GBCM followed by a subscript number corresponding to the activation temperature in °C (i.e., GBCM$_{150}$, GBCM$_{200}$, GBCM$_{300}$ and GBCM$_{350}$). As observed in Fig. 9, the best catalytic performance is obtained with GBCM$_{300}$ (although the global pollutant removal with GBCM$_{350}$ is higher than that observed with GBCM$_{300}$, this removal was mainly attributed to

adsorption on the surface of the material). The higher catalytic activity of GBCM$_{300}$ was ascribed to a combination of properties: the adequate development of porosity, enabling the adsorption of the organic pollutant on its surface, and a basicity of 400 µmol g^{-1} (almost twice higher than that of GBCM$_{350}$), which combined with lower oxygen content led to higher activity for the decomposition of H_2O_2 molecules in close proximity with adsorbed 2-NP molecules. Materials activated at lower temperatures have an important basic character (basicity > 450 µmol g^{-1}), with a low oxygen content (< 3.2%), but also a very poor porous structure, while the material activated at the highest temperature (350 °C) has a significant porosity, but a very high oxygen content (8.6%) combined with a low basicity (250 µmol g^{-1}). Therefore, a balance between the textural and chemical properties is crucial in the synthesis of highly active catalysts for CWPO [104].

3.3.2. Structural defects

Two distinct types of sites can be found in perfect graphene layers of carbon materials: (i) the basal plane sites, which are associated with the sp^2-hybridized aromatic carbon atoms forming the surface of the basal planes (i.e., within the graphene sheet) and (ii) the edge sites, which are the terminal sites of graphene layers [154,197]. The latter are usually considered more electrochemically active than the former, due to the presence of higher amounts of delocalized unpaired π electrons [154,197].

Structural defects may have been traditionally seen as imperfections in materials that could significantly decrease their performance [198]. However, at the nanoscale, defects can be extremely useful since they may be exploited to generate novel materials and applications [198]. In the particular case of CWPO, the presence of defects in the structure of carbon materials has also been addressed and related with increased process efficiency, both when macroscale [171] and nanoscale carbon materials [107] are used as catalysts.

The influence of the structural characteristics of activated carbons on their efficiency in the catalytic decomposition of H_2O_2 was first reported by Rey et al. [171], in a work studying three different activated carbons (CM, CN and CC) before and after different modifications (hydrochloric acid lixiviation, oxidation with nitric acid and heat treatment under N_2 atmosphere). Based on screening results performed with the pristine and with the modified activated carbons, the authors have concluded that oxygen-containing surface groups partially explained the results obtained, but some other important feature should also be playing a significant role [171]. Bearing this in mind, the authors further explored the carbon materials treated with N_2, where most of the oxygen-containing functionalities had been removed. An astonishing breakthrough was made when the apparent global H_2O_2 decomposition rate constant (k_d) was plotted against parameters related with the structural ordering of the activated carbons, obtained by Raman, temperature-programmed oxidation (TPO) and X-ray photoelectron spectroscopy (XPS). As observed in Fig. 10, higher k_d values were found for the most disordered activated carbons. This effect was ascribed to the increased surface density of electron-rich regions, which could act as active sites for the decomposition of H_2O_2 according to an electron-transfer mechanism [171]. In addition, the authors have concluded that micropore entrances could also be regions with more sites of this type [171].

Similar results were found in a very recent work performed in our group, dealing with the synthesis and application of graphene-based materials in the CWPO of 4-nitrophenol solutions with relatively high concentration (5 g L^{-1}) [107]. Graphene-based materials were reported as active and stable catalysts for CWPO processes for the first time and the amount of defects in the structure of reduced graphene oxides (inferred through Raman spectroscopy) was related with enhanced H_2O_2 decomposition. Although not directly supported by quantification of the HO$^\bullet$ formed during the process, this effect was ascribed to the confinement of electron-rich regions caused by structural defects, leading to an increased electron density at those regions, which act as active sites for the catalytic decomposition of H_2O_2, increasing the formation of HO$^\bullet$ [107], as depicted in Fig. 11.

3.4. Adsorptive interactions

The adsorption of organic molecules on carbon materials depends on the adsorbent texture (surface area and pore size), surface chemistry (functional groups) and ash content [193,199,200], and on the adsorbate (molecular weight, polarity, pK_a, molecular size and functional groups) and solution properties (pH, adsorbate concentration and the presence of other possible adsorbates) [200–203]. Two distinct types of interactions may occur between the adsorbate and the adsorbent [200,204,205]: (i) electrostatic interactions, when the adsorbate is dissociated under the experimental conditions used, and (ii) dispersive interactions, with the π–π dispersion interaction mechanism being the most widely accepted [204–206]. Usually, dispersive interactions are predominant when the pollutant is in the molecular form, while electrostatic interactions are more significant when the pollutant is ionized (normally when the solution pH is very high or very low) [200,207]. Therefore, the surface chemistry and the solu-
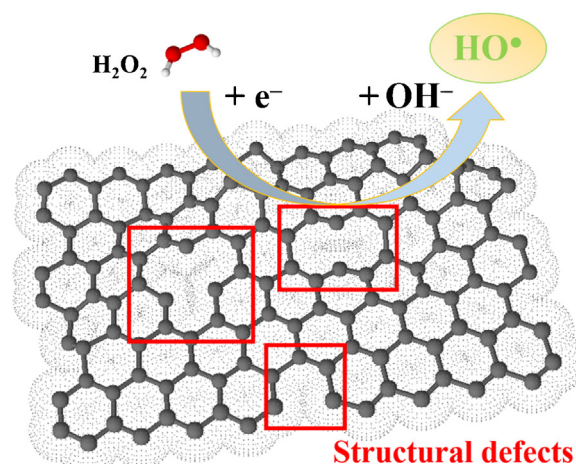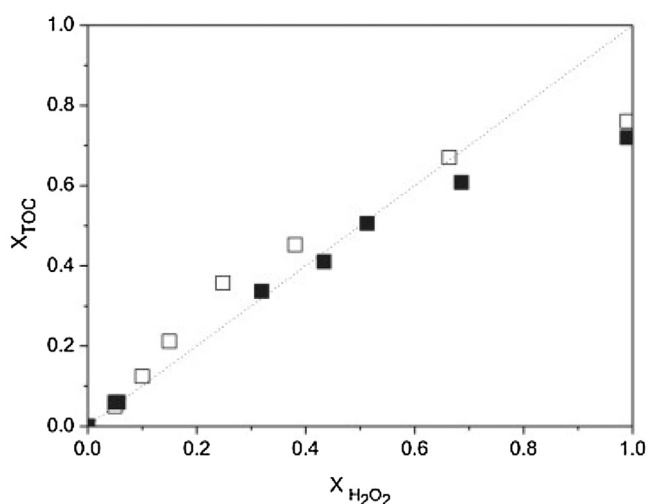

Fig. 11. Representation of electron-rich regions caused by structural defects existing in reduced graphene oxide sheets, which act as active sites for the formation of HO$^\bullet$. Adapted from [107].

tion pH may be considered the most important factors controlling the adsorption process [208]. In the particular case of CWPO, competition phenomena between H_2O_2 and pollutant molecules for reaction with HO$^\bullet$ has been reported by several authors [7,41,47,61]. Recent findings lead to conclude that the efficiency of the CWPO process increases with increasing pollutant concentration adsorbed nearby the sites were HO$^\bullet$ are generated, since in this way non-efficient parasitic reactions between H_2O_2 and HO$^\bullet$ are inhibited [72,104,107].

Domínguez et al. [72] explained the inhibition of parasitic scavenging reactions on the surface of carbon catalysts based on the assumption that a significant coverage of the carbon surface by the pollutant molecules should decrease the rate of HO$^\bullet$ formation from H_2O_2 decomposition and, at the same time, that would make the pollutant more easily available for reaction with HO$^\bullet$. Bearing this in mind, the authors anticipated that the selectivity towards pollutant oxidation and mineralization would be enhanced, in detriment of the scavenging reactions [72]. The demonstration was done by carrying out CWPO experiments with phenol at a relatively high concentration (5 g L^{-1}) and a pollutant/catalyst mass ratio of 2. Two commercial activated carbons (AC-M and AC-P) were used as catalysts and unprecedented H_2O_2 consumption efficiencies close to 100% were achieved, as concluded when total organic carbon (TOC) removals were plotted against H_2O_2 decomposition (cf. Fig. 12). As observed, 100% H_2O_2 consumption efficiency ($X_{TOC} = X_{H2O2}$) is maintained in the case of AC-M up to H_2O_2 decomposition around 65%, corresponding to 24 h of reaction [72].

We have reached similar conclusions in the work carried out with graphene-based materials (described in Section 3.3.2) [107]. As previously discussed, H_2O_2 decomposition increases with higher amounts of structural defects. However, this does not necessarily lead to higher efficiency of the CWPO processes. In a comparison performed with three reduced graphene oxide (rGO) samples (rGOG, rGOH and rGOV, obtained by reduction of graphene oxide with glucose, hydrazine and vitamin C, respectively), it has been observed that the efficiency of H_2O_2 consumption, measured in terms of total organic carbon (TOC) removal per amount of H_2O_2 decomposed (η_{H2O2}), follows the same sequence as 4-nitrophenol adsorption on the surface of the rGO samples (cf. Fig. 13), instead of the H_2O_2 decomposition sequence. The authors concluded that the balance between a more controlled catalytic decomposition of H_2O_2, together with higher pollutant concentration nearby the formed HO$^\bullet$, leads to the highest efficiency of the CWPO process [107]. In addition, these observations suggest that n_{H2O2} is favoured
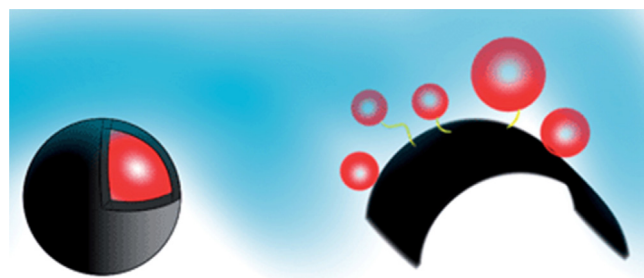
Fig. 12 graph region

Fig. 14. Representation of the two general classes of nanostructured hybrid magnetic carbon materials: carbon encapsulated magnetic nanoparticles (left) and carbon nanostructures decorated with magnetic nanoparticles (right). Carbon material is shown in black, whereas magnetic particles are represented by red spheres; yellow chains correspond to optional molecular linkers. Reprinted from [209], Copyright© 2012, with permission from The Royal Society of Chemistry [License number: 3761881181315]. (For interpretation of the references to color in this figure legend, the reader is referred to the web version of this article.)

Fig. 12. Total organic carbon (TOC) vs. H_2O_2 conversions obtained when using (□) AC-M and (■) AC-P. Experiments performed with $[phenol]_0 = 5.0\,g\,L^{-1}$, $[catalyst] = 2.5\,g\,L^{-1}$, T = 80 °C, pH 3.5 and $[H_2O_2]_0 = 25.0\,g\,L^{-1}$. Reprinted from [72], Copyright© 2013, with permission from Elsevier [License number: 3761880832616].
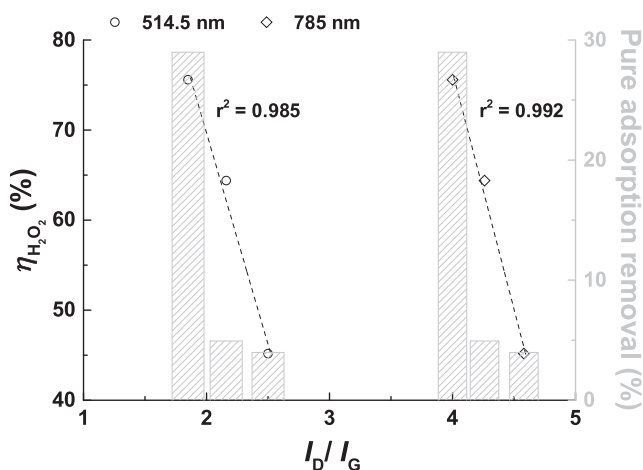
Fig. 13. Total organic carbon (TOC) removal per amount of H_2O_2 decomposed ($\eta_{H_2O_2}$, circles and squares/left axis) and removal of 4-nitrophenol by pure adsorption (bars/right axis) vs. intensity ratios of the D bands relative to the G mode (I_D/I_G) for the rGO samples, obtained by Raman spectroscopy. Points represent experimental data, while lines represents the linear fittings. Experiments performed with $[4\text{-nitrophenol}]_0 = 5.0\,g\,L^{-1}$, $[catalyst/adsorbent] = 2.5\,g\,L^{-1}$, T = 50 °C, pH 3.0 and, in CWPO runs, $[H_2O_2]_0 = 17.8\,g\,L^{-1}$.
Adapted from [107].

by higher pollutant concentrations at the surface of the catalysts, which was ascribed to a more efficient use of the HO• formed near to the adsorbed molecules [107].

Despite all the significant improvements that have been made, especially in recent years, carbon materials, when used as catalysts on their own, still show lower performances in CWPO in comparison with metal-based catalysts [39,41,81,83,129,170]. At the same time, carbon materials with metals within their structure, arising from synthesis precursors and procedures, have been shown to be active and stable catalysts in CWPO, revealing low leaching levels [65,91,103,122]. Other authors have also suggested the preparation of carbon materials with iron within the carbonaceous structure, as suitable catalysts for CWPO with limited Fe leaching [25]. Bearing this in mind, the synthesis of highly stable carbon-based nanostructured composites (resistant to leaching phenomena) containing metallic nanomaterials (e.g. iron, cobalt, nickel and their alloys, and/or ferrite), may be considered the next

step in the evolution of catalysts for CWPO. In this way, the possible synergistic effects that can arise from the combination of the high catalytic activity of iron or other metal species with the proven catalytic properties of carbon-based materials in CWPO could be explored, but always assessing catalyst stability simultaneously. The magnetic properties of these nanostructured materials would be an additional advantage to the process, enabling in situ magnetic separation—thus avoiding typical systems for separation of the homogeneous, or even of the non-magnetic heterogeneous powders used as catalysts in CWPO. This trend (cf. Fig. 1) is suggested by the increasing number of publications regarding the use of hybrid magnetic carbon nanocomposites in CWPO processes: 1 work in 2011 [123], 4 works in 2012 and 2013 [22,37,54,124] and 9 works in 2014 [14,15,29–31,52,94,101,109]. In 2015, 8 works have been published up to the end of November [9,10,12,13,27,93,99,127].

4. Application of nanostructured hybrid magnetic carbon materials in the catalytic wet peroxide oxidation of organic pollutants

Hybrid magnetic carbon materials are composed of carbon nanostructures (mainly sp^2-hybridized aromatic carbon atoms) of various dimensionalities (e.g., 0D fullerene, 1D carbon nanotubes and 2D graphene sheets) and magnetic nanoparticles [209]. As shown in Fig. 14, two general classes of these hybrid materials are usually considered: (i) carbon encapsulated magnetic nanoparticles, which are core-shell structures with a carbonaceous shell and a core made of magnetic materials, and (ii) carbon nanostructures decorated with magnetic nanoparticles, in which the magnetic material is embedded or linked to the carbon structure, without being protected against the environment by a carbonaceous shell [209].

Several techniques for the synthesis of carbon-based nanostructured composites containing magnetic nanomaterials have been explored and improved in recent years [209,210], as described in a recent review [210] and summarized in Fig. 15. Methods such as (i) filling process, (ii) template-based synthesis, (iii) chemical vapour deposition, (iv) hydrothermal/solvothermal method, (v) pyrolysis procedure, (vi) sol-gel process, (vii) detonation induced reaction and (viii) self-assembly method, have led to considerable progress and unprecedented prospects for the use of these type of materials in several applications. In particular, these developments opened a window of opportunity, not only for the investigation of their catalytic properties in CWPO, but also for the development of in-situ magnetic separation systems. Thus, the works dealing with
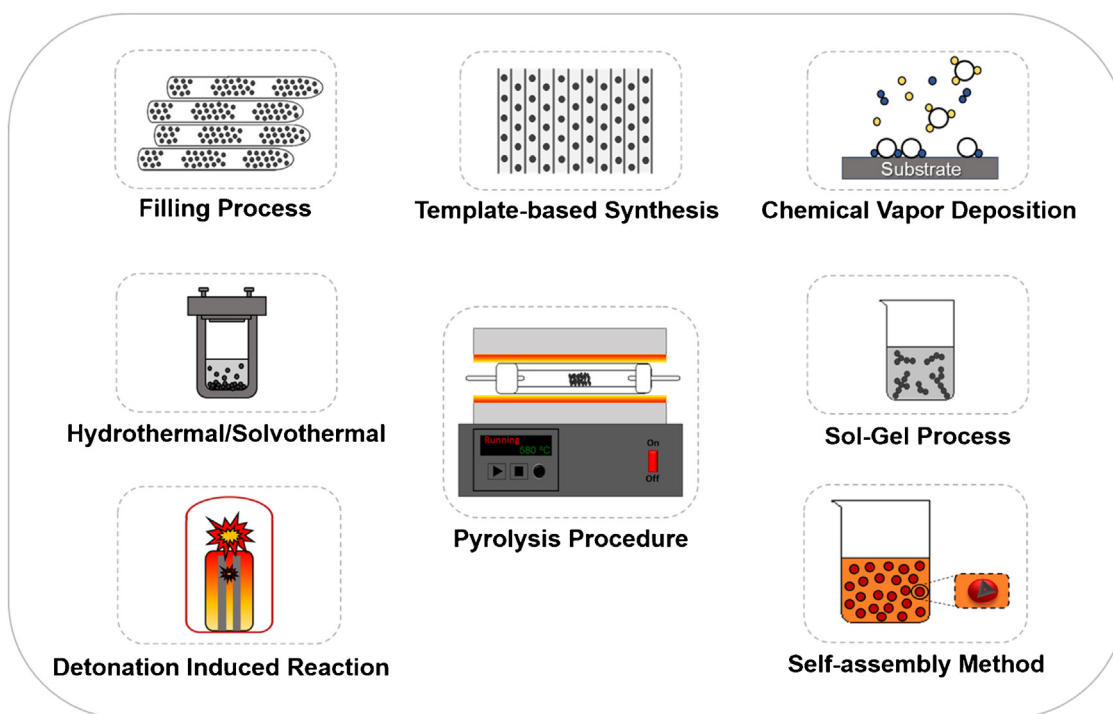
Fig. 15. Main synthesis techniques used for the preparation of hybrid magnetic carbon nanocomposites.

the application of hybrid magnetic carbon materials in CWPO are thoroughly reviewed in the following Sections.

4.1. Carbon nanostructures decorated with magnetic nanoparticles

Several hybrid magnetic composites in which the magnetic material is embedded in the carbon structure have been reported as highly active, efficient and stable catalysts for CWPO applications. Since these hybrid materials can exhibit very distinct textural, structural and surface chemical properties, the literature review performed in this Section is organized according to the carbon material used in the synthesis of the nanostructured composites.

4.1.1. Multiwalled carbon nanotubes

The possible synergistic effects that have been claimed regarding the application of hybrid magnetic carbon materials in CWPO were evidenced in the work performed by Hu et al. in 2011 [123], which, to the best of our knowledge, first reported the application of this kind of nanostructured composites in CWPO processes. The high catalytic activity of magnetite (Fe_3O_4) for the CWPO of 17α-methyltestosterone was increased when this magnetic material was grown on multiwalled carbon nanotubes (MWCNT), resulting in the material named Fe_3O_4/MWCNT, as detailed in Table 6. The performance of Fe_3O_4/MWCNT at 20 °C and $pH_{solution} = 5$ (85.9% pollutant removal) was enhanced when compared to the sum of the removals obtained with Fe_3O_4 (62.0%) and MWCNT (11.0%) on their own (+12.9%, cf. Fig. 16 and Table 6), and it was ascribed to the enrichment of pollutant molecules in the vicinity of the active sites due to adsorptive interactions on the surface of the carbon material [123], which is in line with the findings reported in Section 3.4. The authors claimed that the organic molecules are first adsorbed on the surface of the catalyst and then attacked by HO•, while the Fe species are regenerated directly on the catalyst without significant diffusion into the solution [123]. As also observed in Fig. 16, the decomposition of H_2O_2 is lower when applying the Fe_3O_4/MWCNT catalyst, suggesting that the effi-

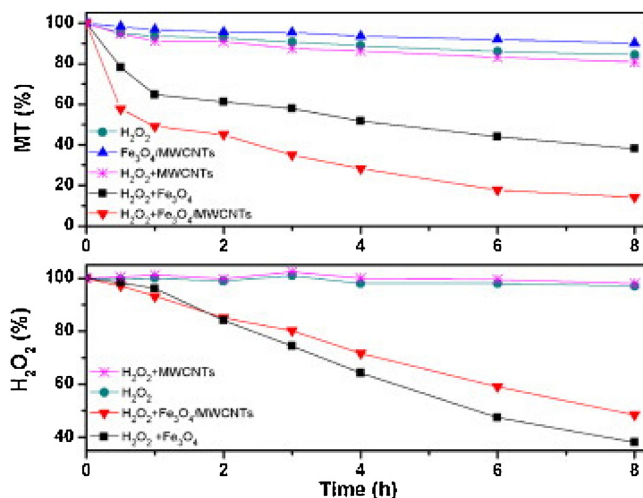**Fig. 16.** 17α-Methyltestosterone (MT) concentration decay (above) and decomposition of H_2O_2 (bellow), under different conditions. Experiments performed with $[MT]_0 = 0.21\,mg\,L^{-1}$, $[H_2O_2]_0 = 0.18\,g\,L^{-1}$, $[Fe_3O_4] = 2.0\,g\,L^{-1}$, $[Fe_3O_4/MWCNT] = 2.0\,g\,L^{-1}$, $[MWCNT] = 0.02\,g\,L^{-1}$, T = 50 °C and pH 5. Reprinted from [123], Copyright© 2011, with permission from Elsevier [License number: 3761890203877].

ciency of H_2O_2 consumption is also increased when compared to that obtained with Fe_3O_4. In addition, the participation of Fe_3O_4 at the surface of the hybrid material in the CWPO process was proven by the authors, since Fe^{2+} in the outermost layer was partially oxidized to Fe^{3+} during the reaction, as corroborated by XPS analysis of the Fe_3O_4/MWCNT catalyst before and after the CWPO process. Specifically, Fe^{3+} and Fe^{2+} contribute with 68.3 wt.% and 31.7 wt.% of the total Fe atoms (corresponding to the Fe_3O_4 crystal structure) on the surface of the fresh catalyst, respectively, whereas the contribution of Fe^{2+} decreased to 13.3 wt.% in the catalyst after reaction [123]. Finally, the authors concluded that the novel hybrid magnetic carbon catalyst would be of potential application in CWPO due to

Table 6

Summary on the use of multiwalled carbon nanotubes decorated with magnetic nanoparticles in CWPO: description of the catalyst, operating conditions and catalytic performance of each catalyst (pollutant removal and Fe leached to the treated waters).

| Authors	Catalyst	Operating conditions	Pollutant	H_2O_2 stoichiometric ratio[a]	Pollutant removal	$[Fe]_{leaching}$ (mg L^{-1})
Hu et al. [123]	Multiwalled carbon nanotubes (1 wt.%) decorated with Fe_3O_4 nanoparticles (Fe_3O_4/MWCNT), prepared by in situ growth of Fe_3O_4 nanoparticles on modified MWCNT surface (sulphuric acid/nitric acid treatment), by chemical oxidation of Fe^{2+}, followed by co-precipitation at 95 °C under N_2 atmosphere	Batch experiments [Catalyst] = 2.0 g L^{-1} $[H_2O_2]_0$ = 0.18 g L^{-1} T = 20 °C $pH_{solution}$ = 5 t = 8 h	17α-Methyltestosterone (0.212 mg L^{-1})	143	85.9% (0.011 mg g^{-1} h^{-1}) 79.4% (in the 7th consecutive reuse)	0.59[b]
	Fe_3O_4 nanoparticles, prepared as described above, but without adding MWCNT MWCNT, supplied by Alpha Nano Technology	[MWCNT] = 0.020 g L^{-1} (corresponding to the 1 wt.% of MWCNT)			62.0% (0.008 mg g^{-1} h^{-1}) 11.0% (0.001 mg g^{-1} h^{-1})	Not addressed Not addressed
	Fe^{3+} (origin not addressed)	$[Fe^{3+}]$ = 0.001 g L^{-1}			35.6% (9.43 mg g^{-1} h^{-1})	Not addressed
Hu et al. [124]	Multiwalled carbon nanotubes decorated with Fe_3O_4 nanoparticles (Fe_3O_4/MWCNT), prepared as described by Hu et al. [123]	Batch experiments [Catalyst] = 2.0 g L^{-1} $[H_2O_2]_0$ = 0.18 g L^{-1} T = 20 °C $pH_{solution}$ = 7 (and 5[c]) t = 8 h	17α-Methyltestosterone (0.212 mg L^{-1})	143	50.5% (0.007 mg g^{-1} h^{-1})	Not addressed
	Fe_3O_4 nanoparticles prepared as described by Hu et al. [123]				43.0% (0.006 mg g^{-1} h^{-1})	Not addressed
Variava et al. [54]	Fe_xO_y-decorated multiwalled carbon nanotubes (Fe_xO_y-MWCNT), prepared by in situ growth of Fe nanoparticles on treated MWCNT (polyethylene glycol) by a polyol-mediated microwave-assisted method performed at 200 °C	Batch experiments [Catalyst] = 0.5 g L^{-1} $[H_2O_2]_0$ = 0.52 g L^{-1} T = 35 °C $pH_{solution}$ = 7 t = 1 h	Orange G (50.0 mg L^{-1})	2.9	98.0% (98.0 mg g^{-1} h^{-1}) 73.0% (in the 5th consecutive reuse)	<2.0
	Fe_3O_4-MWCNT hybrid materials prepared by a solvothermal method using acid treated MWCNT (nitric acid) and iron (III) acetylacetonate in a mix solution of glycol and ultrapure water at various temperatures in the range 200–270 °C	Batch experiments [Catalyst] = 0.5 g L^{-1} $[H_2O_2]_0$ = 0.51 g L^{-1} Unknown temperature	Orange II (87.6 mg L^{-1})	1.3	94.0%[d] (329 mg g^{-1} h^{-1})	Not addressed
Deng et al. [37]	Powdered Fe_3O_4 (synthesis procedure not addressed)	$pH_{solution}$ = 3.5 t = 0.5 h			15.8% (55.4 mg g^{-1} h^{-1})	Not addressed
	Nanometer-size Fe_3O_4 (synthesis procedure not addressed)				37.1% (130 mg g^{-1} h^{-1})	Not addressed
Zhou et al. [109]	MWCNT decorated with Fe_3O_4 (Fe_3O_4/MWCNT), prepared by a solvothermal method using iron (III) acetylacetonate and n-octylamine in n-octanol at 240 °C	Batch experiments [Catalyst] = 0.5 g L^{-1} $[H_2O_2]_0$ = 3.40 g L^{-1} T = 30 °C $pH_{solution}$ = 5 t = 4 h	Tetrabromobisphenol A (10.0 mg L^{-1})	109	95.1% (4.76 mg g^{-1} h^{-1}) 93.2% (in the 10th consecutive reuse)	Not addressed
	Fe_3O_4 nanoparticles (synthesis procedure not addressed)				39.4% (1.97 mg g^{-1} h^{-1})	Not addressed
Cleveland et al. [101]	MWCNT decorated with Fe_3O_4 nanoparticles (Fe_3O_4/MWCNT), prepared by in situ chemical oxidation and co-precipitation, slightly adapting the procedure described by Hu et al. [123]	Batch experiments [Catalyst] = 0.5 g L^{-1} $[H_2O_2]_0$ = 0.04 g L^{-1} T = 50 °C $pH_{solution}$ = 3 t = 4 h	Bisphenol A (68.5 mg L^{-1})	0.1	90.0% (30.8 mg g^{-1} h^{-1}) 89.0% (in the 5th consecutive reuse)	Not addressed
Wang et al. [15]	Fe_3O_4–multiwalled carbon nanotube magnetic hybrid material (Fe_3O_4-MWCNT) prepared by in situ growth of Fe_3O_4 nanoparticles on acid treated MWCNT (nitric acid) by co-precipitation of Fe^{2+} and Fe^{3+} at 50 °C under N_2 atmosphere	Batch experiments [Catalyst] = 0.3 g L^{-1} $[H_2O_2]_0$ = 13.6 g L^{-1} T = room temperature $pH_{solution}$ = 5.5 t = 12 h	Methylene blue (10.0 mg L^{-1})	221	99.8% (2.77 mg g^{-1} h^{-1})	0.25[e]

[a] Obtained by dividing the amount of H_2O_2 employed by the stoichiometric amount needed for the complete mineralization of the pollutant considered.

[b] Maximum value, obtained in the 3rd consecutive reuse of Fe_3O_4/MWCNT in the CWPO of 17α-methyltestosterone.

[c] The results obtained at pH 5 are the same as those described by Hu et al. [123].

[d] Removal obtained with the Fe_3O_4-MWCNT sample produced at 260 °C.

[e] Value obtained in measurements performed without H_2O_2, at pH 5 and 6.
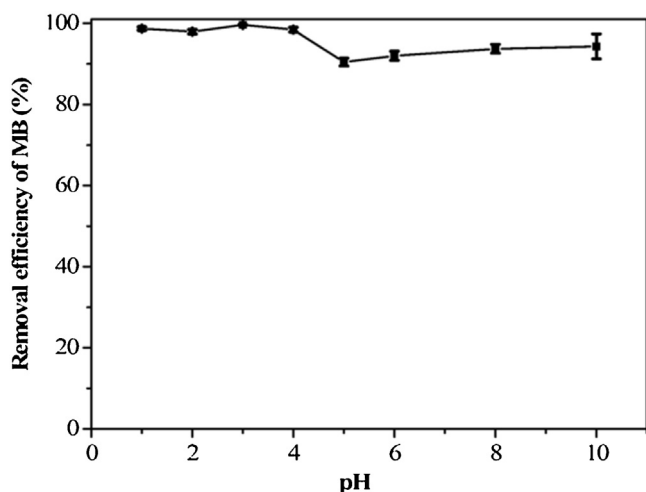
Fig. 17. Influence of the initial solution pH on the removal of methylene blue (MB) by CWPO when using the Fe_3O_4-MWCNT catalyst ($0.3\,g\,L^{-1}$). Experiments performed at room temperature during 2 h, with $[MB]_0 = 10\,mg\,L^{-1}$ and $[H_2O_2]_0 = 13.61\,g\,L^{-1}$. Reprinted from [15], Copyright© 2014, with permission from The Royal Society of Chemistry [License number: 3761890418678].


Fig. 18. Magnetic saturation curves of the Fe_3O_4-MWCNT composites produced at different temperatures, measured at room temperature using a vibrating sample magnetometer. Inset: photograph of magnetic separation of the composites from an aqueous suspension. Reprinted from [37], Copyright© 2012, with permission from Elsevier [License number: 3761911315093].

its good structural stability, low iron leaching, simple separation, stable catalytic activity in consecutive reuse experiments (the pollutant degradation slightly decreases from 85.9%, in the first use, to 79.4%, in the seventh use) while regeneration is not needed [123]. The degradation mechanism of 17α-methyltestosterone by CWPO was further investigated by Hu et al. [124] in a work performed under the same operating conditions described in the legend of Fig. 16. At this time, the authors performed a kinetic study that suggested the intrinsic reactions on the oxide surface (including sorption and oxidation) as the rate-limiting step for the degradation process, rather than the rate of diffusion of the solutes to the surface [124].

In 2012, Variava et al. [54] reported a work in which Fe nanoparticles were also grown in MWCNT, but this time using a microwave-assisted polyol method, resulting in the composite named Fe_xO_y-MWCNT, as described in Table 6. This composite was able to catalyse the degradation of orange G by CWPO without the need to acidify the reaction mixture, being effective at neutral pH. Therefore, the authors have concluded that Fe_xO_y-MWCNT is a promising catalyst for CWPO, since the treated waters do not require either a process to remove dissolved Fe species, or the neutralization of highly acidic solutions, which, as discussed in Section 2.1, are typical drawbacks of the Fenton process [54]. Although residual dye and degradation by-products are adsorbed on the surface of the catalyst, leading to partial deactivation, a simple and basic regeneration procedure allows the catalyst to be consecutively reused with some decrease on the efficiency of orange G elimination by CWPO (from 98% in the first use, to 73% in the fifth consecutive reuse) [54].

A wider tolerance to the solution pH has been observed in the work of Wang et al. [15], in which a Fe_3O_4-MWCNT magnetic nanocomposite, prepared as described in Table 6, was used in the CWPO of methylene blue under different operating conditions. As shown in Fig. 17, methylene blue can be efficiently removed in the pH range 1.0–10.0, with efficiencies in the range 88.1–98.7%, after 2 h of reaction; therefore, the authors concluded that this wide range of working pH is very attractive for the treatment of real wastewaters [15]. Nevertheless, Fe levels above $2\,mg\,L^{-1}$ were leached into the treated waters when the initial solution pH was lower than 2 [15].

Fe_3O_4-MWCNT hybrid composites were first reported as superparamagnetic materials in a work performed by Deng et al. [37],
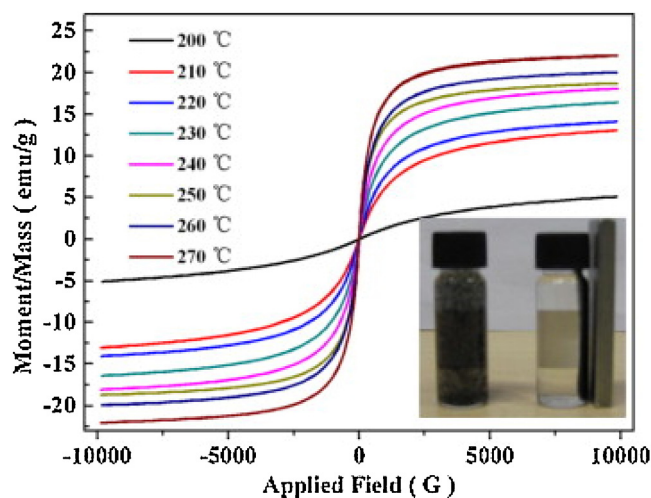
in which distinct samples of Fe_3O_4-MWCNT were prepared by solvothermal synthesis at different temperatures, as described in Table 6. The magnetization measurements given in Fig. 18 show the high magnetic sensitivity of the Fe_3O_4-MWCNT samples produced at different temperatures. The superparamagnetism of these nanostructured composites was attributed to the measured coercivity and remnant magnetization values close to zero [37].

The results obtained by these authors also show that pure Fe_3O_4 nanoparticles present a narrow size distribution and a uniform distribution over the MWCNT surface, as can be observed in the micrograph (Fig. 19a) obtained by transmission electron microscopy (TEM) of the Fe_3O_4-MWCNT sample prepared at 260 °C (here shown as an illustrative example of a carbon nanostructure decorated with magnetic nanoparticles) and in the histogram of size distribution over the MWCNT surface (Fig. 19b). That same Fe_3O_4-MWCNT sample was used in the CWPO of orange II with $pH_{solution} = 3.5$. As observed in Table 6, the Fe_3O_4-MWCNT catalyst displays a significantly enhanced catalytic activity when compared to that of powdered Fe_3O_4 and nanometric Fe_3O_4. This increased catalytic performance was ascribed to the homogeneous dispersion of the Fe_3O_4 nanoparticles, which increases the active sites available for H_2O_2 decomposition [37].

The same conclusion was obtained by Zhou et al. [109] using a Fe_3O_4/MWCNT hybrid material synthesized by a solvothermal method in the CWPO of tetrabromobisphenol A at 30 °C and $pH_{solution} = 5$ (cf. Table 6). In addition, the stability of the Fe_3O_4/MWCNT catalyst was thoroughly assessed against that of Fe_3O_4, through 10 consecutive reutilization experiments. As observed in Fig. 20a, the amount of tetrabromobisphenol A remaining at the end of the 10th cycle is 6.8%, corresponding to a pollutant removal of 93.2%. When this value is compared to that observed in the 1st use of the Fe_3O_4/MWCNT catalyst (95.1%, cf. Table 6) only a decrease of 1.9% is observed during the 10 cycles considered, confirming the excellent stability of the catalyst for CWPO [109]. In addition, the saturation magnetization of the Fe_3O_4/MWCNT catalyst after the 10th cycle is $16.9\,emu\,g^{-1}$ (cf. Fig. 20b), which represents only a decrease of 1.1% from its original value; on the contrary, the saturation magnetization of Fe_3O_4 decreases 15.8% in the same process [109]. This effect was also observed by XPS analysis of Fe_3O_4/MWCNT and Fe_3O_4, as synthesized and after the 10th CWPO cycle (cf. Fig. 20c–f). Fig. 20c and d, shows that no significant changes occur after 10 consecutive reuses of the Fe_3O_4/MWCNT
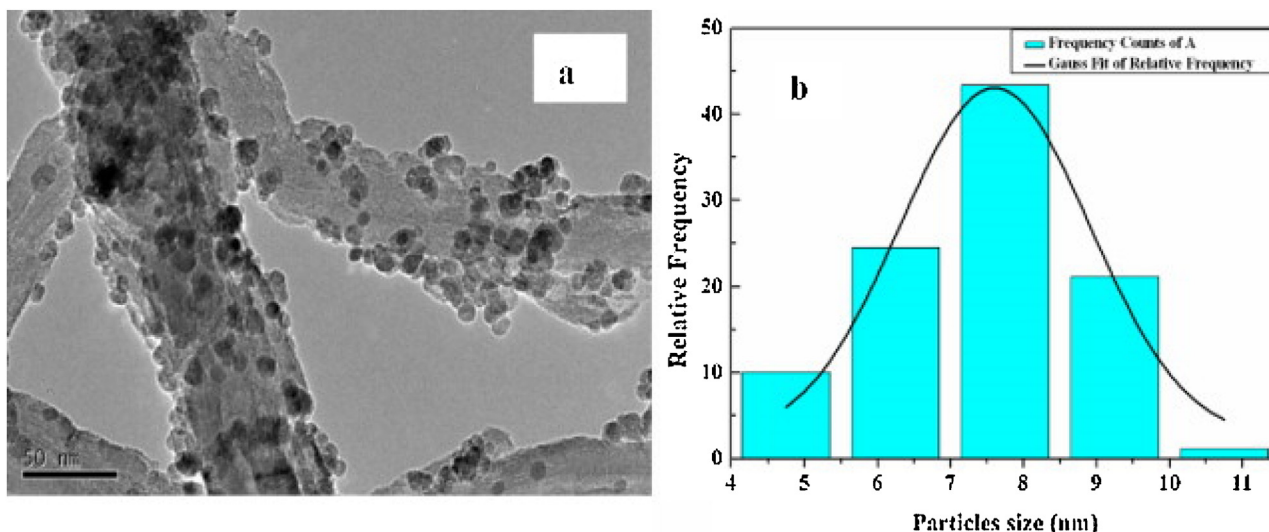
Fig. 19. (a) TEM micrograph of one sample of the Fe_3O_4-MWCNT magnetic hybrid materials produced by J. Deng et al.; (b) histogram of Fe_3O_4 particle size distribution in the same sample. Reprinted from [37], Copyright© 2012, with permission from Elsevier [License number: 3761911315093].

catalyst in the CWPO of tetrabromobisphenol A. For instance, peak areas indicate that 32.4% of the total iron content on the surface of the Fe_3O_4/MWCNT catalyst is in the Fe^{2+} state, a value that decreases to 30.0% after the 10th CWPO cycle; on the contrary, the surface concentration of Fe^{2+} decreases from 32.7% down to 27.8% when Fe_3O_4 is used in 10 CWPO cycles. Thus, the authors concluded that the reduction of Fe^{3+} in the CWPO process is more efficient when MWCNT are combined with Fe_3O_4, which is beneficial for the regeneration of the active sites [109].

Knowing whether the toxicity of the by-products formed during CWPO is lower or higher than that of the parent compounds is a crucial issue to evaluate if the risk for human and environmental health actually decreases/increases with the degradation of the initial pollutants. In the particular case of CWPO processes using hybrid magnetic carbon catalysts, this question was first addressed by Cleveland et al. [101] in a work dealing with the use of Fe_3O_4 attached to multiwalled carbon nanotubes (Fe_3O_4/MWCNT, as described in Table 6) for the elimination of aqueous bisphenol A—an endocrine disrupting agent. Biotoxicity tests performed with the treated waters revealed minimal inhibition of *E. coli* due the presence of by-products resulting from the CWPO of bisphenol A performed at 50 °C and $pH_{solution}$ = 3, whereas significant biotoxicity effects were initially observed for bisphenol A aqueous solutions (inhibition in the range 54–100%, depending on the pollutant concentration). In the light of these results, the authors concluded that the CWPO of bisphenol A is compatible with further biological treatments [101].

4.1.2. Graphene-based materials

The participation of HO• formed during the catalytic decomposition of H_2O_2 at the surface of nanostructured hybrid magnetic carbon materials in CWPO processes was first evidenced in a work performed by Liu et al. [22], in which a magnetically separable nanocomposite catalyst was used in the CWPO of methylene blue at 25 °C and neutral pH. Fe_3O_4 nanoparticles were embedded in the graphene oxide (GO) structure by a co-precipitation method, followed by reduction with hydrazine, resulting in the Fe_3O_4/rGO hybrid composite, as described in Table 7. CWPO experiments performed with this material in the presence and absence of *tert*-butanol—a strong HO• scavenger [211], have shown that the degradation of methylene blue is greatly suppressed with the addition of *tert*-butanol before the reaction, putting into evidence the role of HO• in the CWPO process. Specifically, the degrada-

tion of methylene blue obtained after 2 h of reaction drops from 98.6% down to 57.0%, upon addition of *tert*-butanol [22]. Taking these results into consideration, the authors proposed a possible mechanism for the elimination of methylene blue by CWPO in the presence of Fe_3O_4/rGO, as shown in Fig. 21. Briefly, the HO• radicals formed by the catalytic decomposition of H_2O_2 at the surface of Fe_3O_4 nanoparticles are responsible for the degradation of methylene blue molecules adsorbed at the surface of the Fe_3O_4/rGO composite; with the degradation of methylene blue, the adsorption equilibrium changes and more pollutant molecules are transferred from the solution to the surface of Fe_3O_4/rGO, resulting in a cyclic process [22].

Liu et al. [22] have also compared the performance of the Fe_3O_4/rGO catalyst in the CWPO of methylene blue to that of Fe_3O_4 and rGO. As referred above, the degradation of methylene blue is up to 98.6% when the Fe_3O_4/rGO catalyst is used, while removals of only 17.7% and 24.5% (cf. Table 7) are obtained when using Fe_3O_4 and rGO, respectively; therefore, the pollutant removal obtained with the Fe_3O_4/rGO catalyst (98.6%) is far superior to that of the sum of the individual contributions (i.e., 42.2%), which, once again, puts into evidence the synergistic effect that arises from the combination of Fe_3O_4 with carbon-based materials, this time by using the Fe_3O_4/rGO hybrid material.

Fe_3O_4 magnetic nanoparticles decorated with graphene oxide (GO-Fe_3O_4) were also reported as active catalysts in a work performed by Chang et al. [52], in which a GO-Fe_3O_4 composite was prepared by co-precipitation of iron salts onto GO sheets, as described in Table 7. Once synthesized, the performance of the GO-Fe_3O_4 catalyst in the CWPO of rhodamine B was evaluated at 25 °C and neutral pH, against that of Fe_3O_4. As observed in Table 7, the degradation rate of rhodamine B is higher when using the GO-Fe_3O_4 catalyst, leading to the conclusion that the presence of GO makes a significant contribution to the degradation of rhodamine B.
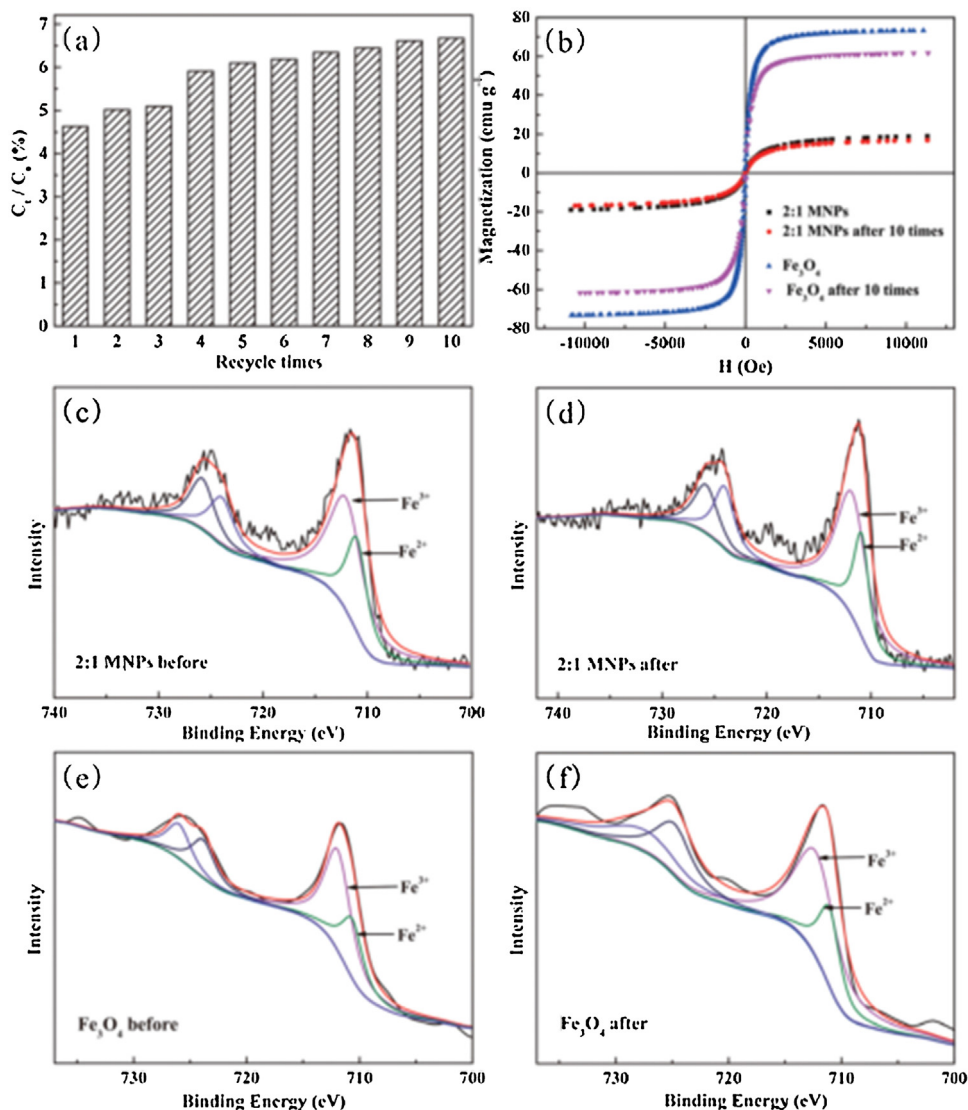
The influence of GO loading in the structural and functional features of a GO-Fe_3O_4 nanocomposite prepared by a similar procedure (cf. Table 7) was thoroughly addressed in the work of Zubir et al. [29]. Based on detailed characterization of a set of GO-Fe_3O_4 materials synthesized with GO loadings in the range 5–25 wt.%, these authors proposed the formation of two very different nanocomposite structures, depending on the GO load. As shown in Fig. 22, GO loadings below 10 wt.% lead to the formation of structure I, while GO loadings above 10 wt.% lead to the formation of structure II. The formation of the proposed structures

Table 7

Summary on the use of graphene-based materials decorated with magnetic nanoparticles in CWPO: description of the catalyst, operating conditions and catalytic performance of each catalyst (pollutant removal and Fe leached to the treated waters).

Authors	Catalyst	Operating conditions	Pollutant	H_2O_2 stoichiometric ratio[a]	Pollutant removal	$[Fe]_{leaching}$ ($mg\,L^{-1}$)
Liu et al. [22]	Reduced graphene oxide (rGO) decorated with Fe_3O_4 nanoparticles (Fe_3O_4/rGO), prepared by co-precipitation of Fe^{2+} and Fe^{3+} in the presence of graphene oxide (10 wt.%) at 90 °C under N_2 atmosphere, followed by reduction with hydrazine at 90 °C under N_2 atmosphere	Batch experiments $[Catalyst] = 0.3\,g\,L^{-1}$ $[H_2O_2]_0 = 2.04\,g\,L^{-1}$ $T = 25$ °C $pH_{solution} = 7$			98.6% ($32.9\,mg\,g^{-1}\,h^{-1}$) 90.6% (in the 5th consecutive reuse)	0.22
	Fe_3O_4 nanoparticles, prepared by co-precipitation of Fe^{2+} and Fe^{3+} at 90 °C under N_2 atmosphere	$t = 2$ h	Methylene blue (20.0 mg L^{-1})	16.5	17.7% ($5.90\,mg\,g^{-1}\,h^{-1}$)	Not addressed
	Reduced graphene oxide (rGO) obtained from reduction of graphene oxide (produced from natural graphite according to a modified Hummers method) with hydrazine at 90 °C under N_2 atmosphere	$[rGO] = 0.03\,g\,L^{-1}$ (corresponding to the 10 wt.% of rGO)			24.5% ($81.7\,mg\,g^{-1}\,h^{-1}$)	Not addressed
Chang et al. [52]	Graphene oxide (GO) decorated with Fe_3O_4 nanoparticles ($GO-Fe_3O_4$), prepared by co-precipitation of Fe^{2+} and Fe^{3+} in the presence of GO at 60 °C under N_2 atmosphere	Batch experiments $[Catalyst] = 0.2\,g\,L^{-1}$ $[H_2O_2]_0 = 8.12\,g\,L^{-1}$ $T = 25$ °C	Rhodamine B (10.0 mg L^{-1})	147	88.3% ($44.2\,mg\,g^{-1}\,h^{-1}$)	Not addressed
	Fe_3O_4 nanoparticles (synthesis procedure not addressed)	$pH_{solution} = 7$ $t = 1$ h			60.7% ($30.4\,mg\,g^{-1}\,h^{-1}$)	Not addressed
	Graphene oxide-iron oxide ($GO-Fe_3O_4$) nanocomposite prepared by co-precipitation of Fe^{2+} and Fe^{3+} in the presence of GO (5 wt.%) at room temperature	Batch experiments $[Catalyst] = 0.2\,g\,L^{-1}$ $[H_2O_2]_0 = 0.75\,g\,L^{-1}$			98.0% ($57.2\,mg\,g^{-1}\,h^{-1}$)	Not addressed
Zubir et al. [29]	Fe_3O_4 nanoparticles prepared by co-precipitation of Fe^{2+} and Fe^{3+} at room temperature	$T = 25$ °C $pH_{solution} = 3$ $t = 3$ h	Orange II (35.0 mg L^{-1})	4.9	70.5% ($41.1\,mg\,g^{-1}\,h^{-1}$)	Not addressed
	GO produced from natural graphite according to a modified Hummers method, followed by exfoliation by ultrasonication				12.5% ($7.29\,mg\,g^{-1}\,h^{-1}$)	Not addressed
	Graphene oxide-iron oxide ($GO-Fe_3O_4$) nanocomposite prepared as described above for Zubir et al. [29]	Batch experiments $[Catalyst] = 0.5\,g\,L^{-1}$ $[H_2O_2]_0 = 0.29\,g\,L^{-1}$ $T = 25$ °C $pH_{solution} = 3$ $t = 1.5$ h			76.0% ($35.5\,mg\,g^{-1}\,h^{-1}$)	Not addressed
Zubir et al. [31]	$GO-Fe_3O_4$ nanocomposite prepared as described above for Zubir et al. [29], but in the presence of 1 wt.% of GO		Orange II (35.0 mg L^{-1})	1.9	45.0% ($21.0\,mg\,g^{-1}\,h^{-1}$)	
	$GO-Fe_3O_4$ nanocomposite prepared as described above for Zubir et al. [29], but in the presence of 0.5 wt.% of GO				48.0% ($22.4\,mg\,g^{-1}\,h^{-1}$)	Not addressed
	Reduced graphene oxide decorated with Fe_3O_4 nanoparticles (Fe_3O_4-rGO), prepared by co-precipitation of Fe^{2+} and Fe^{3+} in the presence of GO at 80 °C, followed by reduction with hydrazine at 90 °C	Batch experiments $[Catalyst] = 0.1\,g\,L^{-1}$ $[H_2O_2]_0 = 0.03\,g\,L^{-1}$ $T = 25$ °C $pH_{solution} = 3$ $t = 1$ h	Methylene blue (50.0 mg L^{-1})	0.1	54.5% ($273\,mg\,g^{-1}\,h^{-1}$)	Not addressed
Yang et al. [12]	Nanoscale zero valent iron immobilised on magnetic Fe_3O_4-reduced graphene oxide composite ($Fe^0-Fe_3O_4-rGO$), prepared by reduction of Fe^{2+} by sodium borohydride in the presence of Fe_3O_4-rGO at room temperature under N_2 atmosphere				98.0% ($490\,mg\,g^{-1}\,h^{-1}$) 68.8% (in the 5th consecutive reuse)	2.0
	Fe_3O_4 nanoparticles (synthesis procedure not addressed)				23.6% ($118\,mg\,g^{-1}\,h^{-1}$)	Not addressed
	Fe^0 nanoparticles (origin not addressed)				77.3% ($387\,mg\,g^{-1}\,h^{-1}$)	Not addressed

[a] Obtained by dividing the amount of H_2O_2 employed by the stoichiometric amount needed for the complete mineralization of the pollutant considered.

Fig. 20. (a) Percentage of tetrabromobisphenol A (TBBPA) remaining at the end of each of 10 consecutive CWPO cycles performed during 4 h with the Fe_3O_4/MWCNT catalyst; (b) magnetic saturation curves of Fe_3O_4/MWCNT (MNPs) and Fe_3O_4, measured at room temperature using a vibrating sample magnetometer; XPS spectrum of Fe in the Fe_3O_4/MWCNT (MNPs) (c) before and (d) after 10 CWPO cycles; and XPS spectrum of Fe in the Fe_3O_4 (e) before and (f) after 10 CWPO cycles. Experiments performed with $[TBBPA]_0 = 10\,mg\,L^{-1}$, $[catalyst] = 0.5\,g\,L^{-1}$, T = 30 °C, pH 5 and $[H_2O_2]_0 = 3.40\,g\,L^{-1}$. Reprinted from [109], Copyright© 2014, with permission from The Royal Society of Chemistry [License number: 3761920010657].

was ascribed to the dispersion effect of GO, as previously reported for GO and nanowires [212], or GO and polystyrene [213]. Structure I is obtained when the Fe_3O_4 nanoparticles are intercalated between the GO sheets; in this case, hydroxylated Fe complexes are able to homogeneously anchor onto both the surfaces and edges of exfoliated GO sheets through oxygen-containing functional groups, while further condensation of complexes leads to the formation of nuclei and growth of Fe_3O_4 crystallites onto GO sheets [29]. On the other hand, structure II is formed when the deposition of Fe_3O_4 nanoparticles occurs mainly onto the external surface of the GO sheets, due to the previous stacking of the GO sheets; in this case, the anticipated GO stacking was ascribed to the reduction of the degree of exfoliation as the concentration of GO increases, since high GO loadings may induce a dominant effect of GO stacking due to $\pi-\pi$ interactions around the carbon basal plane of GO sheets [29].

The GO-Fe_3O_4 nanocomposites synthesized by Zubir et al. [29] were tested in the CWPO of orange II at 25 °C and $pH_{solution} = 3$. The main results are shown in Fig. 23. As observed, the perfor-

mance of the nanocomposites gradually decreases with increasing GO loading, the highest catalytic activity being obtained with a GO loading of 5 wt.%. In this case, the synergistic effect arising from the combination of Fe_3O_4 with carbon-based materials is once again demonstrated: the degradation of orange II is up to 88.6% when using the GO-Fe_3O_4 catalyst, while removals of 70.5% and 12.5% are obtained when using Fe_3O_4 and GO, respectively (as shown in Fig. 23 and Table 7). The authors claimed four significant contributions to this synergistic effect: (i) high surface area of exfoliated GO sheets promotes high dispersion of the Fe_3O_4 nanoparticles (cf. Fig. 22, structure I); (ii) GO favours orange II adsorption, which provides higher pollutant concentration near to the active sites; (iii) GO presents delocalized unpaired π electrons and electron transfer features that facilitate the transfer of electrons between GO and the Fe_3O_4 nanoparticles, which is beneficial for the regeneration of active sites; and (iv) partial reduction of GO sheets, which further increases electron transfer and the regeneration of the active sites [29].
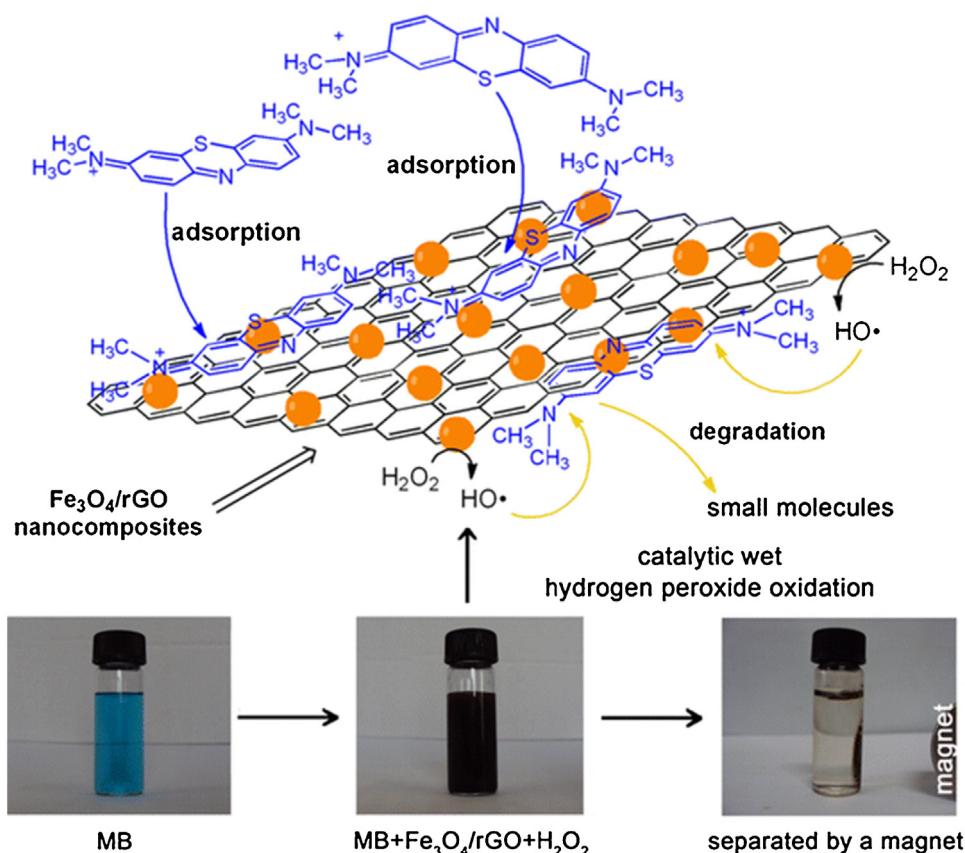
Fig. 21. Mechanism proposed by Liu et al. for the CWPO of methylene blue (MB) when using the Fe_3O_4/rGO catalyst. Inset: photographs of Fe_3O_4/rGO dispersed in solution and of magnetic separation by a permanent magnet after degradation of MB. Reprinted from [22], Copyright© 2013, with permission from Springer Science + Business Media [License number: 3763540153228].
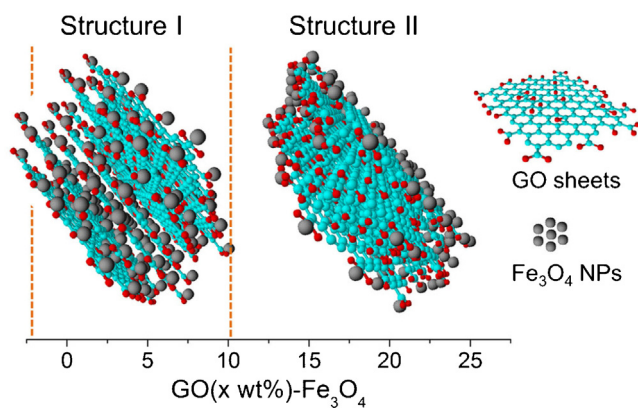
Fig. 22. Different GO-Fe_3O_4 structures proposed by Zubir et al. Reprinted from [29], Copyright© 2014, with permission from Nature Publishing Group [License number: 3761920430748].

GO-Fe_3O_4 nanocomposites with GO loadings below 5 wt.% were also explored by Zubir et al. in a different work [31]; however, as can be seen in Table 7, this approach did not allow the synthesis of hybrid magnetic catalysts with improved performances for the CWPO of orange II. In another work of these authors [30], the kinetics of orange II CWPO were studied considering the optimized GO-Fe_3O_4 catalyst at the optimum operating conditions, using the data reported in their first work mentioned in this review (i.e., Zubir et al. [29]). They concluded that the CWPO of orange II is well described by pseudo-first-order kinetics according to the Langmuir–Hinshelwood mechanism, with the process being dom-inated by the rate of the chemical reactions rather than the rate of mass transfer. In addition, the characterization of the GO-Fe_3O_4 catalyst recovered at the end of the CWPO process revealed that the Fe_3O_4 phase was similar to that of the pristine catalyst, although some minor changes in the specific surface area and pore volume were observed [30].

Zero valent iron has also been assembled on a Fe_3O_4-rGO mag-netic composite by in situ reduction of Fe^{2+} in a work recently reported by Yang et al. [12], resulting in the material named Fe^0-Fe_3O_4-rGO, as detailed in Table 7. Large Fe^0 spheres were wrapped by the Fe_3O_4 nanoparticles anchored on reduced graphene oxide sheets, as shown in Fig. 24c1 and c2. Based on the results obtained in CWPO experiments performed using methylene blue as model pollutant and Fe^0-Fe_3O_4-rGO, Fe_3O_4-rGO, Fe_3O_4 and Fe^0, as cata-lysts (cf. Table 7), the authors concluded that, besides the properties of graphene sheets as good supports and electron conductors, Fe^0 can act as source of electrons to promote a faster regeneration of the active sites [12]. Taking this into consideration, the authors proposed a mechanism for the CWPO of methylene blue with the Fe^0-Fe_3O_4-rGO catalyst, as illustrated in Fig. 25.
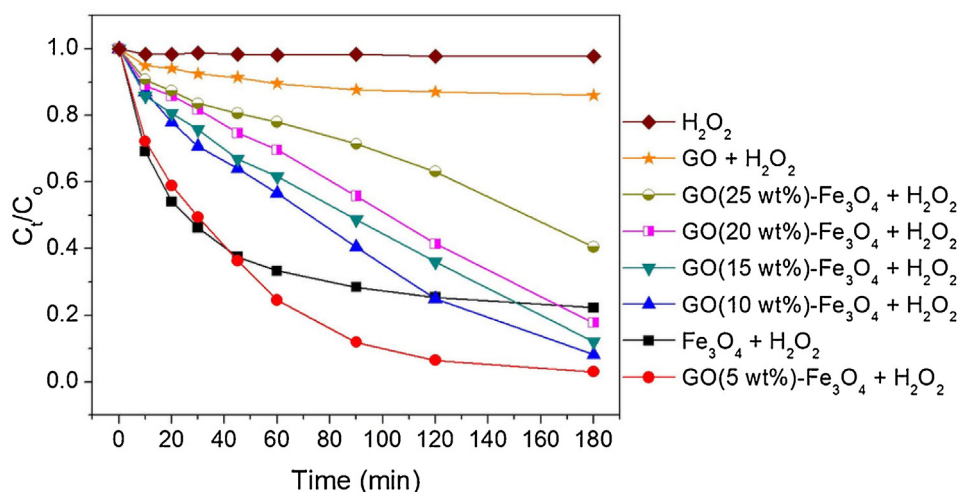
4.1.3. Other carbon materials

Other carbon materials have been used for the preparation of hybrid magnetic composites for CWPO. For instance, hybrid mag-netic composites based on iron-copper bimetallic nanoparticles and ordered mesoporous carbons were reported as active cata-lysts by Wang et al., in a very recent work [99] dealing with the elimination of several recalcitrant organic pollutants in aqueous phase at 25 °C and $pH_{solution}$ = 3. Specifically, the influence of cop-per in iron–copper bimetallic nanoparticles was investigated. For

Table 8
Summary on the use of ordered mesoporous carbons and amorphous carbons decorated with magnetic nanoparticles in CWPO: description of the catalyst, operating conditions and catalytic performance of each catalyst (pollutant removal and Fe leached to the treated waters).

Authors	Catalyst	Operating conditions	Pollutant	H_2O_2 stoichiometric ratio[a]	Pollutant removal	$[Fe]_{leaching}$ $(mg\,L^{-1})$
Wang et al. [99]	Iron-copper bimetallic nanoparticles embedded within ordered mesoporous carbon (CuFe-MC), prepared by inclusion of Fe^{3+} and Cu^{2+} during a "one-pot" block-copolymer self-assembly strategy and in situ reduction	Batch experiments [Catalyst] = 0.3 g L^{-1} $[H_2O_2]_0$ = 1.02 g L^{-1}			93.0% (310 mg g^{-1} h^{-1}) 87.8% (in the 5th consecutive reuse)	0.57
	Iron nanoparticles embedded within ordered mesoporous carbon (Fe-MC), prepared as described above, but without adding Cu^{2+}	T = 25 °C $pH_{solution}$ = 3 t = 1 h	Bisphenol A (100.0 mg L^{-1})	1.9	64.0% (213 mg g^{-1} h^{-1})	Not addressed
	Copper nanoparticles embedded within ordered mesoporous carbon (Cu-MC), prepared as described above, but without adding Fe^{3+}				40.0% (133 mg g^{-1} h^{-1})	Not addressed
Tristão et al. [13]	Fe magnetic nanoparticles dispersed in an amorphous carbon matrix (A8Fe400), prepared by dispersion of iron (III) nitrate nonahydrate in a sucrose solution, followed by calcination at 400 °C under N_2 atmosphere	Batch experiments [Catalyst] = 4.3 g L^{-1} $[H_2O_2]_0$ = 0.97 g L^{-1} Unknown temperature $pH_{solution}$ = 6 t = 3 h	Methylene blue (200.0 mg L^{-1})	0.8	93.0% (14.4 mg g^{-1} h^{-1})	Not addressed
	Fe magnetic nanoparticles dispersed in an amorphous carbon matrix (A8Fe600), prepared as described above, but considering a calcination temperature of 600 °C				94.6% (14.7 mg g^{-1} h^{-1})	Not addressed
	Fe magnetic nanoparticles dispersed in an amorphous carbon matrix (A8Fe800), prepared as described above, but considering a calcination temperature of 800 °C				60.0% (9.30 mg g^{-1} h^{-1})	Not addressed
	Amorphous carbon (A800), prepared by calcination of sucrose at 800 °C under N_2 atmosphere				0.0% (0.00 mg g^{-1} h^{-1})	Not addressed

[a] Obtained by dividing the amount of H_2O_2 employed by the stoichiometric amount needed for the complete mineralization of the pollutant considered.

Fig. 23. Orange II concentration decay curves obtained under different conditions. Experiments performed with $[Orange\ II]_0 = 35.0\ mg\ L^{-1}$, $[catalyst] = 0.2\ g\ L^{-1}$, $T = 25\ °C$, pH 3 and $[H_2O_2]_0 = 0.75\ g\ L^{-1}$. Reprinted from [29], Copyright© 2014, with permission from Nature Publishing Group [License number: 3761920430748].
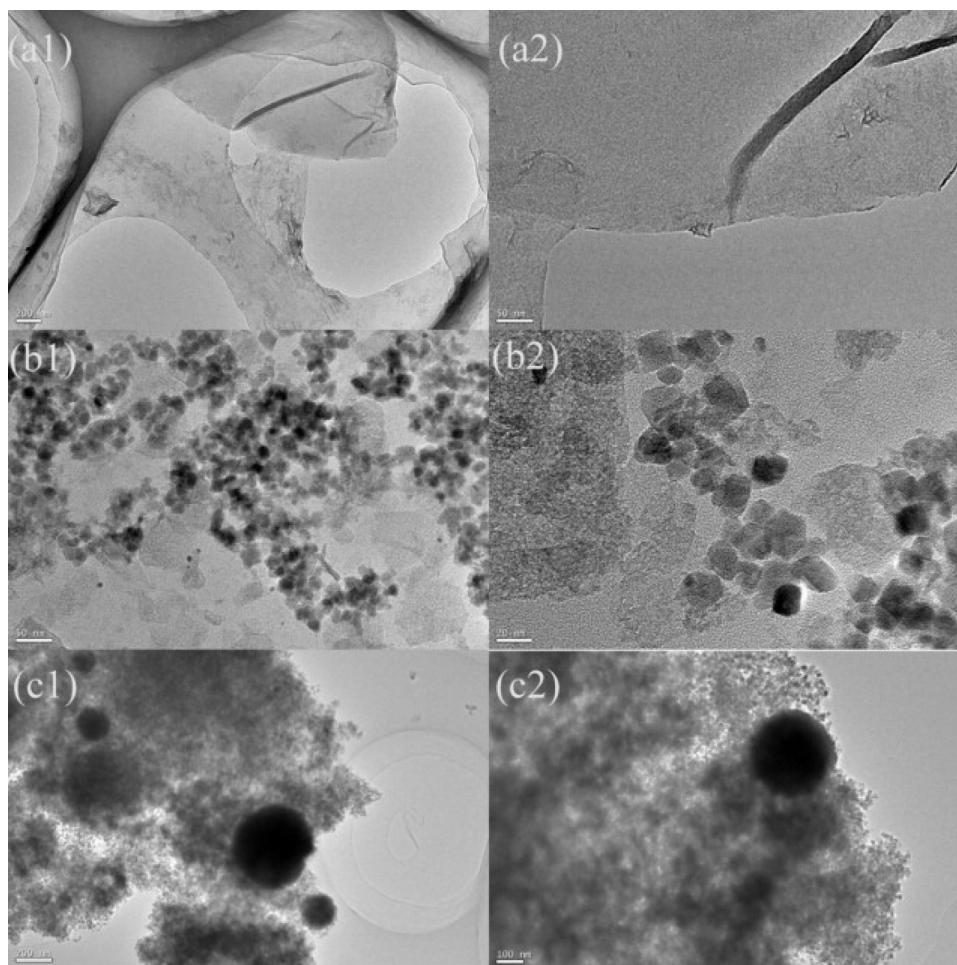

Fig. 24. TEM micrographs of (a1 and a2) graphene oxide, (b1 and b2) Fe_3O_4-rGO and (c1 and c2) Fe^0-Fe_3O_4-rGO. Reprinted from [12], Copyright© 2015, with permission from Elsevier [License number: 3761920605803].

that purpose, a magnetic carbon composite containing iron-copper bimetallic nanoparticles was prepared by inclusion of Fe and Cu precursors during the one-pot synthesis process, resulting in the composite named CuFe-MC, as described in Table 8. For comparison, two monometallic composites were also prepared and denoted as Fe-MC and Cu-MC. When CuFe-MC is compared to Fe-MC, no significant changes are obtained in the average size of the metallic particles or in the specific surface areas of the composites; nevertheless, the Fe content increases from 1.5 wt.% in Fe-MC, up to 2.3 wt.% in CuFe-MC, suggesting that the addition of Cu increases
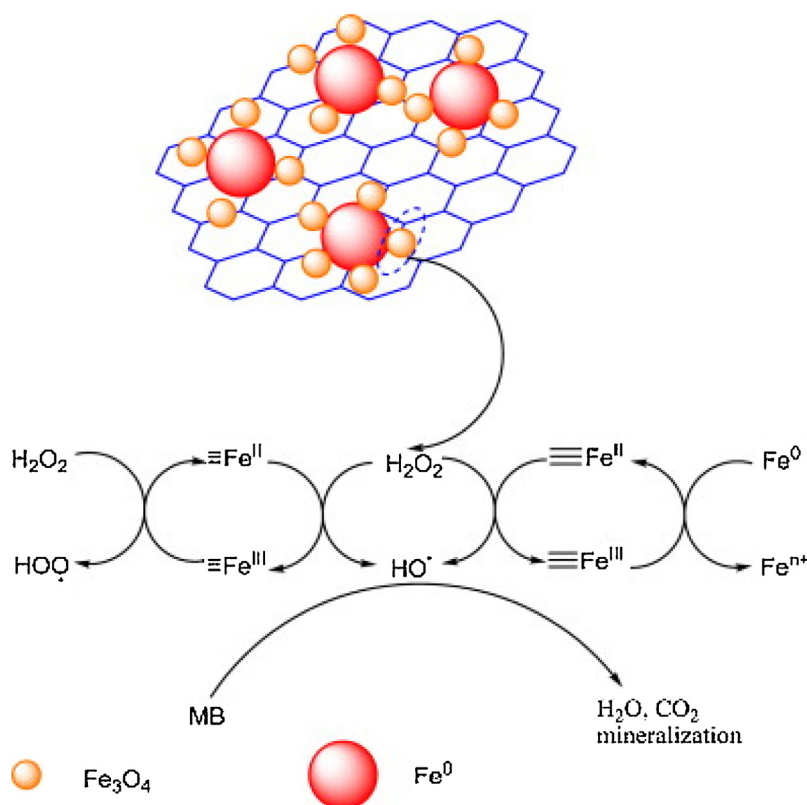
Fig. 25. Mechanism proposed by Yang et al. for the CWPO of methylene blue (MB) when using the Fe^0-Fe_3O_4-rGO catalyst. Reprinted from [12], Copyright© 2015, with permission from Elsevier [License number: 3761920605803].
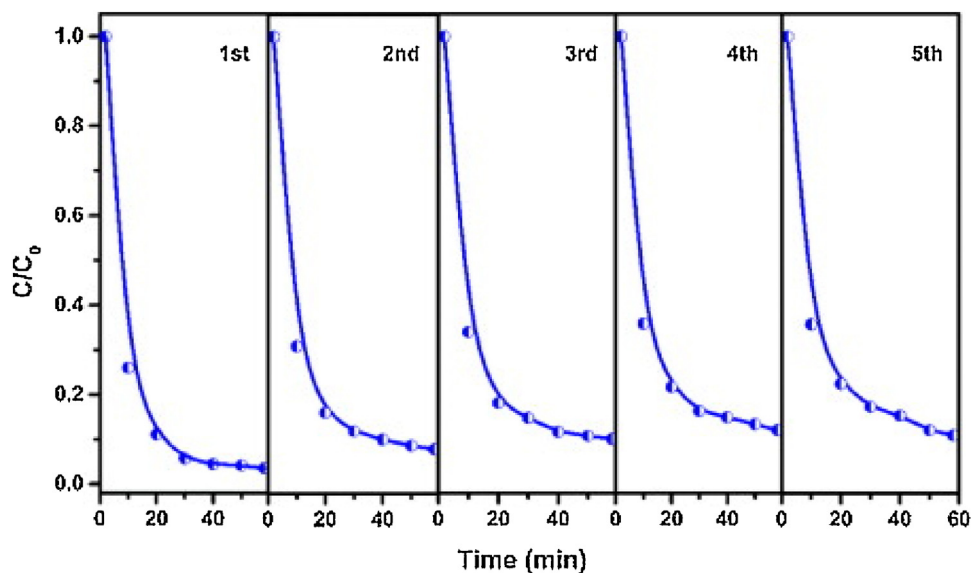

Fig. 26. Bisphenol A concentration decay curves obtained in CWPO runs with consecutive reuse of the CuFe-MC catalyst ($0.3\,g\,L^{-1}$). Experiments performed with [Bisphenol A]$_0$ = $100.0\,mg\,L^{-1}$, [H_2O_2]$_0$ = $1.02\,g\,L^{-1}$, T = $25\,°C$ and pH 3. Reprinted from [99], Copyright© 2014, with permission from Elsevier [License number: 3761920849470].

the loading of Fe at the surface of the composite and, therefore, the number of active sites available for the catalytic decomposition of H_2O_2 [99]. Indeed, the superior performance of the CuFe-MC catalyst in the CWPO of bisphenol A (cf. Table 8) was ascribed to the increased amount of Fe nanoparticles in the ordered mesoporous carbon structure due to the addition of Cu, as well as to four advantages of the composite catalysts based on iron-copper bimetallic nanoparticles and ordered mesoporous carbons: (i) high specific surface area plays a major role in the adsorption of the

pollutant molecules, while the mesoporous structure favours the fast diffusion of reactants and products; (ii) iron-copper bimetallic nanoparticles highly dispersed in the matrix of the composite increase the amount of active sites, therefore pollutant molecules adsorbed on the surface of the composite are instantly decomposed; (iii) the addition of Cu favours the redox cycles of Fe^{3+}/Fe^{2+} and Cu^{2+}/Cu^+, which enhances the activity of the composite; and (iv) the ordered mesoporous carbon can also act as catalyst on its
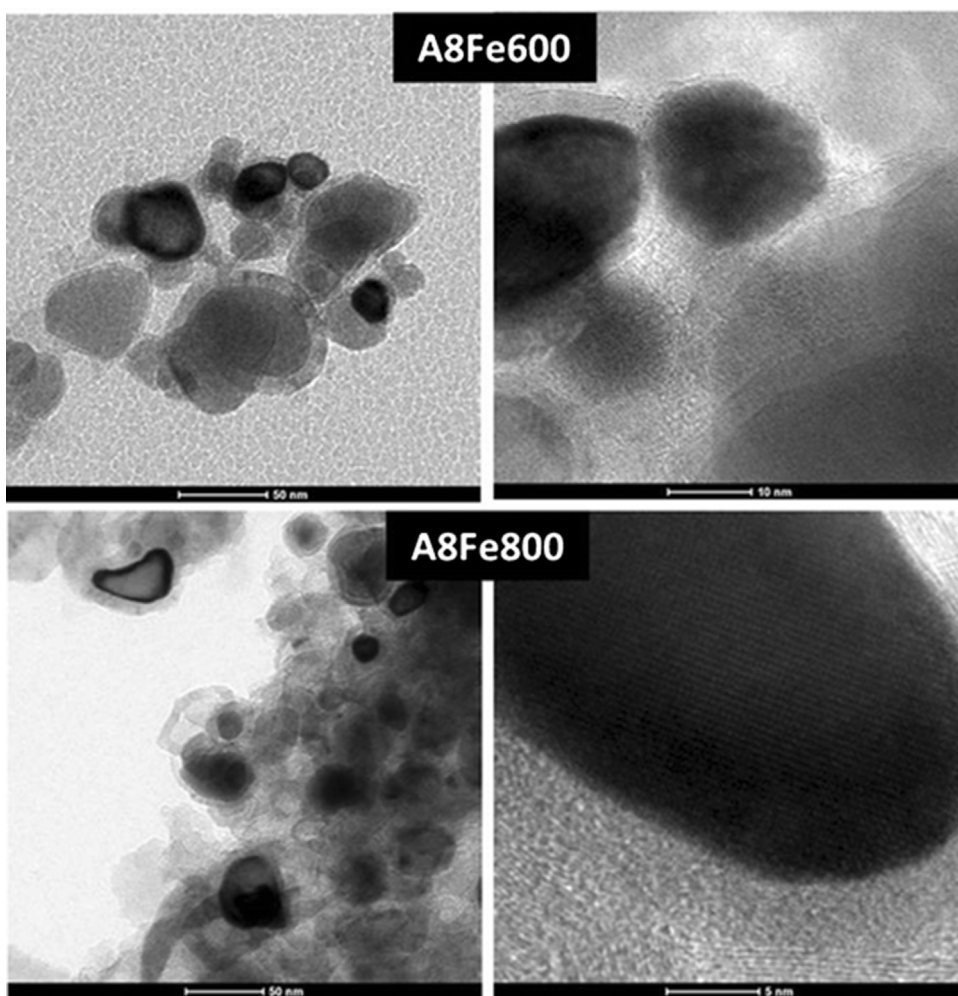
Fig. 27. TEM micrographs of A8Fe600 and A8Fe800. Reprinted from [13], Copyright© 2013, with permission from Springer Science + Business Media [License number: 3763530618389].
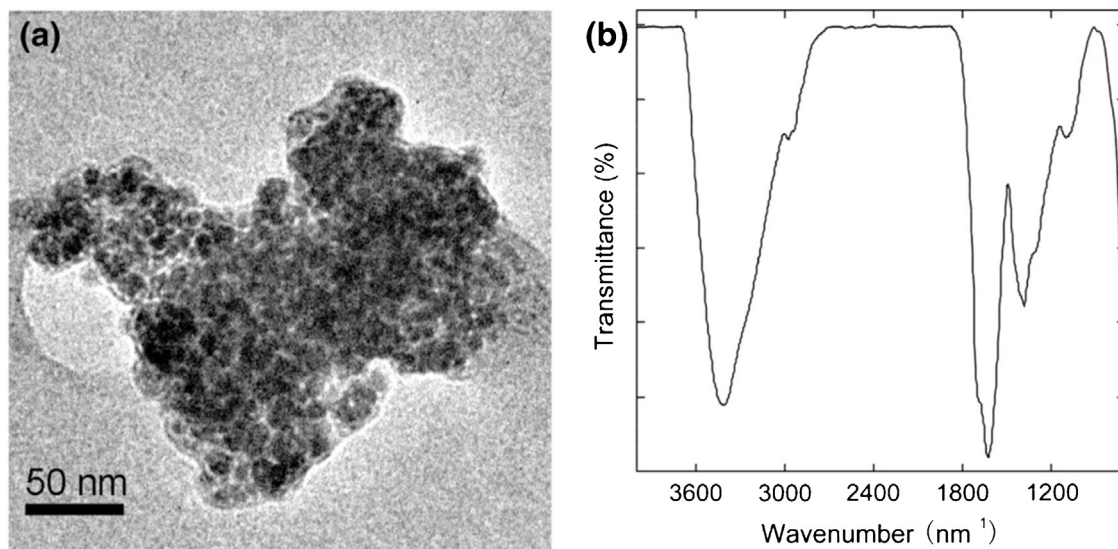
Fig. 28. (a) TEM micrograph and (b) infrared spectra of the Fe_3O_4@C composite. Reprinted from [14], Copyright© 2014, with permission from Springer Science + Business Media [License number: 3763530802165].

own, since it is able to decompose H_2O_2 via formation of highly reactive $HO^\bullet$ [99].

Wang et al. [99] have further studied the stability and reusability of the CuFe-MC catalyst in the CWPO of bisphenol A. Accordingly, a Fe leaching of $0.57\,mg\,L^{-1}$ was obtained in the treated waters at the end of the reaction (cf. Table 8). The authors concluded that the low Fe leaching confirms the enhanced stability of composite catalysts due to the confinement effect of the ordered mesoporous carbon. The reusability study presented in Fig. 26 shows that the CuFe-MC catalyst maintains high activity for the CWPO of bisphenol A even after five consecutive runs, also suggesting that the stability of metallic catalysts is increased when they are embedded within the matrix of ordered mesoporous carbons [99].

Amorphous carbon has also been used for the preparation of hybrid magnetic composites for CWPO processes, as recently reported by Tristão et al. [13]. Fe nanoparticles were dispersed in a carbon matrix through controlled thermal decomposition of iron (III) nitrate nonahydrate in a sucrose aqueous solution at different temperatures (resulting in the materials named A8Fe, followed by the calcination temperature in °C, as described in Table 8) and subsequently tested in the CWPO of methylene blue at $pH_{solution} = 6$. As observed in Fig. 27, Fe particles are effectively within the carbon matrix, which is predominantly composed of amorphous carbon [13]. Regarding the performance of the hybrid magnetic composites in the CWPO of methylene blue, the higher catalytic activity of the two composites that were prepared at lower temperatures
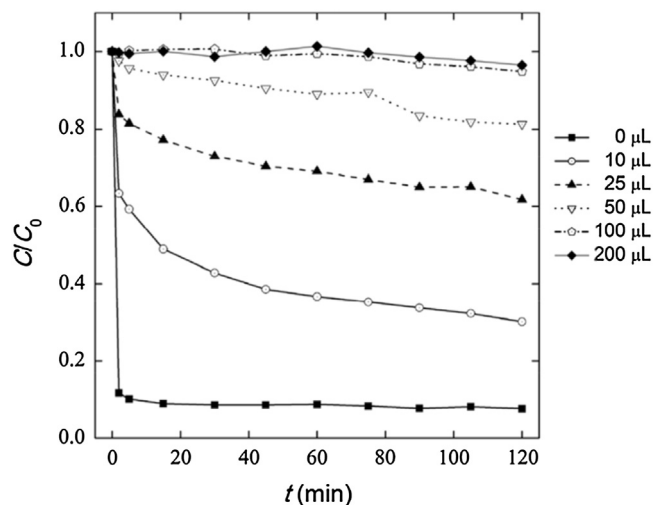
Fig. 29. Influence of different amounts of *tert*-butanol on the CWPO of methylene blue, when using the $Fe_3O_4@C$ catalyst ($0.25\,g\,L^{-1}$). Experiments performed with 20.0 mL of methylene blue aqueous solution ($200\,mg\,L^{-1}$), T = 35 °C, pH 3 and an unknown concentration of H_2O_2. Reprinted from [14], Copyright© 2014, with permission from Springer Science + Business Media [License number: 3763530802165].

(cf. Table 8) was ascribed to the presence of higher amounts of Fe^{2+} species [13].
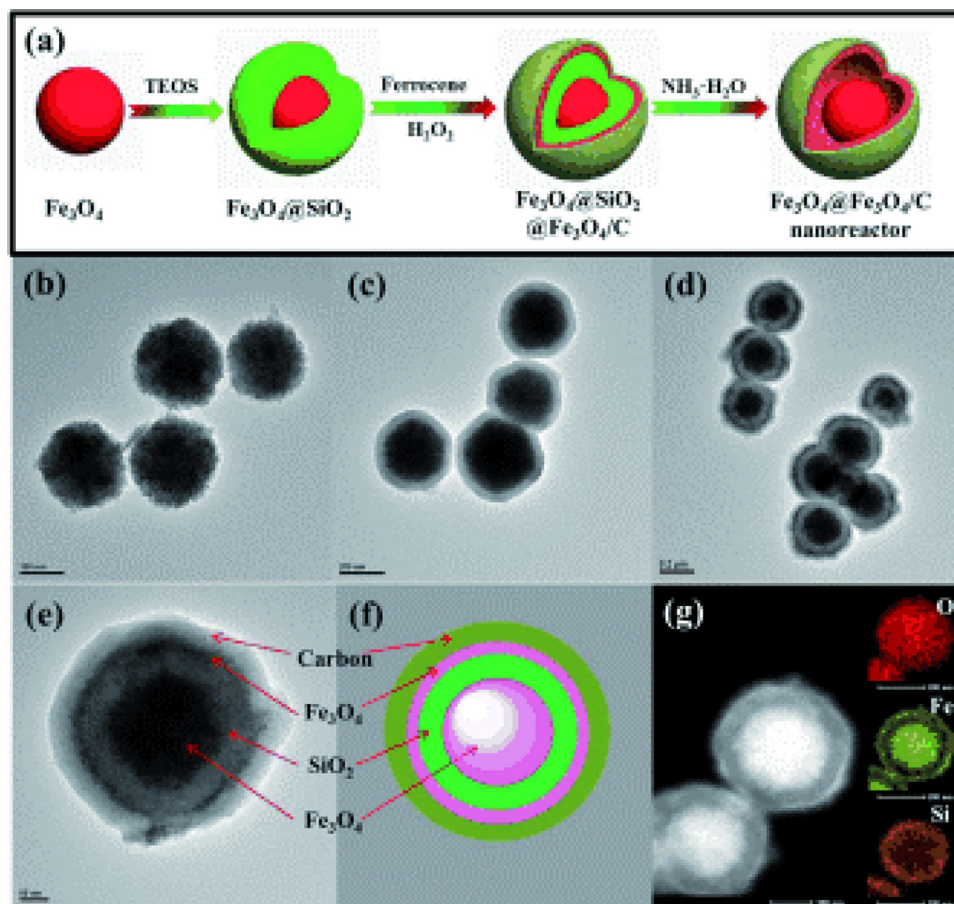
Fig. 30. (a) Illustration of the preparation of the yolk-shell $Fe_3O_4@Fe_3O_4/C$ nanostructured material; TEM micrographs of (b) Fe_3O_4, (c) $Fe_3O_4@SiO_2$ and (d and e) $Fe_3O_4@SiO_2@Fe_3O_4/C$; (f) structural model of $Fe_3O_4@SiO_2@Fe_3O_4/C$; (g) scanning transmission electron microscopy (STEM) micrographs and energy-dispersive X-ray (EDX) mapping of $Fe_3O_4@SiO_2@Fe_3O_4/C$. Reprinted from [94], Copyright© 2014, with permission from John Wiley and Sons [License number: 3761921483345].

Table 9

Summary on the use of carbon encapsulated magnetic nanoparticles in CWPO: description of the catalyst, operating conditions and catalytic performance of each catalyst (pollutant removal and Fe leached to the treated waters).

| Authors	Catalyst	Operating conditions	Pollutant	H_2O_2 stoichiometric ratio[a]	Pollutant removal	$[Fe]_{leaching}$ $(mg\,L^{-1})$
Zhang et al. [14]	Fe_3O_4 core-carbon shell nanoparticles ($Fe_3O_4@C$), prepared by hydrothermal dehydrogenation of glucose at 160 °C in the presence of Fe_3O_4 nanoparticles previously obtained by co-precipitation of Fe^{2+} and Fe^{3+} at room temperature	Batch experiments [Catalyst] = 0.25 g L^{-1} Unknown $[H_2O_2]_0$ T = 35 °C	Methylene blue (200.0 mg L^{-1})	Not applicable	95.3% (381 mg g^{-1} h^{-1})	Not addressed
	Fe_3O_4 nanoparticles, prepared by co-precipitation of Fe^{2+} and Fe^{3+} at room temperature	pH$_{solution}$ = 3 t = 2 h			57.9% (232 mg g^{-1} h^{-1})	Not addressed
Zeng et al. [94]	Yolk-shell nanocomposites with a Fe_3O_4 core and a mesoporous Fe_3O_4/carbon double-layered shell, with a hollow space between them ($Fe_3O_4@Fe_3O_4/C$), prepared as follows: first, Fe_3O_4 nanoparticles were prepared by a solvothermal method using Fe^{3+}, trisodium citrate and sodium acetate in ethylene glycol at 200 °C; core-shell structures composed by a Fe_3O_4 core and a SiO_2 shell ($Fe_3O_4@SiO_2$), were then prepared by coating the Fe_3O_4 nanoparticles through hydrolysis of tetraethyl orthosilicate at room temperature; afterwards, the outer Fe_3O_4/carbon double-layered shell was added by dispersing $Fe_3O_4@SiO_2$ particles, ferrocene and H_2O_2 in acetone, followed by solvothermal treatment at 210 °C; the $Fe_3O_4@Fe_3O_4/C$ nanocomposite was finally obtained by selective etching of the SiO_2 layer with aqueous ammonia at 150 °C	Batch experiments [Catalyst] = 0.5 g L^{-1} $[H_2O_2]_0$ = 0.68 g L^{-1} T = 25 °C pH$_{solution}$ = 4 t = 1.5 h	4-Chlorophenol (200.6 mg L^{-1})	0.8	98.0% (261 mg g^{-1} h^{-1}) 91.0% (in the 4th consecutive reuse)	Not addressed[b]
	Fe_3O_4 nanoparticles were prepared by a solvothermal method using Fe^{3+}, trisodium citrate and sodium acetate in ethylene glycol at 200 °C				36.0% (96.3 mg g^{-1} h^{-1})	Not addressed
Li et al. [93]	Core-shell nanocomposite with a zero valent iron core and a carbonaceous shell (Fe@C core-shell), prepared by coating Fe_2O_3 nanoparticles with cetyltrimethylammonium bromide, resorcinol, formaldehyde and ammonia in a mixed solution of ethanol and water at 35 °C, followed by calcination at 900 °C under N_2 atmosphere to promote carbonization and reduction of the core	Batch experiments [Catalyst] = 1.0 g L^{-1} $[H_2O_2]_0$ = 0.45 g L^{-1} Unknown temperature pH$_{solution}$ = 4 t = 20 min (Fe@C core-shell) t = 12 min (Fe@C yolk-shell)	4-Chlorophenol (100.0 mg L^{-1})	1.0	100.0% (303 mg g^{-1} h^{-1})	Not addressed
	Yolk-shell nanocomposite with a zero valent iron core and a carbonaceous shell (Fe@C yolk-shell), prepared as follows: first, Fe_2O_3 nanoparticles were coated with SiO_2 through hydrolysis of tetraethyl orthosilicate at room temperature; then, the resulting material was coated with resorcinol-formaldehyde resins as described above; afterwards, the SiO_2 layer was removed with aqueous ammonia at 85 °C; the Fe@C yolk-shell nanocomposite was finally obtained by calcination at 900 °C under N_2 atmosphere				100.0% (500 mg g^{-1} h^{-1}) 100.0% (in the 3rd consecutive reuse)	Not addressed

[a] Obtained by dividing the amount of H_2O_2 employed by the stoichiometric amount needed for the complete mineralization of the pollutant considered.

[b] A control experiment was made: $Fe_3O_4@Fe_3O_4/C$ was suspended in a H_2O_2 solution for 45 min at the same conditions of the CWPO experiments, and then removed; the remaining solution was then tested for the degradation of 4-chlorophenol by homogeneous CWPO, a conversion of 4% being obtained after 60 min of reaction.
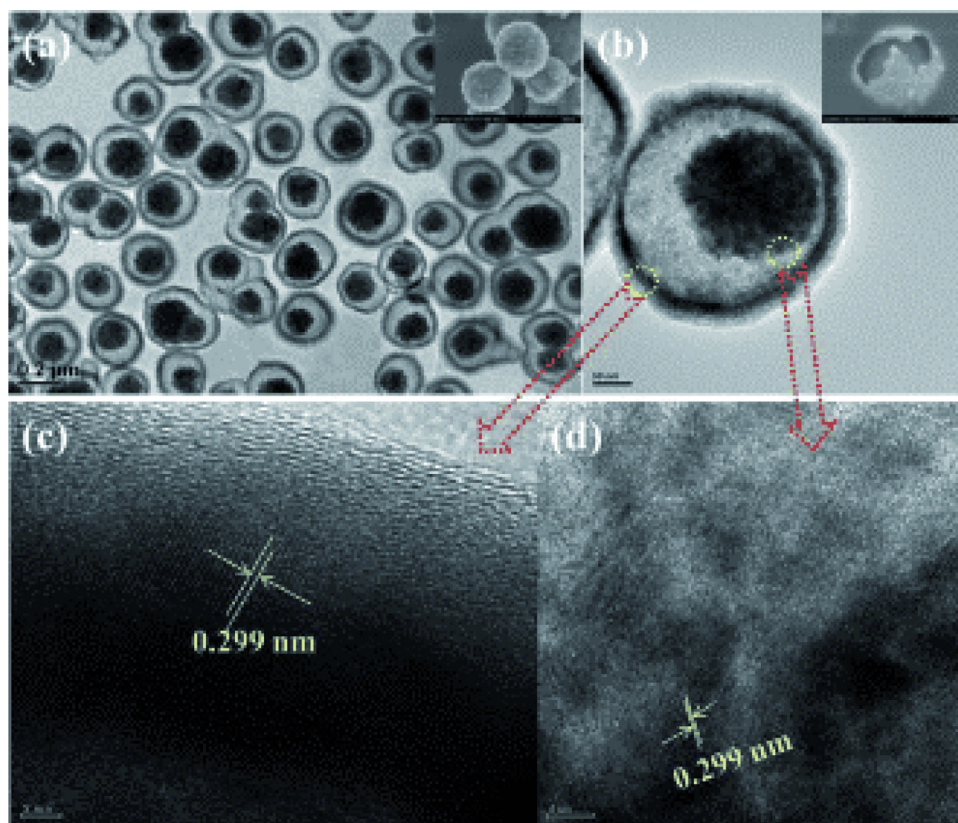
Fig. 31. (a and b) TEM micrographs of $Fe_3O_4@Fe_3O_4/C$; (c and d) high-resolution transmission electron microscopy (HRTEM) micrographs of the shell and core, respectively. Insets in (a) and (b) are scanning electron microscopy (SEM) images of $Fe_3O_4@Fe_3O_4/C$. Reprinted from [94], Copyright© 2014, with permission from John Wiley and Sons [License number: 3761921483345].

4.2. Carbon encapsulated magnetic nanoparticles

To the best of our knowledge, the use of carbon encapsulated magnetic nanoparticles in CWPO processes was first reported in 2014, by Zhang et al. [14]. For this purpose, Fe_3O_4 was prepared by co-precipitation; then, hydrothermal dehydrogenation of glucose was adopted in order to coat the Fe_3O_4 cores with a faintly distinguished carbon layer, as observed in Fig. 28a, resulting in the composite named $Fe_3O_4@C$, as described in Table 9.

Although Zhang et al. [14] have reported the formation of big agglomerates of particles due to magnetic attraction, the catalytic activity of the $Fe_3O_4@C$ catalyst in the CWPO of methylene blue was unequivocally demonstrated at 35 °C and $pH_{solution} = 3$. Indeed, the authors concluded that carbon encapsulation enhances the catalytic activity of the Fe_3O_4 cores. As observed in Table 9, the discoloration efficiency obtained with $Fe_3O_4@C$ (95.3%) is almost twice that obtained with Fe_3O_4 (57.9%). As previously discussed regarding the use of carbon nanostructures decorated with magnetic nanoparticles in CWPO (cf. Section 4.1), this effect was ascribed to an increased concentration of pollutant molecules near to the active sites in which $HO^\bullet$ are formed, due to adsorptive interactions with the carbonaceous shell [14]. In addition, inhibition experiments performed in the presence of *tert*-butanol – a strong $HO^\bullet$ scavenger [211] – confirm the role of $HO^\bullet$ in the CWPO of methylene blue, as shown in Fig. 29 [14].

Novel and complex hierarchical nanoarchitectures, core-shell and hollow structured materials have been developed in recent years, mainly as powerful platforms for controlled drug delivery, confined nanocatalysis and energy storage and conversion [214]. These novel materials, known as yolk-shell nanoparticles or "nanorattles", are nanostructures with a void space between

the core and the shell, which can provide very specific microenvironments [94,214]. Bearing this in mind, Zeng et al. [94] anticipated that yolk-shell structured catalysts could be used in CWPO. Therefore, a yolk-shell nanostructured material with a Fe_3O_4 core, a mesoporous Fe_3O_4/carbon double-layered shell, and a void space between them was synthesized ($Fe_3O_4@Fe_3O_4/C$, as described in Fig. 30a) [94]. The pre-synthesized Fe_3O_4 nanoparticles (cf. Fig. 30b) were first coated with a silica shell through the hydrolysis of tetraethyl orthosilicate to form core-shell structured $Fe_3O_4@SiO_2$ microspheres (cf. Fig. 30c); a double-layer coating was then deposited simultaneously on the surface of $Fe_3O_4@SiO_2$ by hydrothermal reaction with ferrocene and H_2O_2 (cf. Fig. 30d and e); the yolk-like $Fe_3O_4@Fe_3O_4/C$ nanostructured material (cf. Fig. 31) was finally obtained by the selective etching of the silica shell with aqueous ammonia (a more detailed synthesis procedure is given in Table 9) [94].

Once synthesized, the ability of the $Fe_3O_4@Fe_3O_4/C$ catalyst for CWPO was assessed using 4-chlorophenol as model pollutant. As observed in Fig. 32a, the catalytic performance of $Fe_3O_4@Fe_3O_4/C$ obtained at 25 °C and $pH_{solution} = 4$, is superior to that of the other catalysts used in control experiments: 97% pollutant removal is obtained after 210 min of reaction when using Fe_3O_4, while 4-chlorophenol is almost completely eliminated after 60 min of reaction when using the $Fe_3O_4@Fe_3O_4/C$ catalyst. As illustrated in Fig. 32b, this superior performance was ascribed to the synergistic effects that arise from the combination of each part of the $Fe_3O_4@Fe_3O_4/C$ composite: (i) the cavity of the nanostructured material provides a perfect microenvironment where the CWPO process is facilitated due to the confinement of reactants and active sites on both surfaces of the cavity; (ii) the outer carbon layer of the shell helps to increase the pollutant concentration in the cav-
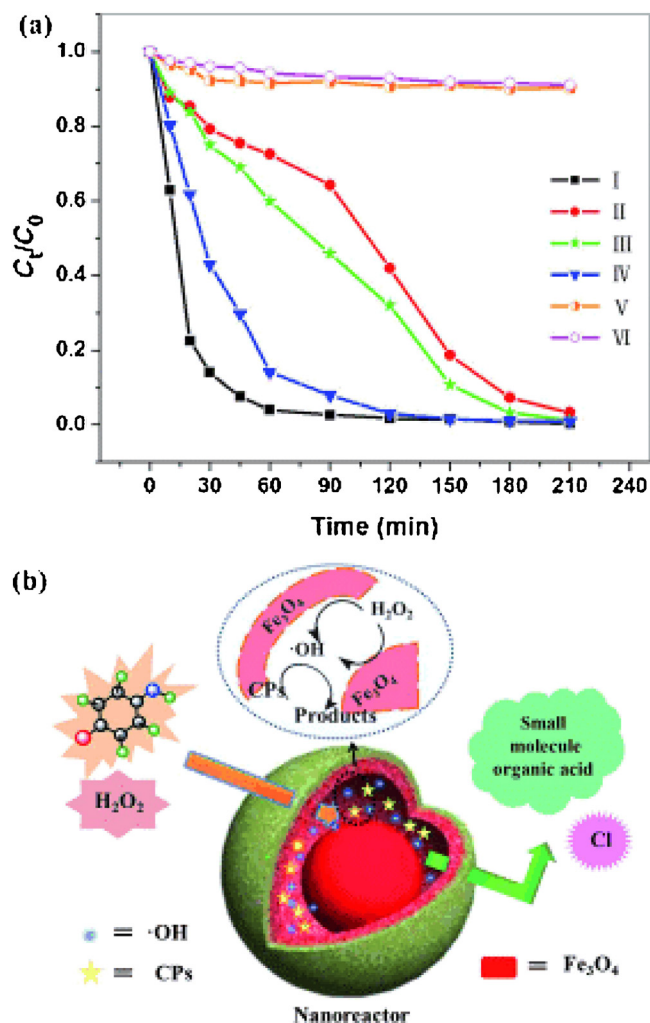
Fig. 32. (a) 4-Chlorophenol concentration decay curves obtained under different conditions: I) $Fe_3O_4@Fe_3O_4/C$; II) Fe_3O_4; III) solid $SiO_2@Fe_3O_4/C$; IV) yolk-like $SiO_2@Fe_3O_4/C$; V) non-catalytic removal (blank); and VI) pure adsorption removal with $Fe_3O_4@Fe_3O_4/C$. Experiments performed with [4-Chlorophenol]$_0$ = 200.6 mg L^{-1}, [catalyst/adsorbent] = 0.5 g L^{-1}, T = 25 °C, pH 4 and, in CWPO runs, [H_2O_2]$_0$ = 0.68 g L^{-1}. (b) Mechanism proposed by T. Zeng et al. for the CWPO of 4-chlorophenol in the yolk-like $Fe_3O_4@Fe_3O_4/C$ catalyst. Reprinted from [94], Copyright© 2014, with permission from John Wiley and Sons [License number: 3761921483345].

ity, while it also (iii) acts as a protection to abate the erosion of the Fe_3O_4 components by the external harsh conditions. In addition, Fe_3O_4 components confer a superparamagnetic character to $Fe_3O_4@Fe_3O_4/C$ [94].

The performance of a magnetic yolk-shell composite (Fe@C yolk-shell) in CWPO was compared to that of more traditional core-shell structures (Fe@C core-shell) in a work reported by Li et al. [93], in which 4-chlorophenol was also used as model pollutant. As shown in Fig. 33 and detailed in Table 9, both composites were produced in a similar way, with a core made of zero valent iron and a carbon shell obtained by carbonization of resorcinol-formaldehyde resins. In this way, the effect of the void space between the core and the shell was assessed at pH$_{solution}$ = 4. As observed in Table 9, 4-chlorophenol is completely removed by CWPO after 20 min of reaction with the Fe@C core-shell catalyst, while the same performance is obtained within 12 min when the Fe@C yolk-shell catalyst is applied. The increased performance of the Fe@C yolk-shell catalyst was ascribed to its unique structure, whose cavity provides numerous active sites for the catalytic decomposition of H_2O_2 at the surface of the core. Nevertheless, the stability of zero-valent

iron and the influence of homogeneous catalysis promoted by the Fe leached into the solution were not addressed in this work, which, as the authors recognized, casts some doubts on the actual extent of heterogeneous catalysis [93].

5. Summary and perspectives

This review demonstrates unequivocally the adequacy of CWPO as water treatment for the elimination of recalcitrant pollutants in aqueous phase.

Features such as (i) stable metal impurities, (ii) basic active sites, (iii) sulphur-containing functionalities, (iv) well-developed surface area and pore texture, (v) adsorptive interactions and (vi) structural defects, were shown to increase the catalytic activity of carbon materials when applied as catalysts on their own. These effects were respectively ascribed to the (i) recognized catalytic activity of metal species, (ii) electron donating character of basic active sites, (iii) presence of thiol surface groups, (iv) higher surface availability, (v) increased pollutant concentration adsorbed nearby the sites were HO• are generated, inhibiting non-efficient parasitic reactions between H_2O_2 and HO•, and to the (vi) increased surface density of electron-rich regions, which may act as active sites for the decomposition of H_2O_2. On the other hand, the presence of acidic oxygen-containing functionalities was shown to decrease the performance of carbon materials in CWPO, due to their electron-withdrawing capacity.

The combination of highly active and magnetically separable iron species with carbon-based materials promotes several synergistic effects that increase the performance of the resulting nanostructured hybrid composites in CWPO. These effects were mainly ascribed to:

- increased adsorptive interactions enhanced by the carbon phase, attracting the pollutant molecules to the vicinity of the active sites where highly oxidizing HO• are generated; this phenomena inhibits non-efficient parasitic reactions involving H_2O_2 and HO•, thus increasing the efficiency of H_2O_2 consumption;
- good structural stability and lower leaching of metal species, due to the confinement effect caused by the carbon phase;
- increased regeneration of active sites, either due to delocalized unpaired π-electrons or to electron transfer features of the carbon-based materials;
- increased dispersion of the active sites, as result of the high specific surface area of the carbon phase;
- the evident CWPO activity of carbon materials on their own.

As a result of these synergies, several of the nanostructured hybrid composites considered in this review were reported as effective catalysts at neutral pH. In this way, the treated waters do not require neutralization before being discharged into natural waters, which is a typical drawback of the Fenton process.

In addition, the magnetic sensitivity of the nanostructured composites allows their easy recycling at the end of the CWPO treatment cycle. Thus, the typical separation step required in the Fenton process for the removal of dissolved Fe species in the treated waters may be avoided. Nevertheless, in order to confirm this feature of the nanostructured hybrid magnetic composites, future works should always evaluate their stability through the measurement of Fe leached into solution during the CWPO process. For the sake of clarity, this is the only approach that allows full evaluation of the extent of the heterogeneous catalysis that is promoted by the composite catalysts.

All the works dealing with CWPO described in this review share a common feature: the experimental runs were always carried out at the atmospheric pressure. This fact, combined with the rela-
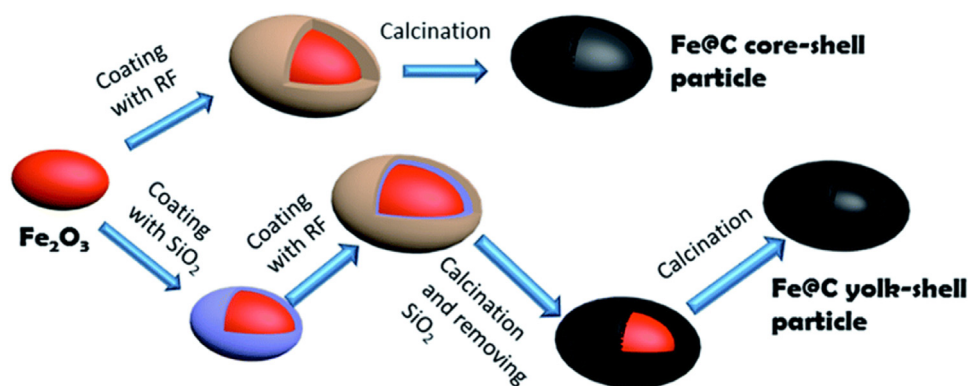
Fig. 33. Synthesis pathways of the Fe@C core-shell and Fe@C yolk-shell hybrid magnetic composites. Reprinted from [93], Copyright© 2015, with permission from The Royal Society of Chemistry [License number: 3761930157656].

tively mild conditions of temperature used (in the range 20–80 °C), confers an increased potential for economically viable applications to the CWPO-based water treatment technologies. On the other hand, the wide range of pollutant concentrations considered in the tests, from 0.212 mg L^{-1} up to 5 g L^{-1}, puts into evidence the suitability of this treatment, not just for the elimination of micro-contaminants present in wastewaters, but also for the removal of organic pollutants from industrial process waters and wastewaters at low to medium concentrations. Nevertheless, the H$_2$O$_2$ consumed per mole of pollutant degraded may be considered excessive in some works where a large excess of H$_2$O$_2$ was employed (H$_2$O$_2$ stoichiometric ratios up to 221). This excessive consumption of H$_2$O$_2$ may hinder the global efficiency of CWPO, as H$_2$O$_2$ is the main reactant employed and the main contributor to the global CWPO process cost. Likewise, in some works the catalyst dosage was in large excess when compared to the pollutant concentration. In fact, pollutant/catalyst mass ratios as low as 0.0001 have been employed, which may favour non-efficient parasitic reactions between H$_2$O$_2$ and HO$^\bullet$, as discussed in Section 3.4. Bearing this in mind, it is important to optimize both H$_2$O$_2$ and catalyst dosages in future works dealing with the application of hybrid magnetic carbon nanocomposites for the degradation of organic pollutants by CWPO.

To the best of our knowledge, studies on large-scale production of hybrid magnetic carbon composites for application in CWPO processes have never been reported in the literature. Therefore, possible limitations on reproducibility of the characteristics of these novel materials should be addressed in future works, in order to evaluate the feasibility of its large-scale use. Another important issue regarding the widespread use of CWPO has to do with some concerns of the scientific community over possible toxicological effects of the by-products resulting from the application of this treatment technology. Therefore, the toxicity of the treated waters should be addressed more often in future studies.

In conclusion, although significant findings and major improvements have been discussed in this review, especially regarding the synthesis and application of highly active and stable nanostructured hybrid magnetic catalysts for CWPO, much is yet to be done in order to promote CWPO as an efficient technology, not only for the treatment and reuse of industrial waters and wastewaters, but also to be able to meet the demanding quality criteria for the reuse of treated waters in urban water cycles. Bearing this in mind, future attempts to improve CWPO-based water treatment technologies may comprise very distinct approaches, such as the proper tuning of the carbon materials, as widely discussed in Section 3, the incorporation of metals with increased performances, as a result of the several studies that have been performed on the subject [144], or the very recent advances on the synthesis of hybrid magnetic

carbon materials for other applications [209,210,215]. In addition, carbon-based hybrid magnetic composites produced from very distinct waste materials such as sewage sludge [56,216], soil [217], foundry waste [218], peanut shells [219] and natural graphite tailings [220], have also been reported as active catalysts for CWPO. In the future, the low cost typically associated with waste materials may contribute to increase even further the commercial viability of CWPO-based water treatment technologies.

Acknowledgments

References

[1] D. Fatta-Kassinos, C. Manaia, T.U. Berendonk, E. Cytryn, J. Bayona, B. Chefetz, J. Slobodnik, N. Kreuzinger, L. Rizzo, S. Malato, L. Lundy, A. Ledin, Environ. Sci. Pollut. Res. 22 (2015) 7183–7186.
[2] J.J. Pignatello, E. Oliveros, A. MacKay, Crit. Rev. Environ. Sci. Technol. 36 (2006) 1–84.
[3] C.W. Jones, Applications of Hydrogen Peroxide and Derivatives, The Royal Society of Chemistry, Cambridge, UK, 1999.
[4] P.R. Gogate, A.B. Pandit, Adv. Environ. Res. 8 (2004) 501–551.
[5] S. Navalon, M. Alvaro, H. Garcia, Appl. Catal. B 99 (2010) 1–26.
[6] V.P. Santos, M.F.R. Pereira, P.C.C. Faria, J.J.M. Órfão, J. Hazard. Mater. 162 (2009) 736–742.
[7] L.C.A. Oliveira, C.N. Silva, M.I. Yoshida, R.M. Lago, Carbon 42 (2004) 2279–2284.
[8] E. Lorençon, D.C. Ferreira, R.R. Resende, K. Krambrock, Appl. Catal. A 505 (2015) 566–574.
[9] C. Bao, H. Zhang, L. Zhou, Y. Shao, J. Ma, Q. Wu, RSC Adv. 5 (2015) 72423–72432.
[10] Y. Shao, L. Zhou, C. Bao, J. Ma, Carbon 89 (2015) 378–391.
[11] J. Ma, L. Zhou, W. Dan, H. Zhang, Y. Shao, C. Bao, L. Jing, J. Colloid Interface Sci. 446 (2015) 298–306.
[12] B. Yang, Z. Tian, L. Zhang, Y. Guo, S. Yan, J. Water Process Eng. 5 (2015) 101–111.
[13] J.C. Tristão, F.G. de Mendonça, R.M. Lago, J.D. Ardisson, Environ. Sci. Pollut. Res. 22 (2015) 856–863.
[14] X. Zhang, M. He, J.-H. Liu, R. Liao, L. Zhao, J. Xie, R. Wang, S.-T. Yang, H. Wang, Y. Liu, Chin. Sci. Bull. 59 (2014) 3406–3412.
[15] H. Wang, H. Jiang, S. Wang, W. Shi, J. He, H. Liu, Y. Huang, RSC Adv. 4 (2014) 45809–45815.
[16] L. Zhou, Y. Shao, J. Liu, Z. Ye, H. Zhang, J. Ma, Y. Jia, W. Gao, Y. Li, ACS Appl. Mater. Interfaces 6 (2014) 7275–7285.
[17] W. Li, T. Sun, F. Li, Ind. Eng. Chem. Res. 53 (2014) 18095–18103.

[18] J. Qian, K. Wang, Q. Guan, H. Li, H. Xu, Q. Liu, W. Liu, B. Qiu, Appl. Surf. Sci. 288 (2014) 633–640.

[19] Y.C. Lee, S.J. Chang, M.H. Choi, T.J. Jeon, T. Ryu, Y.S. Huh, Appl. Catal. B 142–143 (2013) 494–503.

[20] S.B. Lima, S.M.S. Borges, M. Do Carmo Rangel, S.G. Marchetti, J. Braz. Chem. Soc. 24 (2013) 344–354.

[21] M. Gonçalves, M.C. Guerreiro, L.C.A. de Oliveira, C.S. De Castro, J. Environ. Manage. 127 (2013) 206–211.

[22] W. Liu, J. Qian, K. Wang, H. Xu, D. Jiang, Q. Liu, X. Yang, H. Li, J. Inorg. Organomet. Polym. Mater. 23 (2013) 907–916.

[23] G. Nie, Z. Li, X. Lu, J. Lei, C. Zhang, C. Wang, Appl. Surf. Sci. 284 (2013) 595–600.

[24] C.S. Castro, M.C. Guerreiro, L.C.A. Oliveira, M. Gonçalves, A.S. Anastácio, M. Nazzaro, Appl. Catal. A 367 (2009) 53–58.

[25] J.H. Ramirez, F.J. Maldonado-Hódar, A.F. Pérez-Cadenas, C. Moreno-Castilla, C.A. Costa, L.M. Madeira, Appl. Catal. B 75 (2007) 312–323.

[26] H. Haham, J. Grinblat, M.T. Sougrati, L. Stievano, S. Margel, Materials 8 (2015) 4593–4607.

[27] N.A. Zubir, C. Yacou, J. Motuzas, X. Zhang, X.S. Zhao, J.C. Diniz da Costa, Chem. Commun. 51 (2015) 9291–9293.

[28] M.T. Pinho, A.M.T. Silva, N.A. Fathy, A.A. Attia, H.T. Gomes, J.L. Faria, J. Environ. Chem. Eng. 3 (2015) 1243–1251.

[29] N.A. Zubir, C. Yacou, J. Motuzas, X. Zhang, J.C. Diniz da Costa, Sci. Rep. 4 (2014), Article number: 4594.

[30] N.A. Zubir, C. Yacou, X. Zhang, J.C. Diniz da Costa, J. Environ. Chem. Eng. 2 (2014) 1881–1888.

[31] N.A. Zubir, X. Zhang, C. Yacou, J.C. Diniz da Costa, Sci. Adv. Mater. 6 (2014) 1382–1388.

[32] F.M. Duarte, F.J. Maldonado-Hódar, L.M. Madeira, Appl. Catal. B 129 (2013) 264–272.

[33] F.M. Duarte, F.J. Maldonado-Hódar, L.M. Madeira, Appl. Catal. A 458 (2013) 39–47.

[34] Y. Zhao, W.-F. Chen, C.-F. Yuan, Z.-Y. Zhu, L.-F. Yan, Chin. J. Chem. Phys. 25 (2012) 335–338.

[35] Y. Tu, S. Tian, L. Kong, Y. Xiong, Chem. Eng. J. 185–186 (2012) 44–51.

[36] F.M. Duarte, F.J. Maldonado-Hódar, L.M. Madeira, Ind. Eng. Chem. Res. 51 (2012) 9218–9226.

[37] J. Deng, X. Wen, Q. Wang, Mater. Res. Bull. 47 (2012) 3369–3376.

[38] R.S. Ribeiro, N.A. Fathy, A.A. Attia, A.M.T. Silva, J.L. Faria, H.T. Gomes, Chem. Eng. J. 195–196 (2012) 112–121.

[39] F.M. Duarte, F.J. Maldonado-Hódar, L.M. Madeira, Appl. Catal. B 103 (2011) 109–115.

[40] A. Rodríguez, G. Ovejero, J.L. Sotelo, M. Mestanza, J. García, Ind. Eng. Chem. Res. 49 (2010) 498–505.

[41] F.M. Duarte, F.J. Maldonado-Hódar, A.F. Pérez-Cadenas, L.M. Madeira, Appl. Catal. B 85 (2009) 139–147.

[42] Z. Qu, X. Tang, X. Li, K. Chen, D. Ma, Chin. J. Catal. 30 (2009) 142–146.

[43] S.T.T. Le, T.T. Ngo, W. Khanitchaidecha, A. Nakaruk, Bull. Mater. Sci. 38 (2015) 1039–1042.

[44] C. Yang, D. Wang, Q. Tang, J. Taiwan Inst. Chem. Eng. 45 (2014) 2584–2589.

[45] T.D. Nguyen, N.H. Phan, M.H. Do, K.T. Ngo, J. Hazard. Mater. 185 (2011) 653–661.

[46] H.T. Gomes, S.M. Miranda, M.J. Sampaio, A.M.T. Silva, J.L. Faria, Catal. Today 151 (2010) 153–158.

[47] H.T. Gomes, S.M. Miranda, M.J. Sampaio, J.L. Figueiredo, A.M.T. Silva, J.L. Faria, Appl. Catal. B 106 (2011) 390–397.

[48] J.C. García, M.P. Castellanos, Á. Uscátegui, J. Fernández, A.M. Pedroza, C.E. Daza, Univ. Sci. 17 (2012) 303–314.

[49] L. Dąbek, E. Ozimina, A. Picheta-Oleś, Rocz. Ochr. Sr. 13 (2011) 1023–1042.

[50] G. Ersöz, Appl. Catal. B 147 (2014) 353–358.

[51] O. Türgay, G. Ersöz, S. Atalay, J. Forss, U. Welander, Sep. Purif. Technol. 79 (2011) 26–33.

[52] Y.H. Chang, Y.F. Yao, H. Luo, L. Cui, L.J. Zhi, Int. J. Nanomanuf. 10 (2014) 132–141.

[53] Y. Yao, Y. Mao, B. Zheng, Z. Huang, W. Lu, W. Chen, Ind. Eng. Chem. Res. 53 (2014) 8376–8384.

[54] M.F. Variava, T.L. Church, A.T. Harris, Appl. Catal. B 123–124 (2012) 200–207.

[55] L. Sun, Y. Yao, L. Wang, Y. Mao, Z. Huang, D. Yao, W. Lu, W. Chen, Chem. Eng. J. 240 (2014) 413–419.

[56] L. Gu, N. Zhu, H. Guo, S. Huang, Z. Lou, H. Yuan, J. Hazard. Mater. 246–247 (2013) 145–153.

[57] J. Wu, G. Lin, P. Li, W. Yin, X. Wang, B. Yang, Water Sci. Technol. 67 (2013) 572–578.

[58] L. Wang, Y. Yao, L. Sun, W. Lü, W. Chen, Acta Chim. Sinica 71 (2013) 1633–1638.

[59] M. Soria-Sánchez, E. Castillejos-López, A. Maroto-Valiente, M.F.R. Pereira, J.J.M. Órfão, A. Guerrero-Ruiz, Appl. Catal. B 121–122 (2012) 182–189.

[60] I. Mesquita, L.C. Matos, F.M. Duarte, F.J. Maldonado-Hódar, A. Mendes, L.M. Madeira, J. Hazard. Mater. 237–238 (2012) 30–37.

[61] O.P. Pestunova, O.L. Ogorodnikova, V.N. Parmon, Chem. Sustain. Dev. 11 (2003) 227–232.

[62] J.C. Espinosa, S. Navalón, A. Primo, M. Moral, J.F. Sanz, M. Álvaro, H. García, Chem. Eur. J. 21 (2015) 11966–11971.

[63] S.A. Messele, O.S.G.P. Soares, J.J.M. Órfão, C. Bengoa, F. Stüber, A. Fortuny, A. Fabregat, J. Font Catal. Today 240 (2015) 73–79.

[64] S.A. Messele, C. Bengoa, F. Stüber, A. Fortuny, A. Fabregat, J. Font, Desalin. Water Treat. 57 (2016) 5155–5164.

[65] M.T. Pinho, H.T. Gomes, R.S. Ribeiro, J.L. Faria, A.M.T. Silva, Appl. Catal. B 165 (2015) 706–714.

[66] C.M. Domínguez, P. Ocón, A. Quintanilla, J.A. Casas, J.J. Rodríguez, Appl. Catal. B 144 (2014) 599–606.

[67] C.M. Domínguez, A. Quintanilla, J.A. Casas, J.J. Rodriguez, Chem. Eng. J. 253 (2014) 486–492.

[68] S.A. Messele, O.S.G.P. Soares, J.J.M. Órfão, F. Stüber, C. Bengoa, A. Fortuny, A. Fabregat, J. Font, Appl. Catal. B 154–155 (2014) 329–338.

[69] F. Martínez, I. Pariente, C. Brebou, R. Molina, J.A. Melero, D. Bremner, D. Mantzavinos, J. Chem. Technol. Biotechnol. 89 (2014) 1182–1188.

[70] T. Wanchun, L. Fen, W. Junli, L. Jiehua, L. Xiaoxi, Tech. Equip. Environ. Pollut. Control 5 (2013) 1744–1748.

[71] Y.Z. Yang, Y.P. Li, D.W. Yang, F. Duan, H.B. Cao, Huan Jing Ke Xue 34 (2013) 2658–2664.

[72] C.M. Domínguez, P. Ocón, A. Quintanilla, J.A. Casas, J.J. Rodríguez, Appl. Catal. B 140–141 (2013) 663–670.

[73] A. Quintanilla, S. García-Rodríguez, C.M. Domínguez, S. Blasco, J.A. Casas, J.J. Rodriguez, Appl. Catal. B 111–112 (2012) 81–89.

[74] F. Martínez, M.I. Pariente, J.A. Botas, J.A. Melero, A. Rubalcaba, J. Chem. Technol. Biotechnol. 87 (2012) 880–886.

[75] L. Kong, W. Wei, Q. Zhao, J.Q. Wang, Y. Wan, ACS Catal. 2 (2012) 2577–2586.

[76] J. Chun, H. Lee, S.-H. Lee, S.-W. Hong, J. Lee, C. Lee, J. Lee, Chemosphere 89 (2012) 1230–1237.

[77] A. Rey, J. Carbajo, C. Adán, M. Faraldos, A. Bahamonde, J.A. Casas, J.J. Rodriguez, Chem. Eng. J. 174 (2011) 134–142.

[78] J. Li, J. Gu, H. Li, Y. Liang, Y. Hao, X. Sun, L. Wang, Microporous Mesoporous Mater. 128 (2010) 144–149.

[79] R.-M. Liou, S.-H. Chen, C.H. Huang, M.Y. Hung, J.S. Chang, C.L. Lai, Water Sci. Technol. 61 (2010) 1489–1498.

[80] R.-M. Liou, S.-H. Chen, J. Hazard. Mater. 172 (2009) 498–506.

[81] O. Taran, E. Polyanskaya, O. Ogorodnikova, V. Kuznetsov, V. Parmon, M. Besson, C. Descorme, Appl. Catal. A 387 (2010) 55–66.

[82] A. Rey, M. Faraldos, J.A. Casas, J.A. Zazo, A. Bahamonde, J.J. Rodríguez, Appl. Catal. B 86 (2009) 69–77.

[83] Q. Liao, J. Sun, L. Gao, Colloids Surf. A 345 (2009) 95–100.

[84] A.M. Dehkordi, A.A. Ebrahimi, Ind. Eng. Chem. Res. 48 (2009) 10619–10626.

[85] Z.G. Meng, J. Wang, L. Fu, F.L. Yang, S.W. Hu, J. Xi'an Univ. Archit. Technol. 41 (2009) 571–574.

[86] J.A. Zazo, A.F. Fraile, A. Rey, A. Bahamonde, J.A. Casas, J.J. Rodriguez, Catal. Today 143 (2009) 341–346.

[87] J.M. Britto, S.B.d. Oliveira, D. Rabelo, M.d.C. Rangel, Catal. Today 133–135 (2008) 582–587.

[88] A. Rey, M. Faraldos, A. Bahamonde, J.A. Casas, J.A. Zazo, J.J. Rodríguez, Ind. Eng. Chem. Res. 47 (2008) 8166–8174.

[89] J.C. Moreno, V.M. Sarria, Á.D. Polo, L. Giraldo, Inf. Technol. 18 (2007) 67–72.

[90] J.A. Zazo, J.A. Casas, A.F. Mohedano, J.J. Rodríguez, Appl. Catal. B 65 (2006) 261–268.

[91] F. Lücking, H. Köser, M. Jank, A. Ritter, Water Res. 32 (1998) 2607–2614.

[92] W. Liu, L. Xu, X. Li, C. Shen, S. Rashid, Y. Wen, W. Liu, X. Wu, RSC Adv. 5 (2015) 2449–2456.

[93] X. Li, F. Gai, B. Guan, Y. Zhang, Y. Liu, Q. Huo, J. Mater. Chem. A 3 (2015) 3988–3994.

[94] T. Zeng, X. Zhang, S. Wang, Y. Ma, H. Niu, Y. Cai, Chem. Eur. J. 20 (2014) 6474–6481.

[95] F. Duan, Y. Yang, Y. Li, H. Cao, Y. Wang, Y. Zhang, J. Environ. Sci. 26 (2014) 1171–1179.

[96] H.-H. Huang, M.C. Lu, J.N. Chen, C.T. Lee, Chemosphere 51 (2003) 935–943.

[97] X. Yang, P.F. Tian, C. Zhang, Y.Q. Deng, J. Xu, J. Gong, Y.F. Han, Appl. Catal. B 134–135 (2013) 145–152.

[98] J.R. Kim, S.G. Huling, E. Kan, Chem. Eng. J. 262 (2015) 1260–1267.

[99] Y. Wang, H. Zhao, G. Zhao, Appl. Catal. B 164 (2015) 396–406.

[100] D. Zhou, C. Wang, Y. Zhao, Chin. J. Environ. Eng. 8 (2014) 5284–5288.

[101] V. Cleveland, J.-P. Bingham, E. Kan, Sep. Purif. Technol. 133 (2014) 388–395.

[102] W. Zhou, Z. Cheng, X. Quan, B. Chen, Huagong Xuebao/CIESC J. 64 (2013) 936–942.

[103] R.S. Ribeiro, A.M.T. Silva, J.L. Figueiredo, J.L. Faria, H.T. Gomes, Appl. Catal. B 140 (2013) 356–362.

[104] R.S. Ribeiro, A.M.T. Silva, M.T. Pinho, J.L. Figueiredo, J.L. Faria, H.T. Gomes, Catal. Today 240 (Part A) (2015) 61–66.

[105] Y. Wang, H. Wei, P. Liu, Y. Yu, Y. Zhao, X. Li, W. Jiang, J. Wang, X. Yang, C. Sun, Catal. Today 258 (Part 1) (2015) 120–131.

[106] Y. Yu, H. Wei, L. Yu, T. Zhang, S. Wang, X. Li, J. Wang, C. Sun, RSC Adv. 5 (2015) 41867–41876.

[107] R.S. Ribeiro, A.M.T. Silva, L.M. Pastrana-Martínez, J.L. Figueiredo, J.L. Faria, H.T. Gomes, Catal. Today 249 (2015) 204–212.

[108] A. Georgi, F.D. Kopinke, Appl. Catal. B 58 (2005) 9–18.

[109] L. Zhou, H. Zhang, L. Ji, Y. Shao, Y. Li, RSC Adv. 4 (2014) 24900–24908.

[110] H.-H. Huang, M.-C. Lu, J.-N. Chen, C.-T. Lee, J. Environ. Sci. Health Part A 38 (2003) 1233–1246.

[111] T.L.P. Dantas, V.P. Mendonça, H.J. José, A.E. Rodrigues, R.F.P.M. Moreira, Chem. Eng. J. 118 (2006) 77–82.

[112] S. Karthikeyan, R. Boopathy, G. Sekaran, J. Colloid Interface Sci. 448 (2015) 163–174.

[113] S. Karthikeyan, R.B. Ahamed, M. Velan, G. Sekaran, RSC Adv. 4 (2014) 63354–63366.
[114] F.M. Duarte, V. Morais, F.J. Maldonado-Hódar, L.M. Madeira, Chem. Eng. J. 232 (2013) 34–41.
[115] Y. Li, H. Fei, Q.-q. Luo, M. Zhang, H.-j. Dai, L. Yin, H.-x. Shi, J. Zhejiang Univ. Sci. 6 (2013) 676–680.
[116] S. Karthikeyan, M.E. Priya, R. Boopathy, M. Velan, A.B. Mandal, G. Sekaran, Environ. Sci. Pollut. Res. 19 (2012) 1828–1840.
[117] S. Karthikeyan, A. Titus, A. Gnanamani, A.B. Mandal, G. Sekaran, Desalination 281 (2011) 438–445.
[118] G. Sekaran, S. Karthikeyan, K. Ramani, B. Ravindran, A. Gnanamani, A.B. Mandal, Environ. Chem. Lett. 9 (2011) 499–504.
[119] P. Bautista, Á.F. Mohedano, N. Menéndez, J.A. Casas, J.J. Rodríguez, Catal. Today 151 (2010) 148–152.
[120] V. Gosu, B.R. Gurjar, R.Y. Surampalli, T.C. Zhang, J. Environ. Chem. Eng. 2 (2014) 1996–2004.
[121] S. Zhang, Y. Han, L. Wang, Y. Chen, P. Zhang, Chem. Eng. J. 252 (2014) 141–149.
[122] C.M. Domínguez, A. Quintanilla, J.A. Casas, J.J. Rodríguez, Sep. Purif. Technol. 129 (2014) 121–128.
[123] X. Hu, B. Liu, Y. Deng, H. Chen, S. Luo, C. Sun, P. Yang, S. Yang, Appl. Catal. B 107 (2011) 274–283.
[124] X.-b. Hu, Y.-h. Deng, Z.-q. Gao, B.-z. Liu, C. Sun, Appl. Catal. B 127 (2012) 167–174.
[125] M. Yang, J. Ma, Y. Sun, X. Xiong, C. Li, Q. Li, J. Chen, Chem. J. Chin. Univ. 35 (2014) 570–575.
[126] J. Ma, M. Yang, F. Yu, J. Chen, J. Colloid Interface Sci. 444 (2015) 24–32.
[127] N. Jaafarzadeh, B. Kakavandi, A. Takdastan, R.R. Kalantary, M. Azizi, S. Jorfi, RSC Adv. 5 (2015) 84718–84728.
[128] M.A. Fontecha-Cámara, M.A. Álvarez-Merino, F. Carrasco-Marín, M.V. López-Ramón, C. Moreno-Castilla, Appl. Catal. B 101 (2011) 425–430.
[129] A. Dhaouadi, N. Adhoum, Appl. Catal. B 97 (2010) 227–235.
[130] Priyanka, V. Subbaramaiah, V.C. Srivastava, I.D. Mall, Sep. Purif. Technol. 125 (2014) 284–290.
[131] S. Hu, H. Yao, K. Wang, C. Lu, Y. Wu, Water Air Soil Pollut. 226 (2015), Article number 155.
[132] A.R. Yeddou, B. Nadjemi, F. Halet, A. Ould-Dris, R. Capart, Miner. Eng. 23 (2010) 32–39.
[133] H.J.H. Fenton, J. Chem. Soc. Trans. 65 (1894) 899–910.
[134] F. Haber, J. Weiss, Naturwissenschaften 20 (1932) 948–950.
[135] F. Haber, J. Weiss, Proc. R. Soc. Lond. A: Math. Phys. Sci. 147 (1934) 332–351.
[136] W.G. Barb, J.H. Baxendale, P. George, K.R. Hargrave, Trans. Faraday Soc. 47 (1951) 462–500.
[137] W.G. Barb, J.H. Baxendale, P. George, K.R. Hargrave, Trans. Faraday Soc. 47 (1951) 591–616.
[138] M. Munoz, Z.M. de Pedro, J.A. Casas, J.J. Rodriguez, Appl. Catal. B 176–177 (2015) 249–265.
[139] J. Barrault, J.M. Tatibouët, N. Papayannakos, Comptes Rendus de l'Académie des Sciences – Series IIC – Chem. 3 (2000) 777–783.
[140] M.C. Pereira, L.C.A. Oliveira, E. Murad, Clay Miner. 47 (2012) 285–302.
[141] P.V. Nidheesh, RSC Adv. 5 (2015) 40552–40577.
[142] S. Rahim Pouran, A.A. Abdul Raman, W.M.A. Wan Daud, J. Cleaner Prod. 64 (2014) 24–35.
[143] M. Muruganandham, R.P.S. Suri, M. Sillanpää, J.J. Wu, B. Ahmmad, S. Balachandran, M. Swaminathan, J. Nanosci. Nanotechnol. 14 (2014) 1898–1910.
[144] A. Dhakshinamoorthy, S. Navalon, M. Alvaro, H. Garcia, ChemSusChem 5 (2012) 46–64.
[145] S. Navalon, A. Dhakshinamoorthy, M. Alvaro, H. Garcia, ChemSusChem 4 (2011) 1712–1730.
[146] S. Navalon, R. Martin, M. Alvaro, H. Garcia, Angew. Chem. Int. Ed. 49 (2010) 8403–8407.
[147] P. Ehrburger, Adv. Colloid Interface Sci. 21 (1984) 275–302.
[148] L.R. Radovic, F. Rodríguez-Reinoso, in: P.A. Thrower (Ed.), Chemistry and Physics of Carbon, Marcel Dekker, New York, 1997, pp. 243–358.
[149] E. Auer, A. Freund, J. Pietsch, T. Tacke, Appl. Catal. A 173 (1998) 259–271.
[150] R. Schlögl, in: G. Ertl, H. Knözinger, J. Weitkamp (Eds.), Preparation of Solid Catalysts, Wiley-VCH Verlag GmbH, Weinheim, Germany, 1999, pp. 150–240.
[151] L.R. Radovic, C. Sudhakar, in: H. Marsh, E.A. Heintz, F. Rodríguez-Reinoso (Eds.), Introduction to Carbon Technologies, University of Alicante Press, Alicante, Spain, 1997, pp. 103–165.
[152] F. Rodríguez-Reinoso, in: J.W. Patrick (Ed.), Porosity in Carbons: Characterization and Applications, Edward Arnold, London, 1995.
[153] F. Rodríguez-Reinoso, Carbon 36 (1998) 159–175.
[154] P. Serp, J.L. Figueiredo, Carbon Materials for Catalysis, John Wiley & Sons, Inc., Hoboken, New Jersey, 2009.
[155] J.L. Figueiredo, J. Mater. Chem. A 1 (2013) 9351–9364.
[156] P. Serp, M. Corrias, P. Kalck, Appl. Catal. A 253 (2003) 337–358.
[157] J.H. Ramirez, C.A. Costa, L.M. Madeira, G. Mata, M.A. Vicente, M.L. Rojas-Cervantes, A.J. López-Peinado, R.M. Martín-Aranda, Appl. Catal. B 71 (2007) 44–56.
[158] R.W. Coughlin, Ind. Eng. Chem. Prod. Res. Dev. 8 (1969) 12–23.
[159] P. Serp, B.F. Machado, Nanostructured Carbon Materials for Catalysis, The Royal Society of Chemistry, Cambridge, UK, 2015.
[160] R.S. Ribeiro, A.M.T. Silva, J.L. Figueiredo, J.L. Faria, H.T. Gomes, Carbon 62 (2013) 97–108.
[161] B.H.J. Bielski, D.E. Cabelli, R.L. Arudi, A.B. Ross, J. Phys. Chem. Ref. Data 14 (1985) 1041–1100.
[162] G.V. Buxton, C.L. Greenstock, W.P. Helman, A.B. Ross, J. Phys. Chem. Ref. Data 17 (1988) 513–886.
[163] H. Christensen, K. Sehested, H. Corfitzen, J. Phys. Chem. 86 (1982) 1588–1590.
[164] A.J. Elliot, G.V. Buxton, J. Chem. Soc. Faraday Trans. 88 (1992) 2465–2470.
[165] M.G. Evans, N. Uri, Trans. Faraday Soc. 45 (1949) 224–230.
[166] L.B. Khalil, B.S. Girgis, T.A.M. Tawfik, J. Chem. Technol. Biotechnol. 76 (2001) 1132–1140.
[167] W.H. Koppenol, J. Butler, J.W. Van Leeuwen, Photochem. Photobiol. 28 (1978) 655–658.
[168] S.-S. Lin, M.D. Gurol, Environ. Sci. Technol. 32 (1998) 1417–1423.
[169] K.G. Linden, C.M. Sharpless, S.A. Andrews, K.Z. Atasi, V. Korategere, M. Stefan, I.H.M. Suffet, Innovative UV Technologies to Oxidize Organic and Organoleptic Chemicals, I. Publishing, London, 2005 (Chapter 8).
[170] A. Rey, A. Bahamonde, J.A. Casas, J.J. Rodríguez, Water Sci. Technol. 61 (2010) 2769–2778.
[171] A. Rey, J.A. Zazo, J.A. Casas, A. Bahamonde, J.J. Rodríguez, Appl. Catal. A 402 (2011) 146–155.
[172] J. Weinstein, B.H.J. Bielski, J. Am. Chem. Soc. 101 (1979) 58–62.
[173] S. Ghafoori, M. Mehrvar, P.K. Chan, Ind. Eng. Chem. Res. 51 (2012) 14980–14993.
[174] T. Schaefer, J. Schindelka, D. Hoffmann, H. Herrmann, J. Phys. Chem. A 116 (2012) 6317–6326.
[175] D.G. Rao, R. Senthilkumar, J.A. Byrne, S. Feroz, Wastewater Treatment: Advanced Processes and Technologies, CRC Press and IWA Publishing, London, UK, 2013.
[176] A. Aguinaco, J.P. Pocostales, J.F. García-Araya, F.J. Beltrán, J. Chem. Technol. Biotechnol. 86 (2011) 595–600.
[177] C.M. Domínguez, A. Quintanilla, P. Ocón, J.A. Casas, J.J. Rodríguez, Carbon 60 (2013) 76–83.
[178] V. Strelko, S. Stavitskaya, N. Tsyba, A. Lysenko, S. Zhuravskii, V. Goba, Russ. J. Appl. Chem. 80 (2007) 389–396.
[179] K.V. Voitko, R.L.D. Whitby, V.M. Gun'ko, O.M. Bakalinska, M.T. Kartel, K. Laszlo, A.B. Cundy, S.V. Mikhalovsky, J. Colloid Interface Sci. 361 (2011) 129–136.
[180] J.L. Figueiredo, M.F.R. Pereira, Catal. Today 150 (2010) 2–7.
[181] D.L. Trimm, in: C. Kemball, D.A. Dowden (Eds.), Catalysis, The Royal Society of Chemistry, London, UK, 1981.
[182] D.E. Weiss, Proceedings of the Fifth Conference on Carbon, Pergamon Press, Inc., New York, N.Y., 1962, pp. 65–72.
[183] J.L. Figueiredo, M.F.R. Pereira, M.M.A. Freitas, J.J.M. Órfão, Carbon 37 (1999) 1379–1389.
[184] J.L. Figueiredo, M.F.R. Pereira, M.M.A. Freitas, J.J.M. Órfão, Ind. Eng. Chem. Res 46 (2007) 4110–4115.
[185] W. Shen, Z. Li, Y. Liu, Recent Pat. Chem. Eng. 1 (2008) 27–40.
[186] H.P. Boehm, M. Voll, Carbon 8 (1970) 227–240.
[187] A. Contescu, C.I. Contescu, K. Putyera, J.A. Schwarz, Carbon 35 (1997) 83–94.
[188] E. Papirer, S. Li, J.-B. Donnet, Carbon 25 (1987) 243–247.
[189] E. Fuente, J.A. Menéndez, D. Suárez, M.A. Montes-Morán, Langmuir 19 (2003) 3505–3511.
[190] M.A. Montes-Morán, J.A. Menéndez, E. Fuente, D. Suárez, J. Phys. Chem. B 102 (1998) 5595–5601.
[191] T.J. Bandosz, C.O. Ania, in: T.J. Bandosz (Ed.), Interface Science and Technology, Elsevier, Amsterdam, 2006, pp. 159–229.
[192] G. Leofanti, M. Padovan, G. Tozzola, B. Venturelli, Catal. Today 41 (1998) 207–219.
[193] S.J. Gregg, K.S.W. Sing, Adsorption, Surface Area and Porosity, 2nd ed., Academic Press, London, 1982.
[194] K. Kaneko, J. Membr. Sci. 96 (1994) 59–89.
[195] J. Rouquerol, D. Avnir, D.H. Everett, C. Fairbridge, M. Haynes, N. Pernicone, J.D.F. Ramsay, K.S.W. Sing, K.K. Unger, in: J. Rouquerol, F. Rodríguez-Reinoso, K.S.W. Sing, K.K. Unger (Eds.), Studies in Surface Science and Catalysis, Elsevier, Amsterdam, 1994, pp. 1–9.
[196] P. Serp, K. Philippot, Nanomaterials in Catalysis, Wiley-VCH Verlag GmbH & Co., Weinheim, Germany, 2013.
[197] W. Jiang, T. Tran, X. Song, K. Kinoshita, J. Power Sources 85 (2000) 261–268.
[198] H. Terrones, R. Lv, M. Terrones, M.S. Dresselhaus, Rep. Prog. Phys. 75 (2012) 062501.
[199] R.C. Bansal, J.B. Donnet, F. Stoeckli, Active Carbon, Marcel Dekker, New York, 1988.
[200] L.R. Radovic, I.F. Silva, J.I. Ume, J.A. Menéndez, C.A.L.Y. Leon, A.W. Scaroni, Carbon 35 (1997) 1339–1348.
[201] F. Haghseresht, S. Nouri, J.J. Finnerty, G.Q. Lu, J. Phys. Chem. B 106 (2002) 10935–10943.
[202] T. Karanfil, J.E. Kilduff, Environ. Sci. Technol. 33 (1999) 3217–3224.
[203] S. Nouri, F. Haghseresht, Adsorpt. Sci. Technol. 20 (2002) 417–432.
[204] C. Moreno-Castilla, Carbon 42 (2004) 83–94.
[205] L.R. Radovic, C. Moreno-Castilla, J. Rivera-Utrilla, in: L.R. Radovic (Ed.), Chemistry and Physics of Carbon, Dekker, New York, 2000.
[206] S. Haydar, M.A. Ferro-Garcíía, J. Rivera-Utrilla, J.P. Joly, Carbon 41 (2003) 387–395.

[207] F. Villacañas, M.F.R. Pereira, J.J.M. Órfão, J.L. Figueiredo, J. Colloid Interface Sci. 293 (2006) 128–136.
[208] C. Moreno-Castilla, J. Rivera-Utrilla, M.V. López-Ramón, F. carrasco-Marín, Carbon 33 (1995) 845–851.
[209] S. Boncel, A.P. Herman, K.Z. Walczak, J. Mater. Chem. 22 (2012) 31–37.
[210] M. Zhu, G. Diao, Nanoscale 3 (2011) 2748–2767.
[211] S. Zhang, X. Zhao, H. Niu, Y. Shi, Y. Cai, G. Jiang, J. Hazard. Mater. 167 (2009) 560–566.
[212] Y. Li, Y. Wu, J. Am. Chem. Soc. 131 (2009) 5851–5857.
[213] S. Stankovich, D.A. Dikin, G.H.B. Dommett, K.M. Kohlhaas, E.J. Zimney, E.A. Stach, R.D. Piner, S.T. Nguyen, R.S. Ruoff, Nature 442 (2006) 282–286.
[214] J. Liu, S.Z. Qiao, J.S. Chen, X.W. Lou, X. Xing, G.Q. Lu, Chem. Commun. 47 (2011) 12578–12591.
[215] J. Tuček, K.C. Kemp, K.S. Kim, R. Zbořil, ACS Nano 8 (2014) 7571–7612.
[216] L. Gu, N. Zhu, P. Zhou, Bioresour. Technol. 118 (2012) 638–642.
[217] M.C. Pereira, L.C.D. Cavalcante, F. Magalhães, J.D. Fabris, J.W. Stucki, L.C.A. Oliveira, E. Murad, Chem. Eng. J. 166 (2011) 962–969.
[218] P.E.F. Oliveira, L.D. Oliveira, J.D. Ardisson, R.M. Lago, J. Hazard. Mater. 194 (2011) 393–398.
[219] L. Zhou, J. Ma, H. Zhang, Y. Shao, Y. Li, Appl. Surf. Sci. 324 (2015) 490–498.
[220] B. Cuiping, G. Wenqi, F. Dexin, X. Mo, Z. Qi, C. Shaohua, G. Zhongxue, Z. Yanshui, Chem. Eng. J. 197 (2012) 306–313.